

CAPITAL UNIVERSITY OF SCIENCE AND
TECHNOLOGY, ISLAMABAD



**An Enhanced Auto-Synchronizer
for Integration of the Virtual
Synchronous Machine into Power
Grid**

by

Muhammad Naeem

A thesis submitted in partial fulfillment for the
degree of Doctor of Philosophy

in the

Faculty of Engineering

Department of Electrical Engineering

2022

An Enhanced Auto-Synchronizer for Integration of the Virtual Synchronous Machine into Power Grid

By

Muhammad Naeem
(DEE161002)

Dr. Saad Mekhilef, Professor
University of Malaya, Kuala Lumpur, Malaysia
(Foreign Evaluator 1)

Dr. Mohamad Kamarol Mohd Jamil, Associate Professor
Universiti Sains Malaysia, Pulau Pinang, Malaysia
(Foreign Evaluator 2)

Dr. Muhammad Ashraf
(Thesis Supervisor)

Dr. Noor Muhammad Khan
(Head, Department of Electrical Engineering)

Dr. Imtiaz Ahmad Taj
(Dean, Faculty of Engineering)

**DEPARTMENT OF ELECTRICAL ENGINEERING
CAPITAL UNIVERSITY OF SCIENCE AND TECHNOLOGY
ISLAMABAD**

2022

Copyright © 2022 by Muhammad Naeem

All rights reserved. No part of this thesis may be reproduced, distributed, or transmitted in any form or by any means, including photocopying, recording, or other electronic or mechanical methods, by any information storage and retrieval system without the prior written permission of the author.

Dedicated to my better half, Asma Kiran Aziz



**CAPITAL UNIVERSITY OF SCIENCE & TECHNOLOGY
ISLAMABAD**

Expressway, Kahuta Road, Zone-V, Islamabad
Phone: +92-51-111-555-666 Fax: +92-51-4486705
Email: info@cust.edu.pk Website: <https://www.cust.edu.pk>

CERTIFICATE OF APPROVAL

This is to certify that the research work presented in the thesis, entitled “**An Enhanced Auto-Synchronizer for Integration of the Virtual Synchronous Machine into Power Grid**” was conducted under the supervision of **Dr. Muhammad Ashraf**. No part of this thesis has been submitted anywhere else for any other degree. This thesis is submitted to the **Department of Electrical Engineering, Capital University of Science and Technology** in partial fulfillment of the requirements for the degree of Doctor in Philosophy in the field of **Electrical Engineering**. The open defence of the thesis was conducted on **September 16, 2022**.

Student Name : Muhammad Naeem (DEE-161002)

The Examination Committee unanimously agrees to award PhD degree in the mentioned field.

Examination Committee :

(a) External Examiner 1: Dr. Abdul Khaliq
Professor
Sir Syed CASE IT, Islamabad

(b) External Examiner 2: Dr. Shaikh Saaqib Haroon
Associate Professor
UET, Taxila

(c) Internal Examiner : Dr. Noor Muhammad Khan
Professor
CUST, Islamabad

Supervisor Name : Dr. Muhammad Ashraf
Professor
CUST, Islamabad

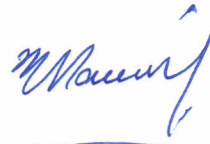
Name of HoD : Dr. Noor Muhammad Khan
Professor
CUST, Islamabad

Name of Dean : Dr. Imtiaz Ahmed Taj
Professor
CUST, Islamabad

AUTHOR'S DECLARATION

I, **Muhammad Naeem (Registration No. DEE-161002)**, hereby state that my PhD thesis titled, '**An Enhanced Auto-Synchronizer for Integration of the Virtual Synchronous Machine into Power Grid**' is my own work and has not been submitted previously by me for taking any degree from Capital University of Science and Technology, Islamabad or anywhere else in the country/ world.

At any time, if my statement is found to be incorrect even after my graduation, the University has the right to withdraw my PhD Degree.



(Muhammad Naeem)

Dated: 16 September, 2021

Registration No : DEE161002

PLAGIARISM UNDERTAKING

I solemnly declare that research work presented in the thesis titled “**An Enhanced Auto-Synchronizer for Integration of the Virtual Synchronous Machine into Power Grid**” is solely my research work with no significant contribution from any other person. Small contribution/ help wherever taken has been duly acknowledged and that complete thesis has been written by me.

I understand the zero tolerance policy of the HEC and Capital University of Science and Technology towards plagiarism. Therefore, I as an author of the above titled thesis declare that no portion of my thesis has been plagiarized and any material used as reference is properly referred/ cited.

I undertake that if I am found guilty of any formal plagiarism in the above titled thesis even after award of PhD Degree, the University reserves the right to withdraw/ revoke my PhD degree and that HEC and the University have the right to publish my name on the HEC/ University Website on which names of students are placed who submitted plagiarized thesis.



(Muhammad Naeem)

Dated: 16 September, 2022

Registration No : DEE161002

List of Publications

It is certified that following publication has been made out of the research work that has been carried out for this thesis:-

1. **M. Naeem**, M. Ashraf, and U. A. Khan, “A Robust Auto-Synchronizer for Synchronverter,” *Computers and Electrical Engineering*, vol. 98, pp. 1-12, 2022.

Muhammad Naeem

Registration No: DEE161002

Acknowledgement

All praises to Allah Who created me and taught me what I didn't know. I am grateful to my supervisor Dr. Muhammad Ashraf who rectified the framework of this thesis and guided me throughout my research. I thank Dr. Umer Amir Khan for the support and motivation he provided during the hard times of this research. He helped in the writeup of publications and continuously backed me up to improve and resubmit the publications.

I also acknowledge Dr. Muhammad Tahir who helped me in learning Latex and other tools and gave useful tips during different stages of this research. His inspirational comments kept me on track continuously. It is also necessary to acknowledge Dr. Aamir Iqbal Bhatti for keeping interest in my research progress. This helped me to stay focused on my objectives.

I am thankful to the Head of my department, Dr. Noor Muhammad Khan, who allowed me to complete my research with dedication. He supported me in managing departmental tasks and responsibilities throughout the degree duration. Thanks to my friends and colleagues at CUST for being well wishers. Finally, special thanks to my family who allowed me to complete this research without creating disturbances.

Muhammad Naeem

Abstract

The increasing demand of energy, scarceness of conventional fuel reserves and increased environmental threats have changed the focus of power grid from conventional resources to renewable energy resources. This trend, although evolving the power system towards the smart grid, deploys a dominant role of inertia-less power electronic converters having the strong tendency to challenge the voltage and frequency stability of the power system. The inherent characteristics of conventional synchronous generators are required to be possessed by these power electronic converters to support the future power grid. Therefore, the idea of Virtual Synchronous Machines (VSM) is encouraged by the researchers so that these power electronic converters appear as synchronous machines from grid point-of-view. Synchronverter, an inverter that mimics real synchronous generator, is exceptional among VSMs because of its simplicity and inertial dynamics. Like conventional synchronous generators, it has ability to support frequency and voltage in power grid. It also has the inherent capability to remain synchronized with the grid without any dedicated synchronization unit. It also offers seamless transfer from grid-connected to stand-alone mode of operation without any change required in the controller. However, it requires a synchronizer to track grid phase and frequency as reference prior to grid connection. Due to complexity, inefficiency, and deteriorating performance of PLL in weak grid, PLL-less synchronization approaches are proposed in literature. Existing PLL-less approaches either lack seamless transfer capability or lead to unwanted delays and uncertainties under adverse grid conditions.

In this research work an enhanced, PLL-less auto-synchronizer for synchronverter is proposed using the concept of Fourier analysis. The Fourier analysis of synchronverter voltage and grid voltage is performed to calculate the phase and magnitude of the fundamental component. The phase and magnitude differences between the two voltages are then minimized by using Proportional Integral gains to synchronize the synchronverter with the grid. The proposed auto-synchronizer ensures uninterrupted power supply capability during synchronization, presents a fast,

and reliable solution of synchronization under adverse grid conditions, and has less computational burden on controller as compared to PLL-based synchronization. The proposed auto-synchronizer is validated by simulations and compared with the existing Differential Root Mean Square Voltage (DRMSV) based synchronizer. Comparison results have shown that the proposed auto-synchronizer has improved the speed and certainty of synchronverter synchronization under adverse grid conditions. Later on, the designed auto-synchronizer is applied to achieve grid-synchronization of synchronverter having Solar Power Plant at the dc bus. Results have shown that the proposed auto-synchronizer can be applied to synchronverter irrespective of the power ratings and nature of the dc source.

To find whether the synchronverter is a promising solution of RERs integration into power grid or not, its performance is not fully investigated yet in literature. The effect of variations in connected load on synchronverter output frequency and voltage in stand-alone mode is not studied to author's best knowledge. As an addition, in this report, the performance of synchronverter is also investigated with variations in local connected load in stand-alone mode and with weak grid conditions in grid-connected mode. Almost all the literature about synchronverter assumes an ideal source at the dc bus. In this research, the effect of intermittent nature of Solar Power Plant on the performance of synchronverter is also investigated in details. Further, the seamless transfer of synchronverter between stand-alone and grid-connected modes of operation is studied. The research outcomes have shown that the synchronverter along with the proposed synchronizer is a promising solution of solar power plant integration into future power grid.

Contents

Author's Declaration	v
Plagiarism Undertaking	vi
List of Publications	vii
Acknowledgement	viii
Abstract	ix
List of Figures	xiv
List of Tables	xviii
Abbreviations	xix
Symbols	xxi
1 Introduction	1
1.1 Current and Future Trends in Power Grid	2
1.2 Virtual Inertia Significance	4
1.3 Virtual Synchronous Machines	5
1.4 Synchronverter	7
1.5 Motivation	7
1.6 Research Objectives	8
1.7 Research Contributions	9
1.8 Thesis Organization	9
2 Literature Review	11
2.1 Review of VSMs Excluding Synchronverter	11
2.1.1 VISMA	12
2.1.2 IEPE's Topology	13
2.1.3 KHI Lab's Topology	13
2.1.4 Ise Lab's Topology	14
2.1.5 Synchronous Power Controller	16

2.1.6	Virtual Synchronous Controller	17
2.1.7	Virtual Synchronous Generator	18
2.1.8	Analysis of VSMs Excluding Synchronverter	19
2.2	Review of Synchronverter	22
2.2.1	Theoretical Concept of Synchronverter	22
2.2.2	Synchronverter Versus Other VSMs	23
2.2.3	Studies and Analysis of Original Synchronverter	24
2.2.4	Modifications in Original Synchronverter	25
2.2.5	Synchronverter Synchronization with Grid	27
2.2.5.1	Phase-Locked Loop Based Synchronization	27
2.2.5.2	Virtual Impedance Based Synchronization	29
2.2.5.3	Virtual Resistance Based Synchronization	31
2.2.5.4	Differential RMS Voltage Based Synchronization	32
2.2.6	Synchronverter Applications	33
2.3	Gap Analysis	36
2.4	Problem Statement	37
2.5	Methodology and Techniques	38
2.6	Applications	39
2.7	Summary	39
3	Design and Evaluation of Synchronverter	41
3.1	Synchronous Generator Model	41
3.2	Design of Synchronverter	46
3.2.1	Synchronous Generator Model	47
3.2.2	Frequency Control Loop	47
3.2.3	Voltage Control Loop	49
3.2.4	LCL Filter	50
3.3	Performance Evaluation of Synchronverter	51
3.4	Simulation Results and Discussions	53
3.4.1	Stand-Alone Performance	54
3.4.2	Grid-Connected Performance	57
3.4.2.1	Grid-Connected Mode with Stable Grid Conditions	57
3.4.2.2	Grid-Connected Performance Following Frequency Event	60
3.4.2.3	Grid-Connected Performance Following Voltage Event	62
3.4.3	Transfer from Grid-Connected to Stand-Alone Mode	65
3.5	Summary	67
4	Design and Evaluation of Proposed Auto-Synchronizer	69
4.1	DRMSV-Based Synchronizer	70
4.1.1	Scenario 1: v_o lags v_g	71
4.1.2	Scenario 2: Significant Difference Between $ v_o $ & $ v_g $	72
4.2	Design of Proposed Auto-Synchronizer	73
4.3	Simulation Results and Discussions	77

4.3.1	Case-I: Grid Synchronization when v_o Led v_g	77
4.3.2	Case-II: Grid Synchronization when v_o Lagged v_g	80
4.3.3	Case-III: Grid Synchronization when $ v_g = 90\%$ of V_n	83
4.3.4	Case-IV: Grid Synchronization when $ v_g = 110\%$ of V_n	87
4.3.5	Seamless Transfer Capability	90
4.4	Summary	93
5	Solar Power Plant Integration into Power Grid	94
5.1	Design of Complete System	95
5.1.1	Solar Power Plant	96
5.1.2	DC-DC Boost Converter	97
5.2	Simulation Results and Discussions	98
5.2.1	Stand-Alone Performance	99
5.2.2	Synchronization with Grid	102
5.2.3	Grid-Connected Mode with Variable Irradiance	105
5.2.4	Grid-Connected Mode Following Frequency Event	110
5.2.5	Grid-Connected Mode Following Voltage Event	112
5.2.6	Transfer from Grid-Connected to Stand-Alone Mode	115
5.3	Summary	118
6	Conclusions and Future Directions	119
6.1	Future Directions	120
	Bibliography	123

List of Figures

1.1	Power grid evolution [13]	2
1.2	Virtual inertia significance in power system [13]	4
1.3	Future power grid with SMs and VSMs [15]	5
1.4	Classification of Virtual Synchronous Machine Topologies [13]	6
2.1	General control scheme of VISMA having grid voltages as input [34]	12
2.2	General control scheme of IEPE Lab's Topology having grid currents as input [34]	13
2.3	Control scheme of KHI Lab's Topology [34]	14
2.4	Control scheme of Ise Lab's Topology [13]	15
2.5	Structure of Synchronous Power Controller [53]	16
2.6	Structure of Virtual Synchronous Controller [63]	17
2.7	General control scheme of Virtual Synchronous Generator [71]	18
2.8	Schematic of Synchronverter [21]	23
2.9	Synchronverter modes of operation	28
2.10	Basic Phase-Locked Loop [107]	28
2.11	Virtual impedance based self-synchronized synchronverter [88]	30
2.12	Virtual resistance based self-synchronized synchronverter [117]	31
2.13	Differential RMS Voltage Based Synchronization [102]	33
3.1	Winding structure of Synchronous Machine [21]	42
3.2	Schematic diagram of synchronverter without synchronizer	47
3.3	Frequency Control Loop	48
3.4	Voltage Control Loop	49
3.5	Stand-alone performance: synchronverter active power P_o and load P_{load}	55
3.6	Stand-alone performance: synchronverter reactive power Q_o and load Q_{load}	56
3.7	Stand-alone performance: synchronverter frequency f_o	56
3.8	Stand-alone performance: synchronverter rms phase voltage v_o	57
3.9	Grid-connected performance with stable grid conditions: synchronverter active power P_o and active power reference P_r	58
3.10	Grid-connected performance with stable grid conditions: synchronverter reactive power Q_o and reactive power reference Q_r	59
3.11	Grid-connected performance with stable grid conditions: synchronverter frequency f_o	59

3.12	Grid-connected performance with stable grid conditions: synchronverter rms phase voltage v_o	60
3.13	Grid-connected performance following a frequency event: synchronverter frequency f_o and grid frequency f_g	61
3.14	Grid-connected performance following a frequency event: synchronverter output current i_o	61
3.15	Grid-connected performance following a frequency event: synchronverter active power P_o	62
3.16	Grid-connected performance following a frequency event: synchronverter reactive power Q_o	62
3.17	Grid-connected performance following a voltage event: synchronverter phase voltage v_o	63
3.18	Grid-connected performance following a voltage event: synchronverter reactive power Q_o	63
3.19	Grid-connected performance following a voltage event: synchronverter frequency f_o	64
3.20	Grid-connected performance following a voltage event: synchronverter active power P_o	64
3.21	Grid-connected performance following a voltage event: synchronverter output current i_o	65
3.22	Transfer from grid-connected to stand-alone mode: synchronverter frequency f_o	66
3.23	Transfer from grid-connected to stand-alone mode: synchronverter rms phase voltage v_o	66
3.24	Transfer from grid-connected to stand-alone mode: synchronverter current i_o	67
4.1	Schematic diagram of DRMSV-based synchronizer [102]	70
4.2	Performance of DRMSV-based self-synchronization [102] when v_o leads v_g by angle θ	71
4.3	Performance of DRMSV-based self-synchronization [102] when v_o lags v_g by angle θ	72
4.4	Performance of DRMSV-based self-synchronization [102] when; (a) v_g becomes 110% of nominal value, (b) v_g drops to 90% of nominal value, (c) RMS difference V_d between v_o and v_g for both cases	73
4.5	Schematic diagram of proposed auto-synchronizer	74
4.6	Case-I: phase difference between v_o and v_g during synchronization	78
4.7	Case-I: RMS difference V_d between v_o and v_g during synchronization	78
4.8	Case-I: synchronverter frequency f_o during synchronization	79
4.9	Case-I: phasor representation of synchronization process with (a) proposed auto-synchronizer, (b) DRMSV-based synchronizer	79
4.10	Case-II: phase difference between v_o and v_g during synchronization	81
4.11	Case-II: RMS difference V_d between v_o and v_g during synchronization	81
4.12	Case-II: synchronverter frequency f_o during synchronization	82

4.13	Case-II: phasor representation of synchronization process with (a) proposed auto-synchronizer, (b) DRMSV-based synchronizer	82
4.14	Case-III: synchronverter phase voltage v_o and grid voltage v_g during synchronization	84
4.15	Case-III: phase difference between v_o and v_g during synchronization	84
4.16	Case-III: RMS difference V_d between v_o and v_g during synchronization	85
4.17	Case-III: phasor representation of synchronization process with (a) proposed auto-synchronizer, (b) DRMSV-based synchronizer	86
4.18	Case-IV: synchronverter phase voltage v_o and grid voltage v_g during synchronization	88
4.19	Case-IV: phase difference between v_o and v_g during synchronization	88
4.20	Case-IV: RMS difference V_d between v_o and v_g during synchronization	89
4.21	Case-IV: phasor representation of synchronization process with (a) proposed auto-synchronizer, (b) DRMSV-based synchronizer	89
4.22	Synchronverter active and reactive power outputs P_o and Q_o , respectively in Case-I	91
4.23	Synchronverter active and reactive power outputs P_o and Q_o , respectively in Case-II	91
4.24	Synchronverter active and reactive power outputs P_o and Q_o , respectively in Case-III	92
4.25	Synchronverter active and reactive power outputs P_o and Q_o , respectively in Case-IV	92
5.1	Schematic diagram of complete model under investigation	95
5.2	Stand-alone performance: synchronverter active power P_o	100
5.3	Stand-alone performance: synchronverter reactive power Q_o	100
5.4	Stand-alone performance: synchronverter frequency f_o	101
5.5	Stand-alone performance: synchronverter line voltage v_o	101
5.6	Grid synchronization with proposed synchronizer: synchronverter frequency f_o	103
5.7	Grid synchronization with proposed synchronizer: active power reference P_r , synchronverter active power P_o , and active power exchanged with grid P_g	103
5.8	Grid synchronization with proposed synchronizer: reactive power reference Q_r , synchronverter reactive power Q_o , and reactive power exchanged with grid Q_g	104
5.9	Grid synchronization with proposed synchronizer: synchronverter line voltage v_o	104
5.10	Grid-connected performance with variable Irradiance level: Irradiance level	105
5.11	Grid-connected performance with variable Irradiance level: SPP voltage V_{PV}	106
5.12	Grid-connected performance with variable Irradiance level: SPP power P_{PV}	106

5.13	Grid-connected performance with variable Irradiance level: active power reference P_r , synchronverter active power P_o , and active power exchanged with grid P_g	107
5.14	Grid-connected performance with variable Irradiance level: synchronverter frequency f_o	107
5.15	Grid-connected performance with variable Irradiance level: reactive power reference Q_r , synchronverter reactive power Q_o , and reactive power exchanged with grid Q_g	108
5.16	Grid-connected performance with variable Irradiance level: synchronverter line voltage v_o	108
5.17	Grid-connected performance with variable Irradiance level: dc-bus voltage V_{DC}	109
5.18	Grid-connected performance following frequency event: grid frequency f_g and synchronverter frequency f_o	110
5.19	Grid-connected performance following frequency event: synchronverter active power P_o and SPP power P_{PV}	111
5.20	Grid-connected performance following frequency event: grid line voltage v_g and synchronverter line voltage v_o	111
5.21	Grid-connected performance following frequency event: synchronverter reactive power Q_o	112
5.22	Grid-connected performance following voltage event: grid line voltage v_g and synchronverter line voltage v_o	113
5.23	Grid-connected performance following voltage event: synchronverter reactive power Q_o	113
5.24	Grid-connected performance following voltage event: grid frequency f_g and synchronverter frequency f_o	114
5.25	Grid-connected performance following voltage event: synchronverter active power P_o and SPP power P_{PV}	114
5.26	Transfer from grid-connected to stand-alone mode: synchronverter frequency f_o	116
5.27	Transfer from grid-connected to stand-alone mode: synchronverter active power P_o and active power exchanged with grid P_g	116
5.28	Transfer from grid-connected to stand-alone mode: synchronverter line voltage v_o	117
5.29	Transfer from grid-connected to stand-alone mode: synchronverter reactive power Q_o and reactive power exchanged with grid Q_g	117

List of Tables

2.1	Literature Review Summary of VSMs Excluding Synchronverter . . .	20
2.2	Literature review summary of original synchronverter	24
2.3	Modifications in original synchronverter	26
2.4	Literature Summary of initial grid-synchronization techniques of synchronverter	34
2.5	Various applications of synchronverter	35
3.1	Parameters used in simulations	52
3.2	Variations in local load connected to synchronverter with ideal source at dc bus	55
3.3	Variations in active and reactive power reference	58
4.1	Synchronizer parameters used in simulations	77
4.2	Comparison of proposed synchronizer with DRMSV synchronizer during synchronization process in Case-I	80
4.3	Comparison of proposed synchronizer with DRMSV synchronizer during synchronization process in Case-II	83
4.4	Comparison of proposed synchronizer with DRMSV synchronizer during synchronization process in Case-III	86
4.5	Comparison of proposed synchronizer with DRMSV synchronizer during synchronization process in Case-IV	90
5.1	Parameters used in simulations	96
5.2	Specifications of PV module used in SPP	97
5.3	Parameters of boost converter	98
5.4	Variations in local load connected to synchronverter with SPP at the dc bus	99
5.5	Comparison of stand-alone performance of synchronverter with dif- ferent dc sources	102
5.6	Irradiance Level in W/m^2	105

Abbreviations

AEDB	Alternative Energy Development Board
AVR	Automatic Voltage Regulator
CSC	Current Source Converter
DNI	Direct Normal Irradiance
DG	Distributed Generation
DFIG	Doubly-Fed Induction Generator
DRMSV	Differential Root Mean Square Voltage
EV	Electric Vehicle
ESD	Energy Storage Device
ESS	Energy Storage System
EPLL	Enhanced Phase-Locked Loop
GHI	Global Horizontal Irradiance
HVDC	High Voltage Direct Current
IPP	Independent Power Producer
LVDC	Low Voltage Direct Current
MPP	Maximum Power Point
MPPT	Maximum Power Point Tracking
NIST	National Institute of Silicon Technology
NTDC	National Transmission and Dispatch Company
NEPRA	National Electric Power Regulatory Authority
PV	Photo-Voltaic
PHEV	Plug-in Hybrid Electric Vehicle
PEC	Power Electronic Converter
PLL	Phase-Locked Loop

PWM	Pulse Width Modulation
POV	Point-of-View
PI	Proportional Integral
RER	Renewable Energy Resource
ROCOF	Rate-of-Change-of-Frequency
RMS	Root Mean Square
SG	Conventional Synchronous Generator
SM	Synchronous Machine
SPP	Solar Power Plant
SPC	Synchronous Power Controller
SOC	State-of-Charge
TET	Total Execution Time
VSM	Virtual Synchronous Machine
VSG	Virtual Synchronous Generator
VSC	Voltage Source Converter
VCO	Voltage Controlled Oscillator
V2G	Vehicle-to-Grid

Symbols

Symbol	Name	Unit
Φ_s	Stator flux linkage	
Φ_e	Rotor flux linkage	
i_a, i_b, i_c	Stator windings currents	
i_e	Excitation current	
M_e	Maximum mutual inductance between stator and rotor	
ψ	Product of mutual inductance and excitation current	
T_e	Induced electric torque	
P_o	Synchronverter output active power	W
P_r	Reference active power	W
Q_o	Synchronverter output reactive power	VAR
Q_r	Reference reactive power	VAR
ω	Rotor angular speed	rad/s
θ	Rotor angle	Deg
e	Induced electromotive force	V
v_g	Grid voltage	V
v_o	Synchronverter output voltage	V
i_o	Synchronverter output current	A
L_1, L_2	Filter inductors	mH
C_f	Filter capacitor	μ F
R_s	Series resistor	Ω
V_{DC}	DC bus voltage	V
V_n	Nominal phase voltage	V

S_n	Nominal power	kVA
f_{sw}	Switching frequency	kHz
f_n	Nominal frequency	Hz
f_o	Synchronverter frequency	Hz
D_f	Damping coefficient	
J	Virtual inertia	
D_v	Voltage droop coefficient	
K	Integrator gain	
τ_f	Frequency loop time constant	s
τ_v	Voltage loop time constant	s
ω_{res}	Resonance frequency	rad/s
V_d	RMS difference between v_o and v_g	V
K_f, I_f	PI gains	
K_v, I_v	PI gains	
V_{Th}	Threshold voltage	V
ω_s	Synchronizer output	rad/s
v_s	Synchronizer output	V
C_{Bi}	Boost converter input capacitor	μF
C_{Bo}	Boost converter output capacitor	μF
L_B	Boost converter inductor	mH
V_{PV}	SPP voltage	V
D_{max}	Maximum duty cycle of boost converter switch	
f_B	Switching frequency of boost converter switch	kHz
I_{PV}	SPP current	A
P_{PV}	SPP Power	kW

Chapter 1

Introduction

The world's population is increasing day-by-day. Increased population means increased demand of resources including water, food, residence, health-care, transportation, and energy, etc. According to [1], the world's energy consumption will be increased by 100% in 2050. This is also linked with the drastic reduction in conventional fuel resources and increased environmental pollution.

This increasing demand of energy, scarceness of conventional fuel reserves and increased environmental threats have changed the focus of power grid from conventional resources to Renewable Energy Resources (RERs) [2]. Therefore, the penetration of RERs into power grid is being increased with each passing day.

Integration of RERs improves system economy, reduces transmission losses, reduces operational cost and limits the carbon footprints [3]. Solar energy is among the leading RERs due to availability of sun on earth surface, easy installation and maintenance, no wear and tear loss, silent operation and zero environmental pollution [4, 5].

This chapter presents technical issues, challenges, and modern solutions related to inverter-dominated power grid. Motivation behind this research work, research objectives, and contributions to the research community are also discussed in this chapter.

1.1 Current and Future Trends in Power Grid

With increasing penetration of RERs, the Synchronous Generator (SG) dominated power grid is being transformed into inverter dominated grid as depicted in Figure 1.1. According to [6]; RERs provide 63% power generation in Portugal, 60% in Denmark and 29% in Spain. Japan has planned to introduce 53 GW of electricity only from Photo-Voltaic (PV) generation by 2030 [7]. Similar trend is seen in Pakistan. Ministry of Science and Technology in Pakistan has taken some drastic steps in development of PV panels during last decade [8]. National Institute of Silicon Technology (NIST) has developed PV modules and other infrastructure for solar power generation. In year 2017-18, National Transmission and Dispatch Company (NTDC) acquired 400 MW from solar Independent Power Producers (IPPs) [9]. During year 2020-21, nineteen (19) new generation licenses having cumulative installed capacity of 50.0264 MW have been issued to solar companies by National Electric Power Regulatory Authority (NEPRA) [10]. Also, 8417 net metering licenses of cumulative capacity of 145.881 MW have been issued to distribution companies during year 2020-21. Currently, Alternative Energy Development Board (AEDB) is pursuing twenty-two solar power projects of 890.80 MW capacity cumulatively [11]. Quaid-e-Azam Solar Park Bahawalpur is the country's largest solar power plant [12].

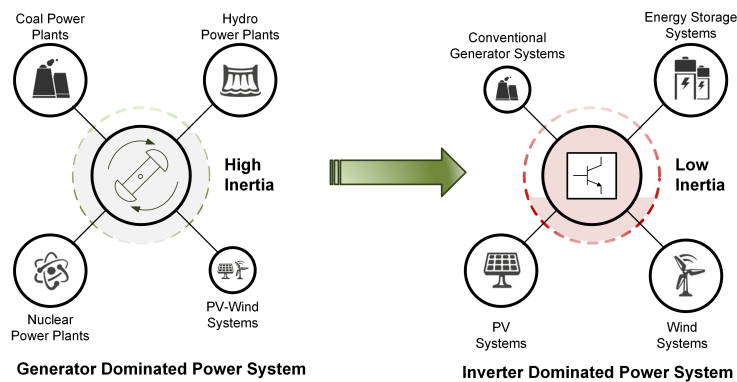


FIGURE 1.1: Power grid evolution [13]

The share of Electric Vehicles (EVs) including Plug-in Hybrid Electric Vehicles (PHEVs) is also increasing all over the world. High shares of EVs is also associated

with the increased penetration of battery chargers in power grid [14].

Almost all RERs, Energy Storage Devices (ESDs), Electric Vehicles (EVs) and so forth are being connected to the grid through solid-state Power Electronic Converters (PECs). Further, most of the modern loads are also being connected through PECs as well [15]. This growing pattern of the inertia-less converters in the conventional grid poses serious problems on grid dynamics and stability [16]. The frequency Nadir and Rate-of-Change-of-Frequency (ROCOF) are going to be higher during fault or load variations due to low rotating inertia in power grid [17]. The frequency Nadir is the minimum value of the frequency reached during transient period following the frequency event.

The renewable energy has intermittent nature with high oscillations and is non-dispatchable too. This nature also affects the stability of the power grid. The stability means the ability of power system to return to steady-state after an incident of disturbance. High penetration of PV panels present technical challenges as well as opportunities to the power system engineers to operate the future power grid [18].

The grid disturbances, like short circuits, voltage sags and dips, and the change in frequency due to frequent switching of heavy loads and generation units interact with the PECs and increase further complexity and uncertainty in operating conditions [19]. Among all, the decreasing inertia of the power system with integrating more PV panels into power grid is a major threat for frequency stability [20].

The current trend in integrating PV panels is the tracking of Maximum Power Point (MPP) i.e. the extraction of maximum power corresponding to an operating point and its injection into the grid. This trend would be appropriate only when PECs have small share of the overall grid capacity. Surely, the small disturbances associated with these resources would be encountered by the inertia possessed by large SGs dominating the grid [13]. But in future, as discussed earlier, RERs will supply a considerable share of the grid capacity. This casual behavior of PECs is not acceptable anymore [21].

1.2 Virtual Inertia Significance

Since the power grid is evolving towards the inverter dominated grid. This evolution is leading towards the reduction in rotating inertia of the power system. As discussed earlier, reduced inertia results in higher ROCOF and lower frequency Nadir. The higher ROCOF and lower frequency Nadir can lead to the cascaded tripping of frequency relays and therefore, can result in blackouts [22]. To resolve this issue, it is required to embed virtual inertia in PECs to increase system stability and RERs integration in future power grid.

Figure 1.2 shows the transient response of power system following a frequency event. It is clear from figure that the frequency Nadir of system without virtual inertia is lower as compared to that with virtual inertia. Also, the ROCOF is higher in system without virtual inertia.

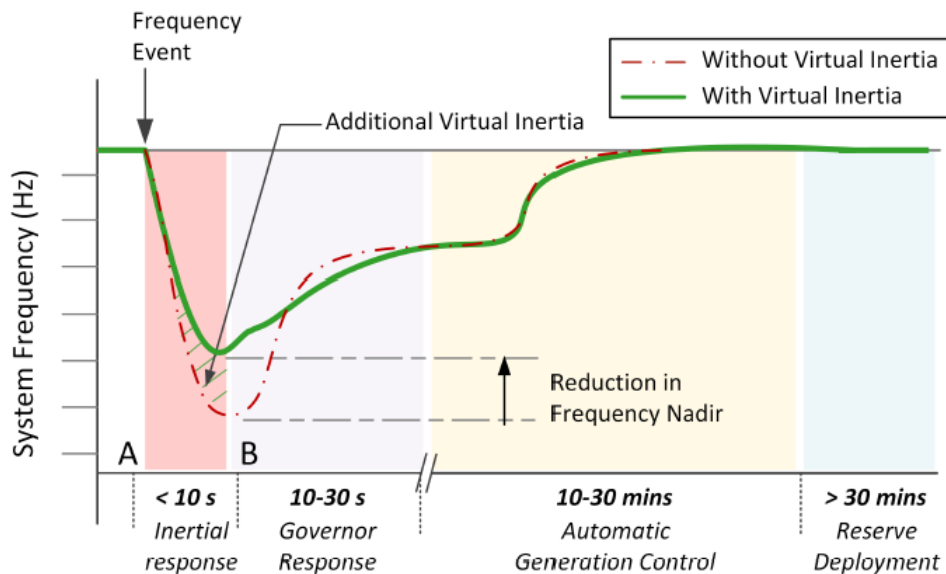


FIGURE 1.2: Virtual inertia significance in power system [13]

To embed virtual inertia in inverter dominated power grid, researchers proposed the idea of emulating Synchronous Machine (SM) essential features in PECs. Such PECs mimic SMs and are broadly termed as Virtual Synchronous Machines (VSMs) [23]. These VSMs support grid during frequency and voltage events.

They are inverters physically, but their behavior is like synchronous machines. With these VSMs, the future power grid can be illustrated as in Figure 1.3.

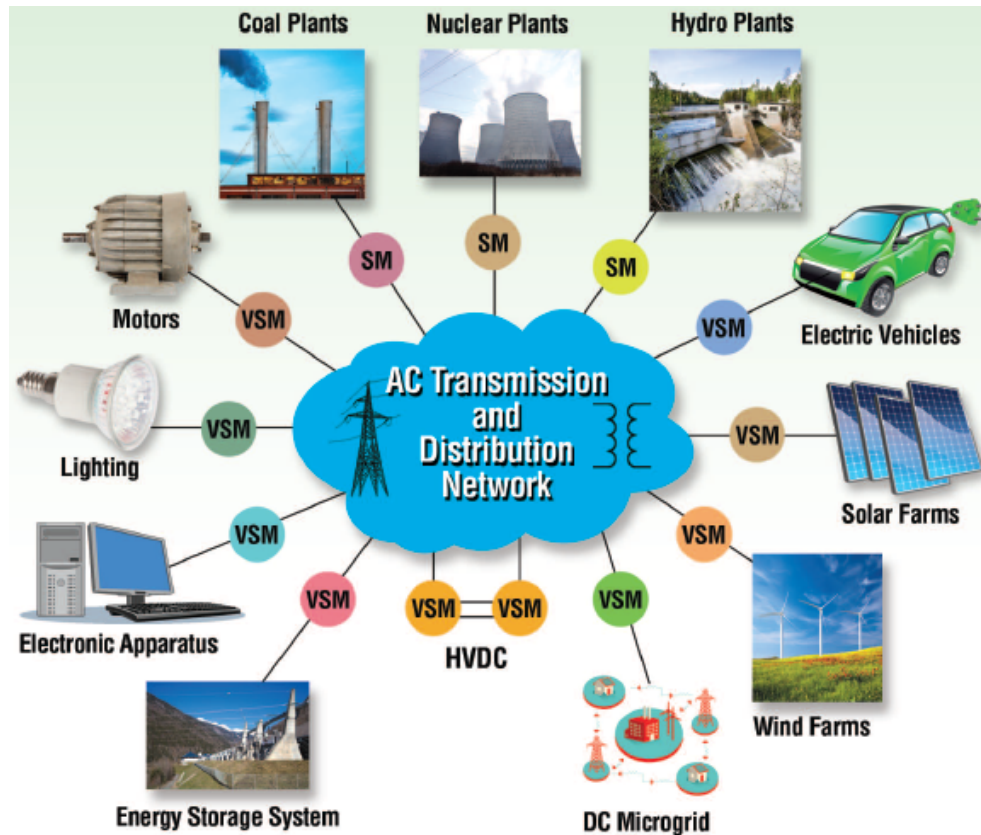


FIGURE 1.3: Future power grid with SMs and VSMs [15]

1.3 Virtual Synchronous Machines

Virtual synchronous machine can either operate as virtual synchronous generator or virtual synchronous motor depending on the direction of energy exchange between the grid and the converter [24]. When PEC is operating as rectifier, it mimics synchronous motor while as inverter, it mimics synchronous generator.

Most of the VSM topologies contain a complete mathematical model of SM [25]. Such topologies include Synchronverter [21], VISMA [26], IEPE's topology [27] and KHI Lab's topology [28].

The mathematical modeling enjoys several advantages over the real SMs such as the parameter values are not constrained by the physical design. Thus, a vast

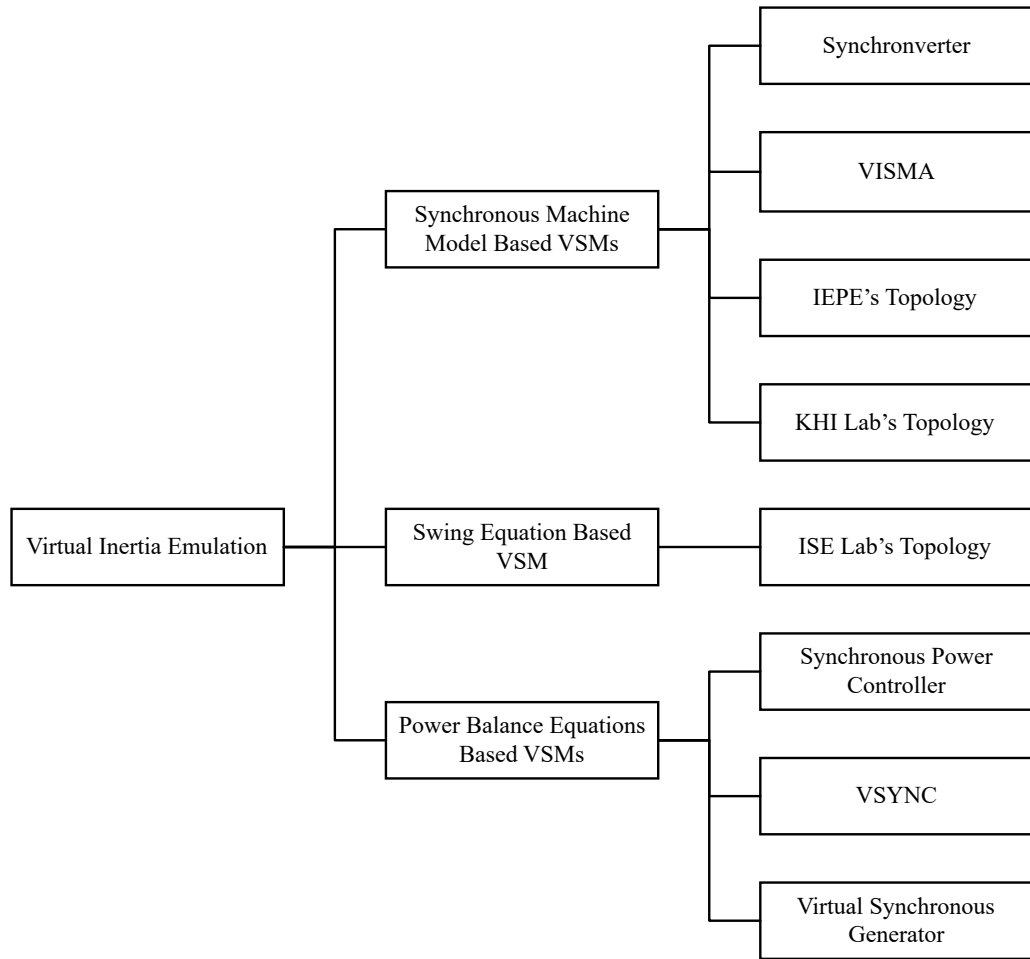


FIGURE 1.4: Classification of Virtual Synchronous Machine Topologies [13]

variety of parameter values can be used that are not even feasible in real machines. These parameters can also be changed during operation unlike real machines [29]. Moreover, the losses associated in these virtual machines impedances are also virtual losses that are directed back to the dc bus and thus, have no effect on system efficiency [21].

Another concept of VSM is the implementation of rotor swing equation associated with real SMs. The detailed mathematical modeling is ignored in this concept. Ise Lab's VSM [7] is the famous topology following this concept.

The other famous topologies including Virtual Synchronous Generator (VSG) [23], Synchronous Power Controller (SPC) [30], and Virtual Synchronous Controller (VSYNC) [31] model the power balance relations of the real SM and emulate inertia. The classification of different VSM topologies is shown in Figure 1.4.

1.4 Synchronverter

Among all the proposed VSMS, synchronverter is the best replication of synchronous generator in terms of simplicity and performance [21]. Like SGs, it has virtual inertia that keeps it synchronized with the grid without any dedicated synchronization unit [32]. It can operate both in stand-alone and grid-connected mode without any change required in the controller circuit. Moreover, it supports system frequency and voltage specially in weak grid [33]. A weak grid is defined as a power grid with a low short-circuit ratio and a low inertia.

Synchronverter can replicate all the essential features of SG required for future power grids [21]. Like SG, careful attention is required in initial synchronization of synchronverter with power grid to prevent high current and power transients at grid-connection. The primary focus of this research is on the initial synchronization of synchronverter having Solar Power Plant (SPP) at the dc bus.

1.5 Motivation

As discussed in Section 1.1, RERs penetration is being increased day by day in power grid all over the world including Pakistan. This trend of installing more and more RERs is leading towards the inverter-dominated power grid. These inertia-less PECs are required to mimic synchronous generator to support frequency and voltage in future power grid.

Synchronverter is one of the Virtual Synchronous Machines that provides both frequency and voltage support to grid. Although the literature [21] claims synchronverter to be the best replication of synchronous generator, however, there is always the room for the improvement. The existing synchronization methods used to synchronize the synchronverter with grid have certain limitations like the absence of seamless transfer capability, unnecessary delays and uncertainties that are discussed in detail in Chapter 2. Therefore, an enhanced auto-synchronizer

is required for synchronverter that overcomes all the limitations of the existing synchronization methods.

The performance of synchronverter is also not fully investigated yet. Existing literature, discussed in Chapter 2, focused on the performance of synchronverter having an ideal source at the dc bus. However, in real scenario, synchronverter is required to integrate RERs into power grid. These RERs have intermittent nature that can affect the synchronverter performance. Therefore, it is required to investigate the performance of synchronverter having a RER connected at dc bus. Moreover, the effect of variations in local connected load on synchronverter also needs to be investigated to study the stand-alone performance of synchronverter.

1.6 Research Objectives

To accommodate increasing number of RERs-based Distributed Generation (DG) in future power grid, VSMs are required instead of inertia-less PECs. This research is carried out to investigate and improve the performance of synchronverter employed for the integration of SPP into power grid.

The key objectives of this research are highlighted in following points.

1. To design an enhanced, PLL-less auto-synchronizer for initial synchronization of synchronverter with grid that ensures power supply to local load during synchronization process.
2. To investigate the effect of variations in local connected load on performance of synchronverter in stand-alone mode of operation.
3. To investigate the dynamic performance of synchronverter having Solar Power Plant connected at dc bus during variations in operating conditions, during grid fluctuations and during transfer between grid-connected and stand-alone modes of operation.

1.7 Research Contributions

Based on the objectives highlighted in Section 1.6, the major contributions of this research are following:

- An enhanced auto-synchronizer is proposed and designed that guaranteed fast and promising synchronization of synchronverter with grid irrespective of the adverse grid conditions. The proposed auto-synchronizer has less computational burden on controller and it ensures power supply to local connected load during synchronization process. Finally, a seamless transfer of synchronverter between grid-connected and stand-alone mode is achieved.
- Detailed investigation of synchronverter performance with variations in local connected load during stand-alone mode of operation is presented.
- A complete performance overview of synchronverter with intermittent nature of SPP is presented in both stand-alone and grid-connected mode. Performance under steady state as well as during transients is included in this study. This overview presents synchronverter as a strong contender for SPP integration into future power grid.

1.8 Thesis Organization

The rest of the report is organized as follows: Chapter 2 presents literature review of various VSM topologies, their significances, pros and cons. Synchronverter is compared with other VSMs and detailed review about synchronverter is given. Gap analysis is presented and problem statement is formulated. Methodology and techniques used in research are explained. Applications of the proposed work are elaborated at the end of Chapter 2.

In Chapter 3, mathematical modeling, complete design of synchronverter control parameters, and grid-side LCL filter is given, assuming an ideal source at the dc bus. Overall performance of synchronverter is evaluated in both stand-alone and

grid-connected modes. Effect of variations in local connected load during stand-alone operation, and the effect of variation in grid conditions during grid-connected mode are focused in this performance evaluation. Simulation results are provided in each case.

In Chapter 4, mathematical modeling, design, significance and working of proposed auto-synchronizer is elaborated in details. Proposed auto-synchronizer is compared with the existing technique to show the improvement in synchronization process. Simulation results are provided to verify the enhanced reliability and certainty of proposed auto-synchronizer.

In Chapter 5, the designed model of synchronverter and proposed auto-synchronizer is extended and applied to the integration of SPP into power grid. Effect of intermittent nature of PV panels on synchronverter performance is evaluated. Validity of the proposed auto-synchronizer in extended system is tested and the seamless transfer of synchronverter between operating modes is studied.

Conclusions are drawn in Chapter 6. Moreover, the future directions are also discussed to encourage future research in this domain.

Chapter 2

Literature Review

During the last decade, researchers have presented several topologies of Virtual Synchronous Machines (VSMs). All these topologies have different practical implementations with different offerings. All have some pros and cons and thus, are suitable for different applications.

This chapter presents the theoretical background of VSM topologies including their control schemes, advantages, and limitations. Literature review of these topologies and the comparison of synchronverter with other VSMs is also presented in this chapter. Based on the literature review, gap analysis is presented in the research direction and problem statement is formulated based on this gap analysis. Finally, the methodology adopted in this research along with the possible applications of this research in power grid is discussed at the end of this chapter.

2.1 Review of VSMs Excluding Synchronverter

This section presents the review of all Virtual Synchronous Machines (VSMs); excluding synchronverter, discusses their control schemes, advantages and limitations. Literature related to all VSMs, other than synchronverter, depicted in Figure 1.4 is summarized here.

2.1.1 VISMA

Beck in [26] presented virtual synchronous machine under the title of "VISMA" for the first time in 2007. The general control scheme of VISMA is illustrated in Figure 2.1. This topology employed the $d - q$ based mathematical model of the Synchronous Generator (SG). Grid voltages are measured and sent to the VISMA controller as reference. Currents are then calculated based on these reference voltages. These currents are then fed into the grid through the hysteresis current-controlled inverter [34].

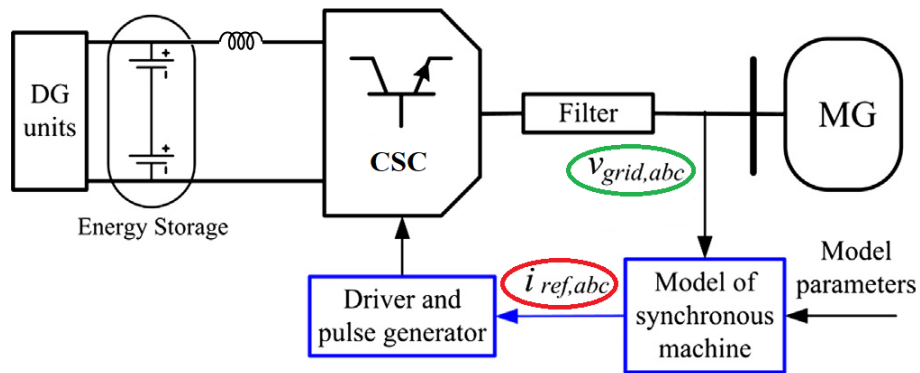


FIGURE 2.1: General control scheme of VISMA having grid voltages as input [34]

References [26, 35–37] used a 7th order model of the synchronous machine including a 5th order electrical and a 2nd order mechanical model in VISMA. This model is discussed in detail in [38]. Although this model emulates all the desired features of the synchronous machine. However, on the other side, it increases the complexity of the controller. To improve the robustness, a three-phase model of synchronous generator based on $d - q$ reference frame is also reported in literature [39].

In [40, 41], 5th order and 4th order models of synchronous machine are implemented in which only stator winding is considered. Low-order models have better dynamic performance under load fluctuations. Also, they have lesser tendency of numerical instability in practical implementation under unbalanced AC voltages and balanced short circuit currents as compared to high-order models [42].

2.1.2 IEPE's Topology

This topology is proposed by Institute of Electrical Power Engineering (IEPE), Russia. IEPE's Topology has the same modeling of synchronous generator as that of VISMA. However, it is a voltage-source inverter [27]. The general control scheme, similar to Figure 2.1, is shown in Figure 2.2.

In IEPE's Topology, the grid currents are measured and sent to the controller as reference. Inverter voltages are then calculated based on these reference currents [27].

This topology is better for stand-alone mode of operation. However, in grid-connected mode, it results in severe transients especially during the synchronization process [13]. Therefore, this topology is not suitable for the integration of SPP into future power grid.

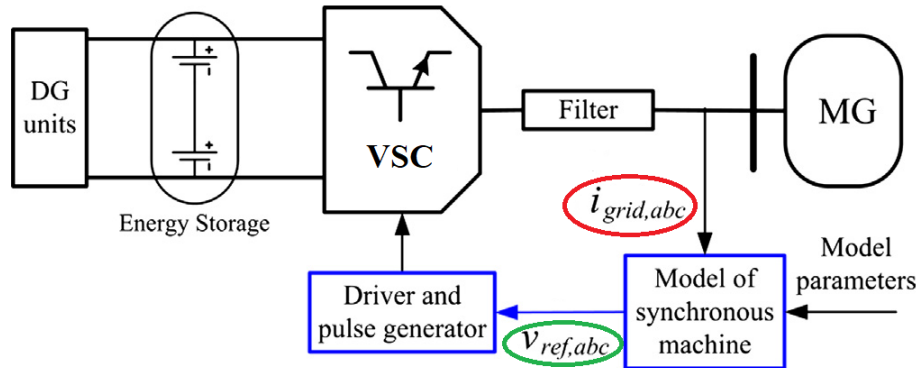


FIGURE 2.2: General control scheme of IEPE Lab's Topology having grid currents as input [34]

2.1.3 KHI Lab's Topology

This topology is proposed by Kawasaki Heavy Industries (KHI) in [28]. KHI Lab's Topology employs the algebraic model of governor and Automatic Voltage Regulator (AVR) to generate the phase angle and voltage references, respectively. These references are then used to generate the current reference based on the phasor representation of SG [43, 44] as shown in Figure 2.3.

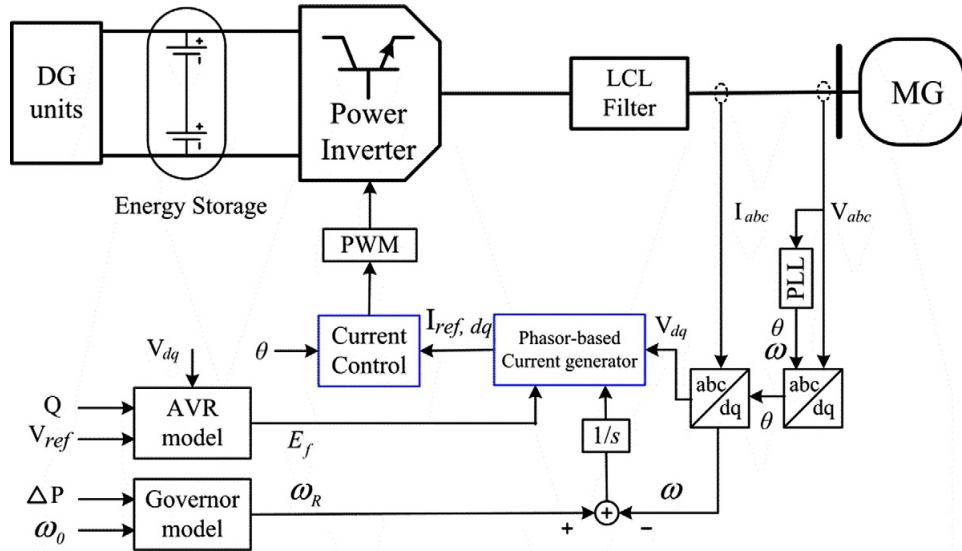


FIGURE 2.3: Control scheme of KHI Lab's Topology [34]

2.1.4 Ise Lab's Topology

This topology is proposed by ISE Laboratory in Osaka University in Japan in [7, 45, 46]. It utilizes only the swing equation of synchronous generator in each control cycle to emulate rotor inertia. Since this topology doesn't include detailed model of synchronous generator, it is simplified version of VSM. Figure 2.4 shows the control scheme of this topology. The swing equation of synchronous generator rotor can be written as:

$$T_m - T_e = J\omega \frac{d^2\phi}{dt^2} \quad (2.1)$$

where, P_m, P_e, J, ω , and ϕ are prime mover input power, SG output power, rotor inertia, rotor angular frequency, and rotor angle of SG respectively. This equation is solved in each control cycle to compute ϕ for generating PWM pulses [16].

The frequency measurement shown in Figure 2.4 is based on Phase-Locked Loop (PLL) [46]. This PLL block is required continuously throughout the operation of this topology. When the set-points for the grid angular frequency and the active power reference is kept constant, the Ise Lab's Topology become equivalent to the traditional droop controller [47].

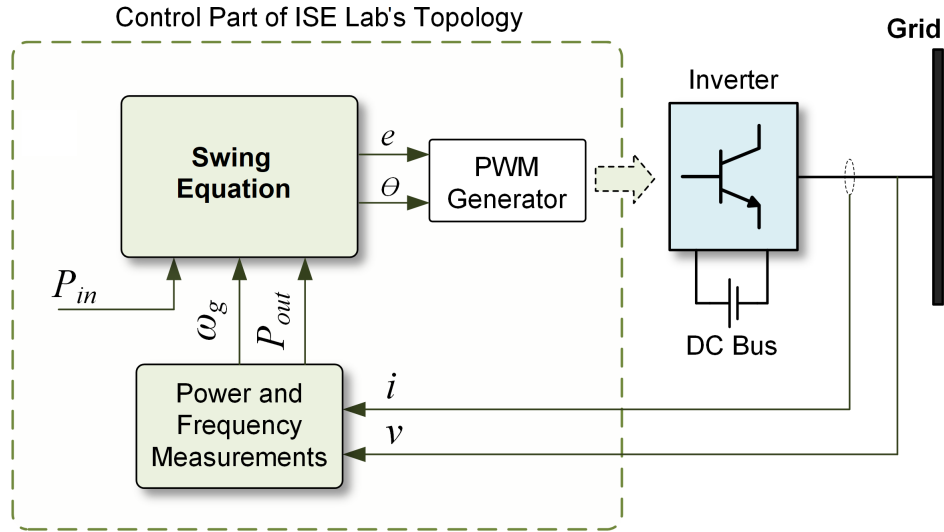


FIGURE 2.4: Control scheme of Ise Lab's Topology [13]

Reference [7] studied the dynamic response of this VSM in both grid-connected and stand-alone modes of operation. Moreover, the operation of same converter in parallel with an SG and with another current-controlled inverter is also studied in [7].

References [48–50] modified Ise Lab's topology by introducing the concept of alternating value of inertia J and other VSM parameters. In [48, 49], the value of virtual inertia J varies based on the rotor acceleration and deceleration during transients. However, in [50], self-tuning algorithm based on optimization problem is proposed.

The optimization problem consists of a cost function which is to be minimized in each cycle to adapt VSM parameters. With these adaptive values of VSM parameters, the transient response of original topology is improved. However, the computation of alternating values puts an extra burden on the controller of the power electronic converter.

Reference [51] modified Ise Lab's Topology to control of HVDC station. In this modification, a inner vector control loop is added for the protection against over-currents. Performance of the modified version is compared with traditional inertia-less technique. Comparison shows that the addition of swing equation to the traditional control provides frequency support to the weak grid.

2.1.5 Synchronous Power Controller

The general structure of Synchronous Power Controller (SPC) proposed by [30, 52] implements a nested loop control with an outer voltage loop and an inner current loop through a virtual admittance [23, 53–55], as shown in Figure 2.5. This nested loop control enabled inherent over-current protection in SPC against transients. This feature was lacking in Ise Lab’s Topology. However, tuning of nested loop is more complex and puts extra burden on PEC controller [13].

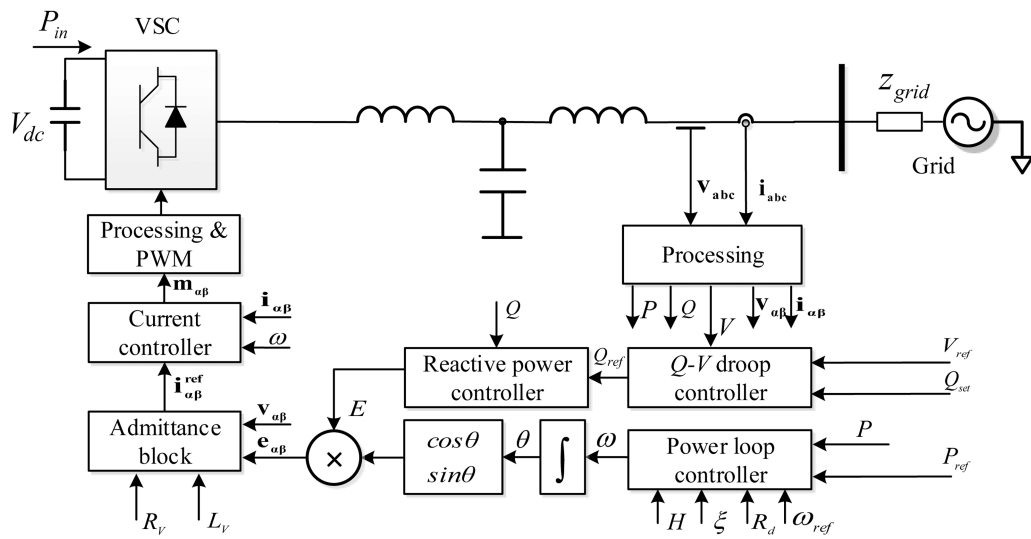


FIGURE 2.5: Structure of Synchronous Power Controller [53]

The SPC of [23] is implemented for a grid-connected Voltage Source Converter (VSC) in [56], for a single-phase bi-directional battery charger in [57], and for a stand-alone VSC in [58]. This particular SPC can either operate in stand-alone mode or with a strong grid. Parameters tuning and stability analysis of SPC is also discussed in detail in both grid-connected and stand-alone modes in [56] and [58–60], respectively. References [25, 60] compared SPC with inertia-less technique and proved that SPC is a better choice for future power grid.

Previously, inverters with other control methods are required to disconnect from the grid during faults which in turn results in loss of distributed generation. In future grid, these distributed generations must offer fault-ride-through capability for a certain time after fault occurs [61]. Reference [62] proposed low-voltage ride

through capability in SPC based on the excitation state of VSG. In this approach, an additional current loop is also designed to suppress the unbalanced currents during asymmetrical faults.

2.1.6 Virtual Synchronous Controller

This topology is proposed by VSYNC research group in [31, 63–65]. In this topology, PLL is used to generate current reference to emulate inertia. In addition to this, PLL also provides phase angle reference for the dq transformation as shown in Figure 2.6.

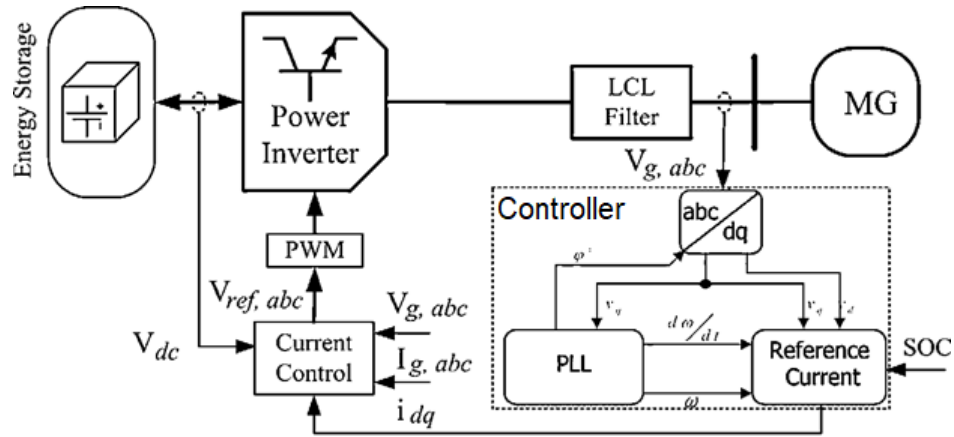


FIGURE 2.6: Structure of Virtual Synchronous Controller [63]

In another VSYNC approach proposed in reference [66], frequency is estimated using zero crossing method and reference current is computed using the following equation:

$$I_r = \frac{J\dot{\omega} + D\omega}{V_{DC}} \quad (2.2)$$

Where, J is inertia, D is damping coefficient, ω is the angular speed and $\dot{\omega}$ is the acceleration of the virtual rotor of the virtual synchronous machine. The variable I_r is the reference current to be computed for the generation of trigger pulses of the power electronic converter. References [67, 68] presented effect of VSYNC parameters on inertial dynamics of Doubly-Fed Induction Generator (DFIG)-based wind turbines.

2.1.7 Virtual Synchronous Generator

In Virtual Synchronous Generator (VSG), a PLL is deployed to estimate RO-COF. Based on this estimation, a power reference is generated using the following equation [34]:

$$P_{VSG} = J \frac{\Delta\omega}{dt} + D\Delta\omega \quad (2.3)$$

Where, $J, D, \Delta\omega$ and $\frac{\Delta\omega}{dt}$ are inertia, damping coefficient, change in frequency, and ROCOF, respectively. Based on this power reference, a current reference is generated for the PWM. A general control scheme of VSG is illustrated in Figure 2.7.

A VSG-based Energy Storage System (ESS) and RERs have been integrated in Guangdong Grid and Hebei North Power Grid, China, respectively, in December 2016 [69]. Hebei North Power Grid consists of 24 photovoltaic VSGs and 5 wind power VSGs. The overall system is the largest VSG-based system in the world with a total capacity of 22 GW [70].

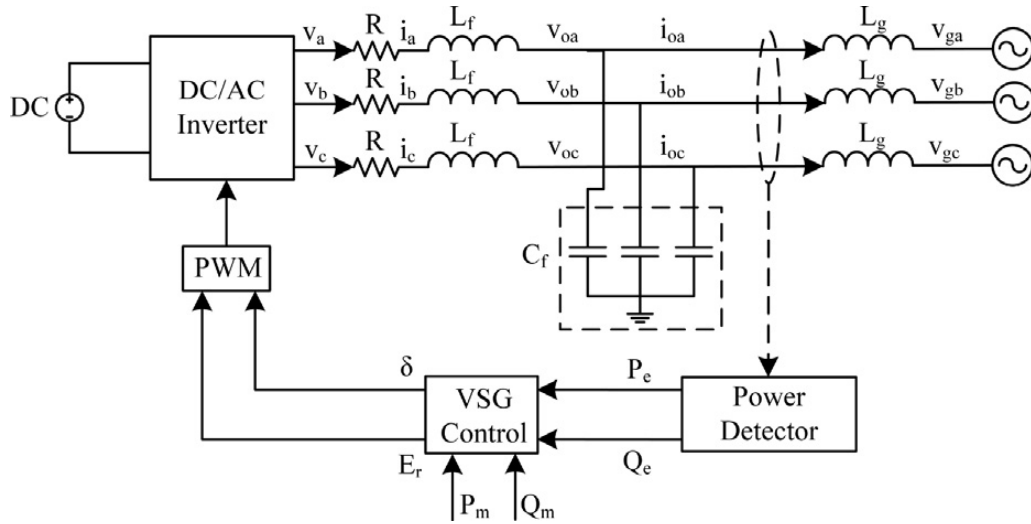


FIGURE 2.7: General control scheme of Virtual Synchronous Generator [71]

An enhanced VSG control for parallel operating inverters in a microgrid is proposed in [72]. The authors enhanced traditional VSG control by adding an adjustable virtual stator reactance based on state-space analysis and voltage estimator in control loop. By this modification, the transient response and active power

damping of VSG is improved.

Parameters design and stability analysis of VSG is performed in [73, 74] for both stand-alone and grid-connected modes of operation. Stability analysis of VSG performing in parallel with other inverters is also presented in [74].

Although the VSGs with constant parameters are proposed, designed, implemented, and tested in various applications, the VSGs with self-tuning and adaptive parameters are also reported in literature [29]. Reference [29] proposed an adaptive algorithm based on rotor acceleration and deceleration during transients. Comparison shows that VSG with adaptive parameters is better than VSG with constant parameters in terms of performance and stability. However, adaptive algorithm puts an extra burden on the VSG controller.

A single-phase bi-directional VSG is used in [75] to integrate a DC microgrid into AC grid. The MPPT-controlled RERs are connected to the DC microgrid along with the parallel connected ESS. The microgrid is then integrated to the grid through single-phase bi-directional VSG to the AC grid. This concept is suitable for short-term and long-term frequency regulation, and power management in both AC and DC sides and thus, it enhances the power system stability.

Reference [76] compared VSG with inertia-less droop controller for a VSC and proved that VSG is better for future grids as it provides frequency regulation to power grid. The VSG has higher damping and lower overshoot than the droop controller. The advantages of droop controller are inherited by the VSG, and additionally, VSG emulates inertia for frequency support.

2.1.8 Analysis of VSMs Excluding Synchronverter

Literature review of VSMs other than synchronverter presented in previous section is summarized in Table 2.1. A lot of work has been done in various aspects of VSMs; from fixed parameters tuning to self-adjusted parameters, from single VSM unit to multiple parallel VSMs, designing of three-phase and single-phase VSMs, and analysis in stand-alone and grid-connected mode.

TABLE 2.1: Literature Review Summary of VSMs Excluding Synchronverter

Contribution	VISMA / IEPE Lab/ KHI Lab	ISE Lab	SPC/ VSYNC/ VSG
Parameters design and stability analysis of VSM in stand-alone and/or grid-connected mode	[27, 40, 44]	[16]	[56, 58–60, 68, 73, 74, 76, 78]
Analysis of VSM operating in parallel with other inverters/S-Gs/VSMs		[7]	[29, 59, 60, 72, 74, 79, 80]
Adaptive parameters for VSM instead of fixed parameters		[48–50]	[29]
VSM with non-ideal source at DC bus	[81]	[49, 50, 82]	[29, 67, 68, 75]
Single-phase VSM			[57, 75]
VSM initial synchronization with grid			[75, 78, 83, 84]
Comparison of VSM with inertia-less techniques	[81]	[7, 49, 51]	[60, 76, 85]
Fault-ride-through capability			[62]
Improved power decoupling in VSM			[79]

Despite of rapid development and applications of these VSMs, they have various limitations that are summarized below [77]:

- VSMs with Current Source Converter (CSC), like VISMA, have certain limitations when used for the integration of SPPs into power grid. One of the problem is the transition of the CSC from grid-connected mode to the stand-alone mode. As, the CSC is not regulating the voltage in grid-connected mode, its controller must be changed entirely when the grid is disconnected. Also, a CSC can continuously inject currents in the grid during faults which

results in extensive high voltage [13]. Therefore, such VSMs are not suitable for integration of SPPs in future power grid.

- All VSMs, specially swing equation based topologies, i.e. Ise Lab's topology, don't represent the same dynamics like SG from grid Point-of-View (POV). Although they emulate inertia, but they lack other features inherited by SG like voltage support, and self-synchronization etc. Therefore, they are not the accurate replication of SG in future power grid.
- All VSMs, except Ise Lab's Topology, reviewed in section 2.1, depend on PLL for the grid-connected operation. They have inaccuracies and stability concerns, specially in weak grid. Due to the dependency on PLL, they have high steady-state errors, frequency variations, voltage sags and harmonic distortions when connected to a weak grid [13].
- VSG utilizes frequency derivative i.e., ROCOF for the generation of reference current as discussed earlier. It is highly prone to noise due to this frequency derivative [13, 34].
- All VSMs discussed in section 2.1 use Park's Transformation for the control signal generation. VISMA used dq based machine model for the control. Park's Transformation increases the overall complexity as well as Total Execution Time (TET) of the controller.
- None of the VSM reported in previous section offers seamless transfer between stand-alone and grid-connected modes of operation. These VSM require certain changes in the controller to operate in other mode after transition from one mode of operation.

A better and accurate replication of SG is required to overcome the above-mentioned limitations. Synchronverter, proposed in [21], is a promising solution of RERs integration in future power grid. Following section presents synchronverter concept briefly and highlights its distinguished features from other VSMs to justify this statement.

2.2 Review of Synchronverter

Synchronverter is the best replication of synchronous generator as it represents the same dynamics from grid point-of-view [21]. This topology is well developed and verified with various applications in literature [86]. Review of literature related to synchronverter is presented in upcoming sections.

2.2.1 Theoretical Concept of Synchronverter

Synchronverter is based on second-order mathematical model of synchronous generator derived using the magnetic flux linkages between stator and rotor winding. Following equations are utilized in synchronverter to emulate SG essential features [21]:

$$T_e = M_e i_e \langle i_s, \widetilde{\sin\theta} \rangle \quad (2.4)$$

$$e = \dot{\theta} M_e i_e \widetilde{\sin\theta} \quad (2.5)$$

$$Q = -\dot{\theta} M_e i_e \langle i_s, \widetilde{\cos\theta} \rangle \quad (2.6)$$

Where, T_e , e , and Q are electromagnetic torque, induced emf and reactive power of SG, respectively, M_e is the maximum value of mutual inductance between rotor and stator winding, i_s is the stator winding current, i_e is the field excitation current and θ is the load angle.

Figure 2.8 shows the schematic diagram of synchronverter. Model of synchronous generator shown in Figure 2.8 consists of Equations (2.4 – 2.6) where J and D_f are inertia and damping coefficient of the virtual rotor of the synchronverter, respectively.

The inertia J of synchronverter supports the grid during disturbances while the damping coefficient D_f maintains the steady-state stability [60]. Complete mathematical modeling and parameter designing of synchronverter is discussed in Chapter 3.

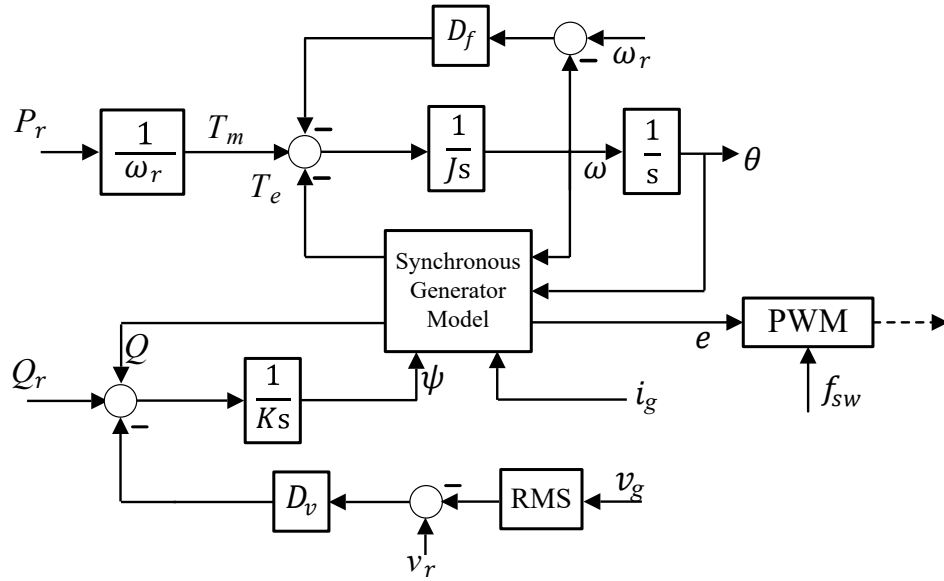


FIGURE 2.8: Schematic of Synchronverter [21]

2.2.2 Synchronverter Versus Other VSMS

Among all the proposed VSMSs, synchronverter is the best replication of synchronous generator because of its simplicity and inertial dynamics [21]. The salient features of synchronverter, that make it better than other VSMSs, are following:

- Unlike other VSMSs, synchronverter represents same dynamics as synchronous generator from grid point-of-view [15].
- Synchronverter doesn't rely on Phase-Locked Loop (PLL) like other VSMSs in grid-connected mode. It has inherent capability to remain synchronized with grid without any dedicated synchronization unit [21].
- Synchronverter doesn't utilize Park's Transformation for the control signal generation. Therefore, the overall complexity and TET of synchronverter is lower than other VSMSs [77].
- Synchronverter has a lower settling time that means there is a lower energy exchange with the DC side as compared to the other VSMSs [13].
- Further, the built-in frequency and voltage control loops of synchronverter improve the grid angle's stability [33].

TABLE 2.2: Literature review summary of original synchronverter

Contributions	References	Details
Parameter Design	[21, 90]	Parameters designing and analysis in grid-connected mode
Stability analysis	[91–93]	Robust stability analysis of synchronverter is performed under different grid conditions
Design of parallel inverters	[94]	Presented coherency-based equivalence method for parallel multilevel inverters for future design and simulations
Synchronverter concept on qZS inverter	[95]	Implemented synchronverter using qZS inverter in an islanded micro-grid

- Synchronverter can operate both in stand-alone and grid-connected mode without any change in the controller circuit [87].
- Synchronverter can support both frequency and voltage specially in a weak grid [88, 89].

In short, synchronverter can replicate all the essential features of SG in both stand-alone and grid-connected mode. Moreover, being independent on PLL, synchronverter is a promising solution to integrate remote area SPPs connected to the weak grid.

2.2.3 Studies and Analysis of Original Synchronverter

Researchers studied and analyzed various aspects of synchronverter during the last decade. Few of the contributions are summarized in Table 2.2. Parameter designing of synchronverter is discussed for both three-phase three-wire and three-phase four-wire PECs in [21] and [90], respectively. Three-phase four-wire converter has the independent neutral line.

Stability analysis of synchronverter, operating in parallel, is performed in [92] using bifurcation theory. Robust stability analysis of synchronverter with LCL filter is performed in [91, 93]. Reference [91] performed stability analysis of a single grid-connected synchronverter under different grid conditions while [93] performed the same for parallel operating synchronverters.

A coherency-based equivalence method is used in [94] to classify the parallel operating synchronverters into coherent groups. Reference [95] implemented synchronverter on qZS inverter in an islanded microgrid.

2.2.4 Modifications in Original Synchronverter

Several modifications have been reported in literature to improve certain aspects of original synchronverter. Table 2.3 summarizes these modifications. Synchronverter with bounded Frequency and voltage is proposed in [32] to keep output frequency and voltage of converter within the specified ranges.

Active voltage feedback control is proposed in [33] that enabled synchronverter to provide primary and secondary frequency regulation without the need of high speed communication system. Self-synchronized synchronverter is proposed in [88] to enable initial synchronization of synchronverter with grid independent of Phase-Locked Loop (PLL).

Reference [96] added feature of DC bus voltage regulation in original synchronverter. It also added fault ride-through capability during unsymmetrical grid faults. A fault ride-through capability is also proposed in [97] in which synchronverter switches to hysteresis control mode to limit the inrush current during faults while injecting appropriate amount of real and reactive power into the grid.

Five modifications are proposed in original synchronverter to improve its stability and dynamic performance in [99]. These modifications included field current control, addition of virtual losses in power formulas, and addition of virtual inductor and virtual capacitor in original synchronverter.

TABLE 2.3: Modifications in original synchronverter

Modifications	Year	References	Details
Bounded Frequency and Voltage	2018	[32]	Kept frequency and voltage of synchronverter within the limits
Active voltage feedback control	2016	[33]	Realized secondary frequency regulation, and fault current limitations in synchronverter
Self-synchronization	2014	[88]	Proposed PLL-less self-synchronization of synchronverter
DC-Bus voltage regulation	2014	[96]	Proposed bidirectional synchronverter with regulation of DC bus voltage. It also embedded fault-ride-through capability in synchronverter.
Mode switching concept	2017	[97]	Proposed mode switching concept during transients for protection against inrush fault currents in synchronverters
Current-controlled Synchronverter	2019	[98]	Proposed current-controlled synchronverter for frequency and voltage regulation in weak grid
Five modifications in original synchronverter	2017	[99]	Proposed virtual inductor, virtual capacitor and field current controller to improve stability and dynamic performance of synchronverter
Decoupling responses	2022	[100]	Decoupled inertial response from primary frequency regulation
Harmonic virtual impedance	2019	[101]	Designed harmonic virtual impedance for current-controlled synchronverter to improve power quality
Single-phase synchronverter	2018	[102]	Designed single phase synchronverter with self-synchronization capability

The inertia and damping coefficient of synchronverter are coupled and adjusting transient response speed can effect steady-state response. References [100, 103] adjusted the transient response speed of synchronverter without affecting steady-state performance by using damping correction loop. Parameters designing and tuning of synchronverter with damping correction loop is discussed in [104, 105].

Current-controlled synchronverter is proposed in [98] for voltage and frequency regulation in weak grid. A harmonic virtual impedance for the same current-controlled synchronverter is designed in [101] to achieve a trade-off in power quality between voltage and current. Single-phase counterpart of synchronverter is presented in [102] for residential roof-top DGs.

2.2.5 Synchronverter Synchronization with Grid

Synchronverter has inherent capability to remain synchronized with grid without any dedicated synchronization unit. Moreover, synchronverter offers seamless transfer from grid-connected to stand-alone mode without any change required in the controller. However, it requires a synchronization unit to track grid phase angle for initial synchronization with grid prior to grid-connection [87].

Figure 2.9 shows the synchronverter operational modes and the transition between them. It is illustrated in Figure 2.9 that a dedicated synchronization unit is only required for initial synchronization with grid. This section presents the review of different synchronization schemes proposed in literature for this initial synchronization of synchronverter with grid. All these synchronization schemes are tabulated in Table 2.4.

2.2.5.1 Phase-Locked Loop Based Synchronization

Phase-locked loop (PLL) was utilized for the initial synchronization of the original synchronverter for the first time in [21]. Later on, references [24, 90, 106] followed the same technique.

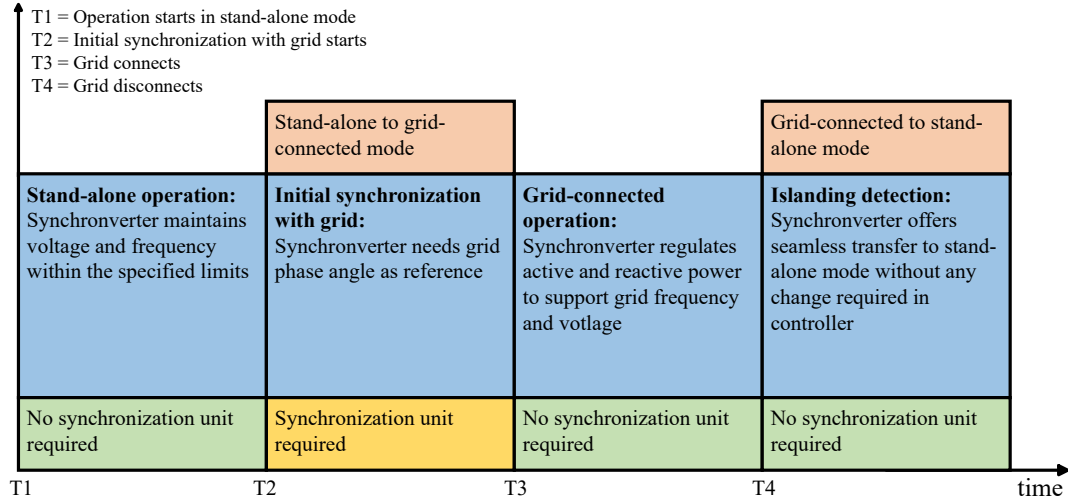


FIGURE 2.9: Synchronverter modes of operation

A basic PLL adopts a control loop containing phase detector, voltage controlled oscillator, and a low pass filter to estimate the phase angle of its input signal [107], as shown in Figure 2.10. It can also provide frequency information of the input signal. However, it can not provide any information about the signal magnitude.

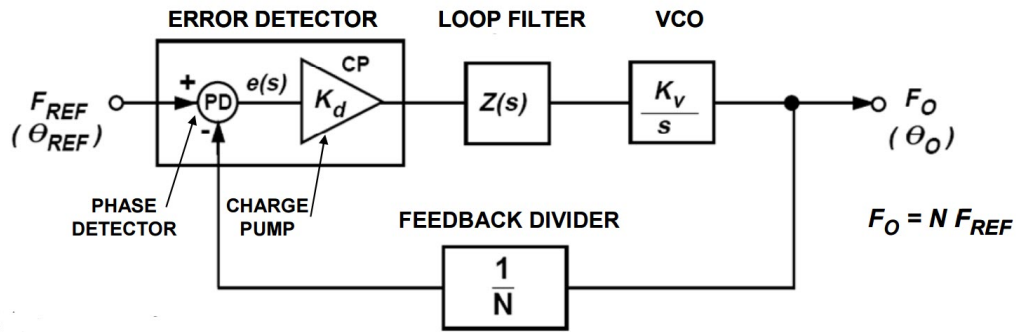


FIGURE 2.10: Basic Phase-Locked Loop [107]

Although an Enhanced PLL (EPLL) is addressed in [108] that can provide information about the voltage magnitude too. However, no evidence of its application on synchronverter is found in literature. PLL has certain disadvantages and limitations when deployed in large numbers in power grid, as discussed below:

- PLL degrades the performance of PEC due to the presence of steady-state errors, harmonic distortions, frequency variations and voltage sags, specially when PEC is connected to a weak grid [77, 109].

- It is quite difficult to tune the PLL parameters to achieve satisfactory performance [110].
- Multiple parallel operating PLLs often compete with each other and can result in loss of synchronism, increased complexity and even instability [111].
- The Voltage Controlled Oscillator (VCO) is the main issue of PLL. It is noise sensitive, prone to switching transients, voltage and frequency variations. Thereby, affecting the stability and performance of PLL [112].

Due to the above-mentioned points, PLL-less synchronization approaches are being addressed in literature. The upcoming sections present the review of these PLL-less synchronization schemes.

2.2.5.2 Virtual Impedance Based Synchronization

First PLL-less self-synchronization approach for initial synchronization of synchronverter is proposed in [88]. Same self-synchronization approach is implemented for unbalanced power grid in [109], for wind farm integration in [113] for single phase synchronverter in [114], for parallel-connected synchronverters in [101], and for droop controllers in [115].

This self-synchronization approach is based on virtual impedance introduced in original synchronverter, as shown in Figure 2.11. During synchronization process, a virtual current is fed into the synchronverter controller instead of actual grid current. This virtual current can be represented as:

$$i_{virtual} = \left(\frac{1}{Ls + R}\right)(e - v_g) \quad (2.7)$$

Where e is the induced electromotive force, represented in Equation 2.5, v_g is the grid voltage, and L and R are the virtual inductor and virtual resistor, respectively. At the same time, the active and reactive power set points are kept 0 during synchronization process. Synchronization is achieved by driving the virtual current

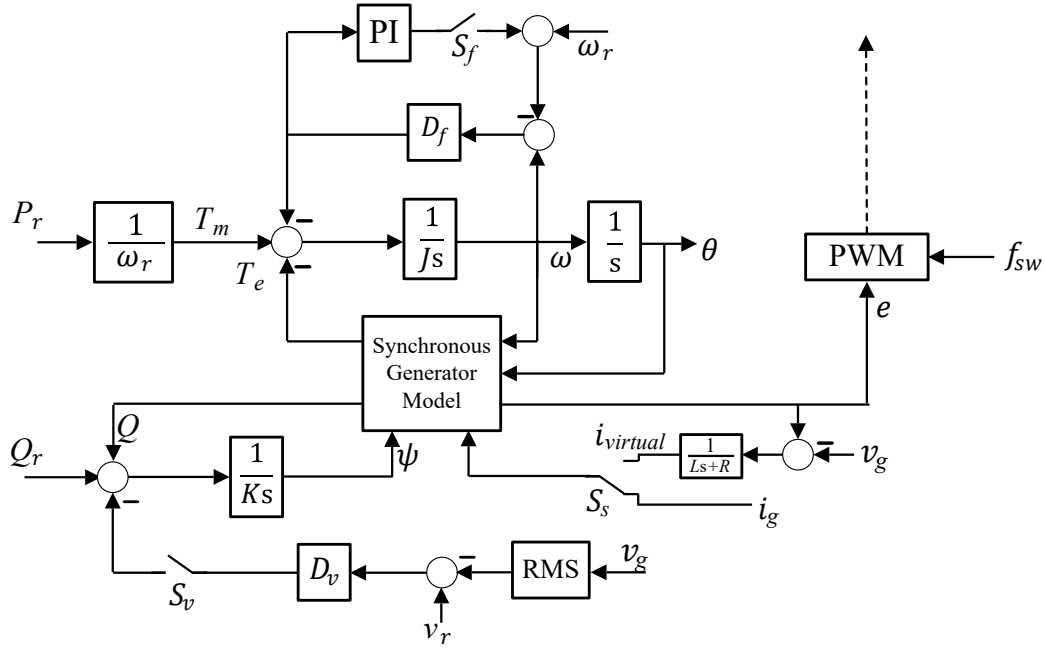


FIGURE 2.11: Virtual impedance based self-synchronized synchronverter [88]

to zero. A PI controller is also used in this approach to regulate the output of damping coefficient block D and to generate the frequency reference.

Although the virtual impedance based self-synchronization is the most common PLL-less synchronization scheme among the researchers, however, it has limitations that are discussed in the following points:

- In this approach, the synchronverter is fed with virtual current instead of actual grid current during synchronization process, and the reference active and reactive powers are kept 0. Due to this, no power can be drawn from synchronverter during synchronization process. It means, the local load must be disconnected from the output during the transition phase from stand-alone to grid-connected mode. This type of synchronization approach is not suitable when a critical local load is connected at synchronverter output. Critical load means a hospital, data center, military unit or an intelligence center that requires uninterrupted power supply all the time.
- Virtual impedance based self-synchronization involves precise tuning of two parameters; virtual inductance and resistance. Smaller values of L and R results in higher $i_{virtual}$ to achieve faster synchronization. However, too

small values may result in frequency oscillations [88]. Virtual inductance L presents unstable eigenvalues that can lead to uncertainties and even unsuccessful synchronization [116].

These two limitations should be properly addressed in self-synchronized synchronverter.

2.2.5.3 Virtual Resistance Based Synchronization

Instead of virtual impedance, this approach deployed a virtual resistance for initial synchronization of synchronverter [117]. In this way, the unstable eigenvalues caused by virtual inductance of [88] are removed.

The schematic diagram of virtual resistance based self-synchronization approach is illustrated in Figure 2.12.

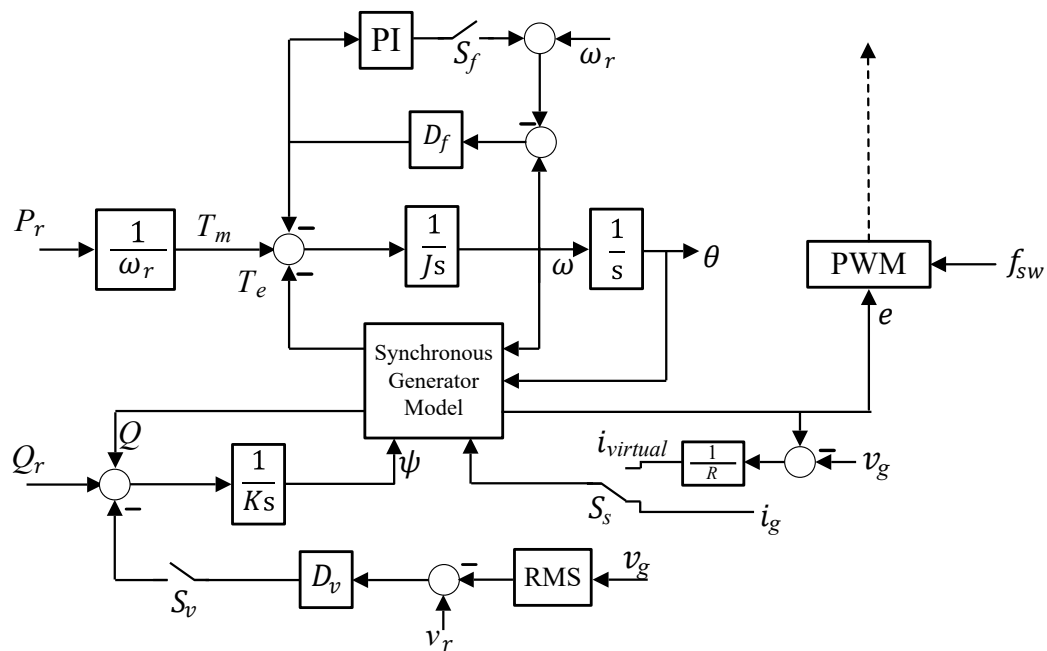


FIGURE 2.12: Virtual resistance based self-synchronized synchronverter [117]

This approach resulted in minimum virtual current peak as compared to that of virtual impedance. However, there are certain limitations associated with this scheme discussed in following points.

- A coordinate transformation with rotational matrices is required when using virtual resistance based self-synchronization [86]. This transformation increases the computational burden on controller.
- In this approach, the synchronverter is fed with virtual current instead of actual grid current during synchronization process, and the reference active and reactive powers are kept 0, similar to that of virtual impedance based self-synchronization. Due to this, no power can be drawn from synchronverter during synchronization process. Therefore, the shortcoming of seamless transfer capability persists in this approach.

2.2.5.4 Differential RMS Voltage Based Synchronization

Realizing the importance of uninterrupted power supply requirement for the critical load, this approach addressed the seamless transfer capability of synchronverter during synchronization process [102].

In this approach, Root Mean Square (RMS) value of the difference between synchronverter and grid voltages is minimized using a PI controller to achieve synchronization. Figure shows the schematic diagram of this approach.

The Differential Root Mean Square Voltage (DRMSV) based synchronization approach added the seamless transfer capability in synchronverter during synchronization process. However, this approach has unwanted delays and uncertainties that are discussed below:

- During synchronization process, this scheme always slowed down the virtual rotor of synchronverter to synchronize with grid. Depending upon the phase angle position of synchronverter voltage, this approach leads to unwanted delays when the synchronverter voltage lags grid voltage.
- When there is significant magnitude difference between synchronverter and grid voltages, i.e. greater than V_{Th} of Figure 2.13, DRMSV-based approach leads to un-successful synchronization.

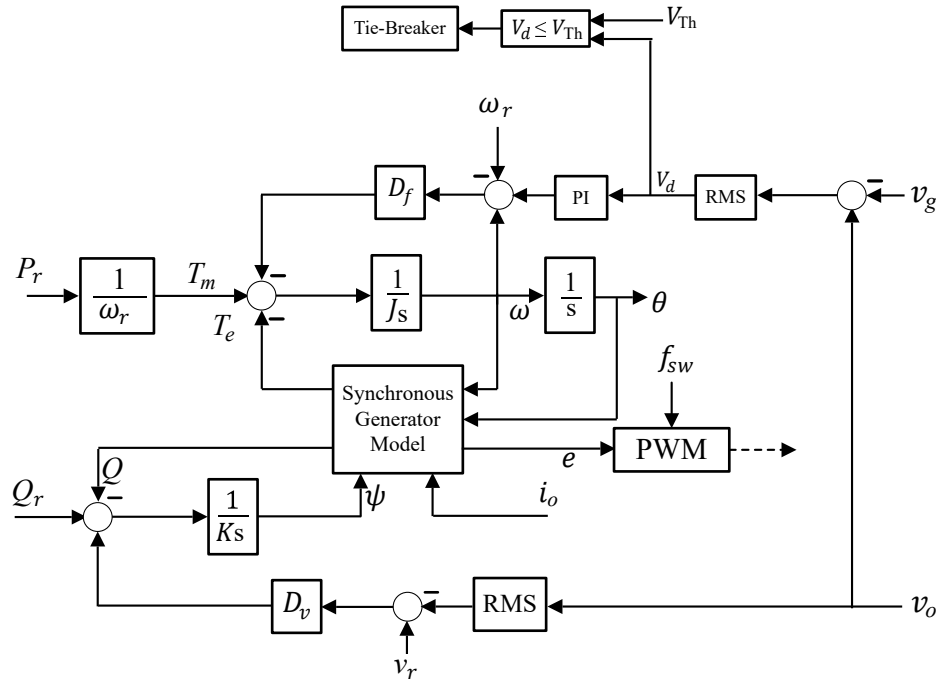


FIGURE 2.13: Differential RMS Voltage Based Synchronization [102]

These limitations are discussed in detail in Chapter 4.

2.2.6 Synchronverter Applications

Right after its invention, synchronverter has been deployed for various applications summarized in Table 2.5. Back-to-back synchronverters were used for integration of wind farm in [24, 118]. The rotor side converter mimicked synchronous motor and served as rectifier as it received power from permanent-magnet synchronous generator and injected it into dc bus. The grid-side converter mimicked synchronous generator and served as inverter as it injected the dc link power into power grid. The rotor-side rectifier controlled the dc-bus voltage while the grid-side inverter tracked Maximum Power Point (MPP). This concept of tracking the MPP and mimicking synchronous machine simultaneously can be extended to SPPs.

Similar scheme of [24] is used for the control and regulation of HVDC transmission system in [33]. Here, the sending-end rectifier behaved as synchronous motor and the receiving-end inverter emulated synchronous generator features. Another

TABLE 2.4: Literature Summary of initial grid-synchronization techniques of synchronverter

Technique	Advantages	Disadvantages	References
Phase-Locked Loop	<ul style="list-style-type: none"> • Most common • Easily available • Seamless transfer 	<ul style="list-style-type: none"> • Complex and time consuming tuning of parameters • Sensitive to noise, harmonics and transients • Degrades performance in weak grid • Brings instability for parallel operating inverters 	[21]
Virtual Impedance	<ul style="list-style-type: none"> • Self-synchronization • Required only during initial synchronization process 	<ul style="list-style-type: none"> • Lacks seamless transfer • Proper tuning of R and L required • Uncertainties 	[88]
Virtual Resistance	<ul style="list-style-type: none"> • Self-synchronization • Required only during initial synchronization process • Better for HVDC system 	<ul style="list-style-type: none"> • Lacks seamless transfer • Requires coordinate transformation 	[116, 117]
DRMSV-Based	<ul style="list-style-type: none"> • Self-synchronization • Required only during initial synchronization process • Seamless transfer • Simpler tuning 	<ul style="list-style-type: none"> • Unwanted delays • Uncertainties 	[102]

TABLE 2.5: Various applications of synchronverter

References	Application	Details
[14]	EVs charging station	Implemented bi-directional synchronverter for V2G charging station for electric vehicles (EVs)
[24]	Wind Farm Grid Integration	Back-to-back synchronverters are used. Rotor-side rectifier emulates synchronous motor and regulates DC bus voltage while grid-side inverter emulates synchronous generator and tracks MPP.
[33]	HVDC system	Proposed improved synchronverte for hybrid multi-terminal HVDC system
[119]	HVDC transmission system	Back-to-back synchronverters are used. Sending-end rectifier emulates synchronous motor and receiving-end inverter emulates synchronous generator.
[120]	LVDC microgrid	Enabled power sharing among dc sources in LVDC microgrid based on synchronverter
[121–123]	Distribution system	Control and regulate distribution systems using soft open point based on back-to-back synchronverters

application of synchronverter in HVDC system is found in [119]. In reference [120] synchronverter is deployed to achieve efficient power sharing among dc sources in LVDC microgrid.

References [121–123] proposed back-to-back synchronverter-based soft open point to transfer power between two adjacent feeders. This soft open point helps in frequency and voltage regulation in feeders and improves system reliability in case of loss of mains in any distribution feeder [122]. Reference [124, 125] applied synchronverter concept on shunt active filter to provide reactive power compensation,

frequency regulation and harmonics mitigation.

Electric Vehicles (EVs) play an important role in transportation system due to their sustainability, energy security and environmental effects. Other than transportation, they can also be crucial for peak load shaving [126], grid-support [127] and demand side management [128]. Synchronverter finds its applications in Vehicle-to-Grid (V2G) charging station for EVs [14]. Reference [129] applied synchronverter-based regenerative braking system for urban rail transit.

2.3 Gap Analysis

Synchronverter got special attention among all VSMS due to its similar dynamics as SG from grid POV. Therefore, researchers during the last decade addressed several issues and concerns about synchronverter design and performance. Section 2.2 reviewed various studies and analyses of synchronverter, different modifications to improve its performance and the synchronization techniques to achieve the initial synchronization with grid.

Some of the aspects about synchronverter are yet to be answered in literature. Following points highlight the research gap in this domain.

- Synchronverter has inherent capability to remain synchronized with grid. However, it requires a synchronization unit for initial synchronization with grid. Due to the complexity, inefficiency, and deteriorating performance of PLL in weak grid, PLL-less synchronization approaches are proposed in literature. Existing PLL-less approaches either lack seamless transfer capability or lead to unwanted delays and uncertainties under adverse grid conditions. An enhanced and promising synchronization technique is still required to overcome all these limitations.
- Almost all the literature about synchronverter assume an ideal source at the dc bus. This means an infinite power can be drawn or supplied to the dc side at any time. This is not true practically. The response of synchronverter

topology would be different from that with ideal source [130]. Reference [24] studied the effect of variations in wind speed on synchronverter performance. Similar studies are presented in [113, 131, 132]. However, the effect of intermittent nature of PV panels on synchronverter performance is still not investigated in literature.

- For the integration of RERs into power grid, ESS is crucial to be connected in parallel with RERs at the dc side of synchronverter for inertia emulation [133–135]. The required storage capacity, charging/discharging and effect of SOC of ESS connected in parallel with RERs, are the issues that are not properly addressed in literature so far.
- Performance of synchronverter with load variations in grid-connected mode is addressed in literature [136]. Steady-state operation of synchronverter in stand-alone mode is also simulated in references [106, 137]. However, effect of variations in connected load on synchronverter output frequency and voltage in stand-alone mode is not studied to author’s best knowledge.
- There are some additional winding termed as damper winding in the rotor of synchronous machines. These winding suppress the hunting and helps synchronous generator to re-synchronize with the grid after frequency disturbances. These damper winding are not yet modeled mathematically in synchronverter.

2.4 Problem Statement

The initial synchronization of synchronverter with grid needs improvement. Existing PLL-less synchronization approaches either lack seamless transfer capability or lead to unwanted delays and uncertainties under adverse grid conditions. Moreover, to find whether the synchronverter is a promising solution of RERs integration into power grid or not, its performance is not fully investigated yet in literature.

Proposed Solutions:

1. To improve the synchronization process, an enhanced, PLL-less auto-synchronizer for initial grid-synchronization of synchronverter is proposed here that
 - (a) ensures uninterrupted power supply to local load during synchronization process,
 - (b) ensures fast synchronization with grid independent of phase angle position of synchronverter voltage with respect to grid voltage,
 - (c) ensures reliability and certainty in synchronization irrespective of the magnitude difference between synchronverter and grid voltages, and
 - (d) has less computational burden on the controller during synchronization.
2. To investigate the performance of synchronverter, following aspects are studied in detail:
 - (a) Effects of variations in local connected load on synchronverter in stand-alone mode of operation.
 - (b) Effects of intermittent nature of SPP on synchronverter performance.
 - (c) Performance of synchronverter having SPP, i.e. the non-ideal source, at dc bus under adverse grid conditions.

2.5 Methodology and Techniques

First, a complete model of original synchronverter is derived from the mathematical model of synchronous generator assuming an ideal source at the dc bus. Then, an enhanced, PLL-less auto-synchronizer is proposed based on Fourier Analysis to achieve fast and reliable initial grid-synchronization of synchronverter under adverse grid conditions.

Finally, the designed system is extended to integrate solar power plant into power grid. The proposed auto-synchronizer is then applied to the final system to test

its validation. All this research is based on simulations performed in MATLAB 9.2/Simulink using SimPowerSystem library.

2.6 Applications

Synchronverter finds its applications in RERs integration into power grid, HVDC transmission, modular multilevel converters, rectifier-fed appliances, static synchronous condensers, EVs charging/discharging stations, and distribution systems. Some of these applications are presented in Section 2.2.6.

The proposed auto-synchronizer can be applied to all the applications where synchronverter having a local connected load is required to be synchronized with grid. Some of the applications are listed below:

- Integration of renewable energy generation based power plant associated with critical centers like hospitals, data centers, military units etc into the power grid
- Integration of distributed generations based hybrid microgrids into power grid
- Charging and discharging of Plug-in Hybrid Electric Vehicles for (V2G) grid support
- Integration of grid-tied roof-top PV panels at residential and commercial units having the facility of net metering into power grid

2.7 Summary

In this chapter, literature review of all the VSMS is presented. Synchronverter is better among all other topologies because of its simplicity and inertial dynamics. It requires a dedicated synchronization unit only during initial synchronization

with grid. Existing PLL-less synchronizers either lack seamless transfer capability or lead to unwanted delays and uncertainties under adverse grid conditions. Moreover, the performance of synchronverter with a non-ideal source at dc bus is not investigated in literature yet. In this work, an enhanced, PLL-less auto-synchronizer is designed for synchronverter to achieve fast and promising synchronization without shutting down the local connected load. In this way the critical load can be attached to the synchronverter output. Moreover, the performance of synchronverter is evaluated in detail having a Solar Power Plant at the dc bus to find whether the synchronverter is a promising solution of RERs integration into power grid or not.

Chapter 3

Design and Evaluation of Synchronverter

Synchronverter presents the same dynamics as that of SG from grid POV. It is based on the second-order model of the synchronous generator. It can replicate all the essential features of synchronous generator in both stand-alone and grid-connected modes of operation.

This chapter presents the mathematical modeling of synchronous machine with some basic assumptions and parameter designing of synchronverter considering an ideal source at the dc side. The performance of synchronverter in stand-alone mode as well as grid-connected mode is investigated and the seamless transfer of synchronverter from grid-connected to stand-alone mode is studied.

Synchronization with grid is elaborated in Chapter 4. Therefore, it is excluded from this chapter.

3.1 Synchronous Generator Model

Mathematical model of synchronous machine is found in literature [138, 139]. For synchronverter, a round-rotor, two-pole synchronous generator is considered in

The stator flux linkages can be expressed as:

$$\begin{aligned}\phi_a &= Li_a - Mi_b - Mi_c + M_{ae}i_e \\ \phi_b &= Li_b - Mi_a - Mi_c + M_{be}i_e \\ \phi_c &= Li_c - Mi_a - Mi_b + M_{ce}i_e\end{aligned}\quad (3.2)$$

Where i_a , i_b , and i_c are the phase currents in stator windings and i_e is the field excitation current in rotor winding. Since, balanced conditions are assumed, following equation holds when neutral line is not connected:

$$i_a + i_b + i_c = 0 \quad (3.3)$$

When the neutral is connected, the sum of three phase currents becomes equal to i_n . Since, balanced condition is assumed in design process, neutral current will also 0 with this assumption. Using Equations (3.1 – 3.3), stator flux linkages can be simplified as:

$$\begin{aligned}\phi_a &= (L + M)i_a + M_e i_e \cos(\theta) \\ \phi_b &= (L + M)i_b + M_e i_e \cos(\theta - \frac{2\pi}{3}) \\ \phi_c &= (L + M)i_c + M_e i_e \cos(\theta - \frac{4\pi}{3})\end{aligned}\quad (3.4)$$

Simplifying Equation (3.4) yields:

$$\begin{bmatrix} \phi_a \\ \phi_b \\ \phi_c \end{bmatrix} = (L + M) \begin{bmatrix} i_a \\ i_b \\ i_c \end{bmatrix} + M_e i_e \begin{bmatrix} \cos \theta \\ \cos(\theta - \frac{2\pi}{3}) \\ \cos(\theta - \frac{4\pi}{3}) \end{bmatrix}\quad (3.5)$$

For the simplification, let $L + M = L_s$, and let the stator flux linkages are equal to Φ_s as:

$$\begin{bmatrix} \phi_a \\ \phi_b \\ \phi_c \end{bmatrix} = \Phi_s \quad (3.6)$$

Let the stator currents are denoted by i_s as:

$$\begin{bmatrix} i_a \\ i_b \\ i_c \end{bmatrix} = i_s \quad (3.7)$$

Also, let:

$$\begin{bmatrix} \cos \theta \\ \cos(\theta - \frac{2\pi}{3}) \\ \cos(\theta - \frac{4\pi}{3}) \end{bmatrix} = \widetilde{\cos\theta} \quad (3.8)$$

Equation (3.4) can be written as:

$$\Phi_s = L_s i_s + M_e i_e \widetilde{\cos\theta} \quad (3.9)$$

The rotor flux linkage can be written as:

$$\Phi_e = L_e i_e + M_{ae} i_a + M_{be} i_b + M_{ce} i_c \quad (3.10)$$

Inserting values of mutual inductances from Equation (3.1) and simplifying rotor flux linkage yields:

$$\begin{aligned} \Phi_e &= L_e i_e + M_e \cos(\theta) i_a + M_e \cos(\theta - \frac{2\pi}{3}) i_b + M_e \cos(\theta - \frac{4\pi}{3}) i_c \\ &= L_e i_e + M_e \begin{bmatrix} i_a \\ i_b \\ i_c \end{bmatrix}^T \begin{bmatrix} \cos \theta \\ \cos(\theta - \frac{2\pi}{3}) \\ \cos(\theta - \frac{4\pi}{3}) \end{bmatrix} \end{aligned} \quad (3.11)$$

After further simplification, the rotor flux linkage obtained in above equation can be written as following equation

$$\Phi_e = L_e i_e + M_e \langle i_s, \widetilde{\cos\theta} \rangle \quad (3.12)$$

Where, $\langle i_s, \widetilde{\cos\theta} \rangle$ is the conventional dot product of stator current i_s and $\widetilde{\cos\theta}$ in real numbers domain.

The rate of change of stator flux can be expressed as:

$$\left. \frac{d\Phi_s}{dt} \right|_{i_s, i_e \text{ constant}} = -\dot{\theta} M_e i_e \widetilde{\sin\theta} \quad (3.13)$$

This rate of change of flux induces electromotive force in stator coils that can be given by Lenz's Law [139]:

$$\begin{aligned} e &= -\frac{d\Phi_s}{dt} \\ &= \dot{\theta} M_e i_e \widetilde{\sin\theta} \end{aligned} \quad (3.14)$$

Where, $\dot{\theta} = \omega$ is the angular speed of synchronous generator rotor in radians per second. The energy stored in the magnetic field of synchronous generator can be written as:

$$\begin{aligned} E &= \frac{1}{2} \langle i_s, \Phi_s \rangle + \frac{1}{2} i_e \Phi_e \\ &= \frac{1}{2} \langle i_s, L_s i_s + M_e i_e \widetilde{\cos\theta} \rangle + \frac{1}{2} i_e (L_e i_e + M_e \langle i_s, \widetilde{\cos\theta} \rangle) \\ &= \frac{1}{2} \langle i_s, L_s i_s \rangle + \frac{1}{2} M_e i_e \langle i_s, \widetilde{\cos\theta} \rangle + \frac{1}{2} L_e i_e^2 + \frac{1}{2} M_e i_e \langle i_s, \widetilde{\cos\theta} \rangle \\ &= \frac{1}{2} \langle i_s, L_s i_s \rangle + \frac{1}{2} L_e i_e^2 + M_e i_e \langle i_s, \widetilde{\cos\theta} \rangle \end{aligned} \quad (3.15)$$

The induced electric torque of the synchronous generator can be found by taking rate of change of stored energy in magnetic field with respect to the rotor movement [53].

$$\begin{aligned} T_e &= -\frac{\partial E}{\partial \theta} \\ &= M_e i_e \langle i_s, \widetilde{\sin\theta} \rangle \end{aligned} \quad (3.16)$$

The generated active power P of the synchronous generator can then be calculated from induced electric torque obtained in above equation and the angular speed of the rotor as [139]:

$$\begin{aligned} P &= \omega T_e \\ &= \dot{\theta} M_e i_e \langle i_s, \widetilde{\sin\theta} \rangle \end{aligned} \quad (3.17)$$

Similarly, the reactive power Q can be expressed as:

$$\begin{aligned} Q &= \dot{\theta} M_e i_e \left\langle i_s, \widetilde{\sin}\left(\theta - \frac{\pi}{2}\right) \right\rangle \\ &= -\dot{\theta} M_e i_e \left\langle i_s, \widetilde{\cos}\theta \right\rangle \end{aligned} \quad (3.18)$$

For simplicity, let the product of maximum mutual inductance between stator and rotor excitation coils and the field excitation current $M_e i_e = \psi$, the Equations (3.14), (3.16) and (3.18) becomes:

$$e = \omega \psi \widetilde{\sin}\theta \quad (3.19)$$

$$T_e = \psi \left\langle i_s, \widetilde{\sin}\theta \right\rangle \quad (3.20)$$

$$Q = -\omega \psi \left\langle i_s, \widetilde{\cos}\theta \right\rangle \quad (3.21)$$

Where, ω is the angular speed of the rotor in radians per second. Equations (3.19 – 3.21) form the basis of synchronverter model.

3.2 Design of Synchronverter

The complete schematic diagram of the synchronverter excluding proposed auto-synchronizer is shown in Figure 3.2. The electrical part consists of three-legged power electronic converter with an LCL filter at the output, the local connected load that requires power supply all the time, tie breaker and the power grid.

Measurement blocks are also shown in Figure 3.2. Measurement block 1 consists of measurement units to measure the values of synchronverter output phase voltage v_o and current i_o . Measurement block 2 measures grid phase voltage v_g .

The controller part of synchronverter contains the synchronous generator mathematical model derived in previous section, frequency control loop, and voltage control loop. As discussed earlier, an ideal source is assumed at the dc side in this chapter. Detailed design of synchronverter including frequency control loop and voltage control loop is described in the upcoming sections.

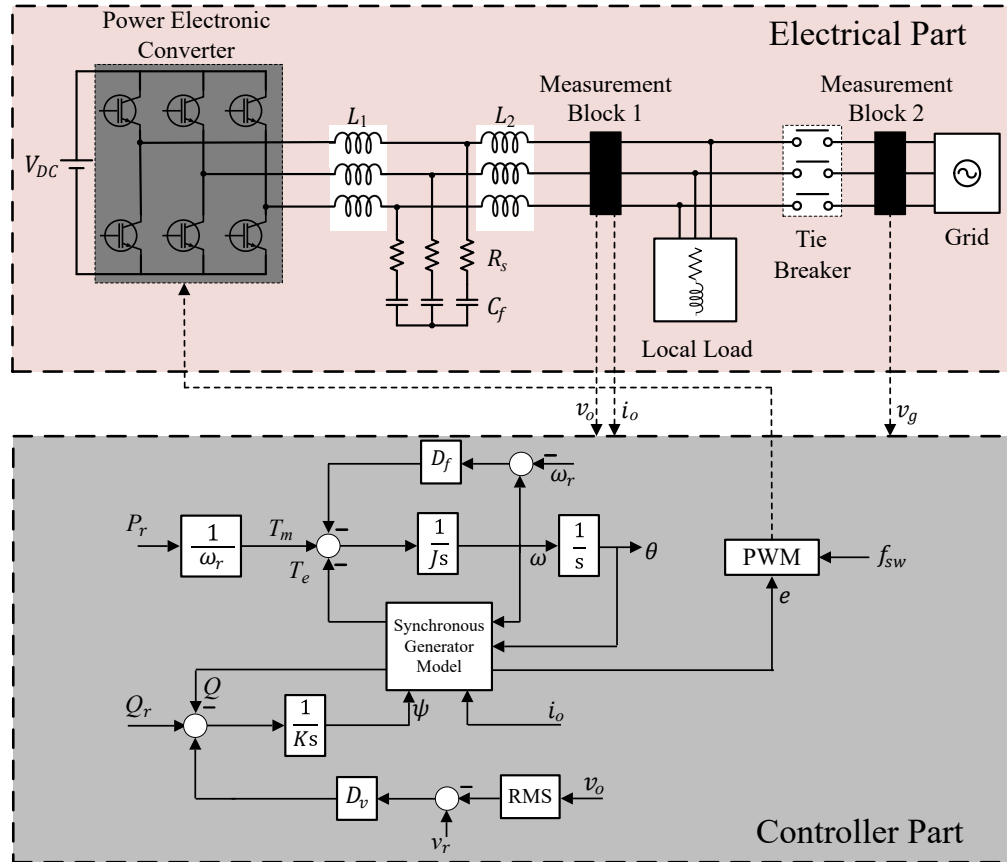


FIGURE 3.2: Schematic diagram of synchronverter without synchronizer

3.2.1 Synchronous Generator Model

The synchronous generator model shown in Figure 3.2 consists of mathematical formulas of virtual induced electromotive force e , virtual electric torque T_e and reactive power Q given by Equations (3.19 – 3.21) derived in Section 3.1. The induced electromotive force e calculated by Equation (3.19) is fed to the Pulse Width Modulation (PWM) block for generating the variable width pulses to drive PEC switches.

3.2.2 Frequency Control Loop

Frequency control loop is analogous to the governor control of the synchronous generator. It is based on the swing equation of the synchronous generator that can be expressed as:

$$J\dot{\omega} = T_m - T_e - D_f(\omega - \omega_r) \quad (3.22)$$

Where J is the moment of inertia of the virtual rotor and D_f is the damping coefficient that acts as feedback gain. Block diagram of frequency control loop is shown in Figure 3.3.

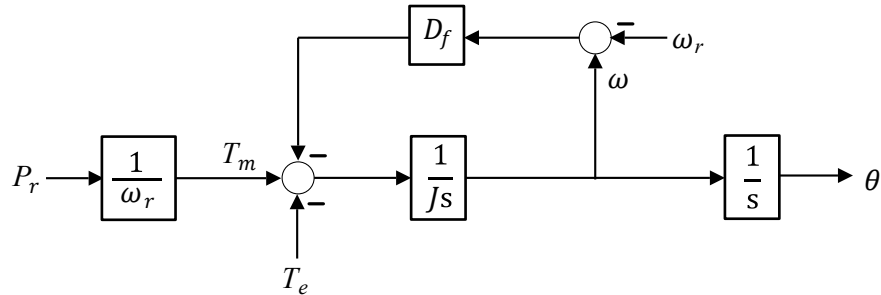


FIGURE 3.3: Frequency Control Loop

P_r is the active power reference, ω_r is the angular speed reference, and T_e is provided by the synchronous generator model block using Equation (3.20). Frequency control loop controls the angular speed ω and rotor angle θ of virtual rotor of synchronverter.

The damping coefficient D_f is represented as [88]:

$$D_f = -\frac{\Delta P_o}{\omega \Delta \omega} \quad (3.23)$$

Here, D_f is selected such as the output power P_o increases or decreases by 100% of the nominal power S_n when the frequency decreases or increases by 0.5% of the nominal value f_n . When ΔP_o is negative, $\Delta \omega$ is positive and vice versa. Therefore, D_f is always positive as defined by Equation (3.23).

The time constant τ_f of the frequency control loop is $\frac{J}{D_f}$. By assuming a value for time constant, J can be chosen as

$$J = D_f \tau_f \quad (3.24)$$

Since, frequency control loop has no delay involved in it, so τ_f can be selected much smaller than the inertial response of synchronous generator [21]. In this way, the frequency control loop responds to the grid dynamics in a quick manner.

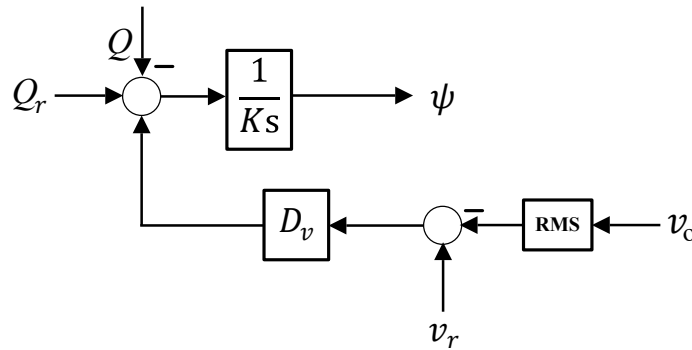


FIGURE 3.4: Voltage Control Loop

Frequency control loop has two nested loops; inner loop is frequency loop and the outer loop is active power loop. These nested loops help synchronverter to provide primary frequency regulation in both stand-alone and grid-connected modes according to the active power-frequency droop characteristics [139].

3.2.3 Voltage Control Loop

Voltage control loop is analogous to the Automatic Voltage Regulator (AVR) of the synchronous generator [138]. Similar to the case of frequency control loop, voltage control loop can be expressed mathematically as:

$$K\dot{\psi} = Q_r - Q + D_v(v_r - v_o) \quad (3.25)$$

Here, K is the integrator gain, ψ is the product of maximum mutual inductance between stator and excitation coils and the field excitation current, Q_r is the reactive power reference, Q is provided by the synchronous generator model block using Equation (3.21), D_v is voltage droop coefficient, and v_r is the reference voltage that is equal to the nominal phase voltage V_n .

Figure 3.4 shows the block diagram of voltage control loop. Voltage droop coefficient D_v is represented as [88]:

$$D_v = -\frac{\Delta Q_o}{\Delta v_o} \quad (3.26)$$

Here D_v is selected such as the output power Q_o increases or decreases by 100% of the nominal power S_n when the voltage decreases or increases by 5% of the nominal voltage V_n . When ΔQ_o is negative, Δv_o is positive and vice versa. Therefore, D_v is always positive as defined by Equation (3.26).

The time constant τ_v of the voltage control loop is $\frac{K}{\omega D_v}$ [88]. By assuming τ_v , K can be selected as:

$$K = \omega D_v \tau_v \quad (3.27)$$

It is clear from Figure 3.4 that the voltage control loop has two sub-loops. The inner loop is voltage loop and outer loop is reactive power loop. Therefore, the voltage control loop regulates the voltage according to the reactive power-voltage droop characteristics [139]. It can have two operating modes as discussed in [88]. First is Q-mode in which the synchronverter produce Q_o according to the reference Q_r irrespective of the difference between v_r and v_g . Second is the Q_D -mode in which the synchronverter takes into account the voltage difference between v_r and v_g in generating Q_o . Therefore, in Q_D -mode, Q_o is deviated from the reference Q_r .

3.2.4 LCL Filter

A filter is required at the output of the PEC to mitigate the harmonics in output current. An LCL filter is used here as shown in Figure 3.2. LCL filter has better damping characteristics and lower voltage drop than LC filter [140]. Values of L_1 , L_2 , C_f and R_s are calculated in literature [141, 142].

In this study, the maximum output current is considered with the 10% fluctuations for filter design as in [141]. Inverter-side inductor L_1 is selected by Equation (3.28) as [142]:

$$L_1 = \frac{3 \cdot V_{DC} \cdot V_n}{6 \cdot f_{sw} \cdot 0.1 \cdot S_n \cdot \sqrt{2}} \quad (3.28)$$

Where V_{DC} is the dc-link voltage, V_n is the nominal phase voltage, S_n is nominal power and f_{sw} is the switching frequency of PEC switches.

The capacitor value C_f affects the power factor. Higher the capacitor, smaller will be the power factor [141]. To keep the power factor closer to unity, the reactive power consumed by filter capacitor should not be more than 5% of the nominal power [142]. Therefore, C_f is calculated by the following equation;

$$C_f = \frac{0.05 \cdot S_n}{\omega_n \cdot (\sqrt{3}V_n)^2} \quad (3.29)$$

Where ω_n is the nominal angular frequency. In this research, ω_n is equal to the ω_r of the synchronverter.

The grid-side inductor L_2 is chosen to attenuate the grid harmonics [141]. Reference [142] used attenuation factor α of 20%. The increase in the attenuation factor will increase the THD in grid current. In this research, $\alpha = 8\%$ is used.

$$L_2 = \frac{\sqrt{\frac{1}{0.08^2} + 1}}{C_f \cdot (2\pi f_{sw})^2} \quad (3.30)$$

To avoid the resonance problem in filter, a resistor R_s is connected in series with the capacitor [141–144]. Its value is selected according to the following equation:

$$R_s = \frac{0.1}{C_f \cdot \omega_{res}} \quad (3.31)$$

Where ω_{res} is the angular resonance frequency that is defined as:

$$\omega_{res} = \sqrt{\frac{L_1 + L_2}{L_1 \cdot L_2 \cdot C_f}} \quad (3.32)$$

All the parameters used in simulations are tabulated in Table 3.1.

3.3 Performance Evaluation of Synchronverter

A synchronverter may operate either in stand-alone or grid-connected mode. In stand-alone mode, voltage and frequency must be kept within the permissible

TABLE 3.1: Parameters used in simulations

Parameters	Symbols	Values
Nominal DC Voltage	V_{DC}	800 V
Damping Coefficient	D_f	20.26
Nominal Phase Voltage	V_n	220 V-rms
Virtual Inertia	J	0.04052
Nominal Power	S_n	10 kVA
Voltage Droop Coefficient	D_v	642
Switching Frequency	f_{sw}	8 kHz
Integrator Gain	K	1284π
Nominal Frequency	f_n	50 Hz
Filter Capacitor	C_f	10 μ F
Filter Inductor	L_1	7.777 mH
Filter Inductor	L_2	0.5343 mH
Series Resistor	R_s	0.7071 Ω
Maximum Local Load	S_L	$8 + j5$ kVA
Voltage Loop Time Constant	τ_v	0.02 s
Frequency Loop Time Constant	τ_f	0.002 s

limits by the synchronverter to supply the local connected load. Whereas, in grid-connected mode, it has to supply real and reactive power based on the droop characteristics of synchronous generator while supporting grid frequency and voltage.

For a synchronverter having a critical local load, continuous output power must be supplied by it all the time. Therefore, the synchronverter should possess the seamless transfer capability from stand-alone mode to grid-connected mode and vice versa.

Upcoming sections evaluate the performance of synchronverter with simulations during:

- Stand-alone mode under variations in local connected load

- Grid-connected mode with stable grid conditions
- Grid-connected mode when grid frequency drops by 0.4% of the nominal value
- Grid-connected mode when grid voltage drops by 20% of the nominal value
- Transition from grid-connected to stand-alone mode of operation

3.4 Simulation Results and Discussions

All the simulations in this chapter were performed to prove that synchronverter has capability to give desired performance in stand-alone and grid-connected mode without a dedicated synchronization unit.

Simulations were performed in MATLAB 9.2/Simulink environment using SimPowerSystem library. The parameters used in the simulations are tabulated in Table 3.1. The ode23tb solver was used with the maximum step size of $1 \mu s$ and minimum required accuracy of 10^{-3} .

All the voltages and currents were measured using three-phase VI measurement blocks having combinations of voltmeters and ammeters. RMS value of the voltage was measured by taking root mean square value over running average window of 20 ms (equal to one cycle of the fundamental frequency).

Since Active and reactive powers are integral quantities, they were computed by first determining the positive sequence of voltage and currents with a running window over one cycle of fundamental frequency. The active and reactive powers were then computed using power formulas. The sample time of all the blocks was $1 \mu s$. The local connected load was series RL load having maximum rating of $8 + j5$ kVA.

Simulations were started at $t = 0$ s and stopped at $t = 15$ s. The breakdown of simulations is as follows:

- Stand-alone performance was studied from $t = 0 - 7$ s.
- Grid-connected performance was studied from $t = 8 - 13$ s with stable grid conditions.
- At $t = 13$ s, grid-connected performance with variation in grid frequency was simulated.
- At $t = 13.5$ s, grid-connected performance with variation in grid voltage magnitude was simulated.
- Finally, at $t = 14$ s, grid was disconnected to verify the seamless transfer of synchronverter from grid-connected mode to stand-alone mode without any change in the controller.

3.4.1 Stand-Alone Performance

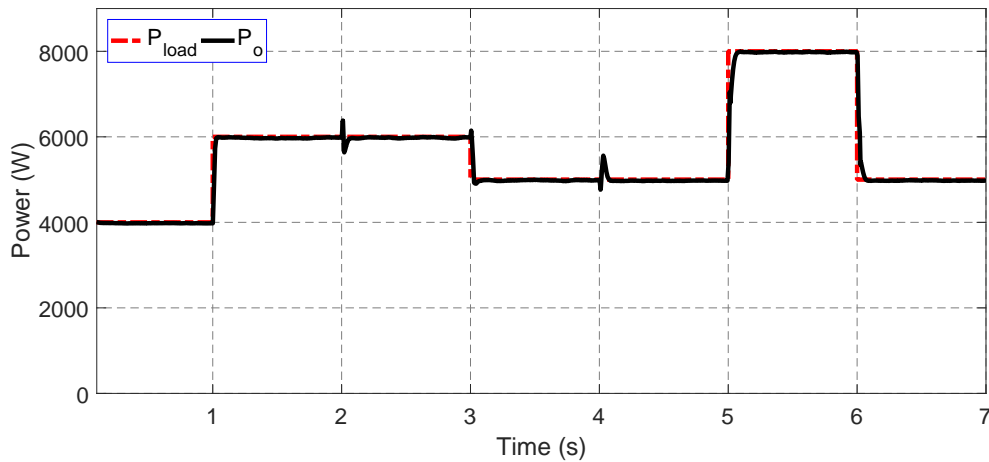
One of the research objectives is the study of stand-alone performance of synchronverter with variations in local connected load. In this part, this performance was evaluated with an ideal source connected at the dc bus. The simulations were started at $t = 0$ s with a load of $4 + j2$ kVA connected to it. Active and reactive loads were varied to study the effect of changes in operating conditions on synchronverter performance.

A load of 2 kW was switched-on at $t = 1$ s. Similarly, a load of 2 kVar was switched-on at $t = 2$ s. The total resistive load was changed to 5 kW at $t = 3$ s and the total inductive load was changed to 1 kVar at $t = 4$ s. Total load on synchronverter was increased to $8 + j5$ kVA at $t = 5$ s and decreased to $5 + j2$ kVA at $t = 6$ s. Table 3.2 shows the active and reactive power load connected to synchronverter at each instant during stand-alone operation. Figures 3.5 and 3.6 depict that the active and reactive power output of the synchronverter was equal to the power demanded by the local load. For the maximum active power change of 3 kW at $t = 5$ s, the response time was 83 ms. Similarly, for the maximum reactive power change of 4000 MVAR at $t = 5$ s, the response time was also 83

TABLE 3.2: Variations in local load connected to synchronverter with ideal source at dc bus

Time Instant	P_{load}	Q_{load}
$t = 0$ s	4000 W	2000 Var
$t = 1$ s	6000 W	2000 Var
$t = 2$ s	6000 W	4000 Var
$t = 3$ s	5000 W	4000 Var
$t = 4$ s	5000 W	1000 Var
$t = 5$ s	8000 W	5000 Var
$t = 6$ s	5000 W	2000 Var

ms. Transients were seen in power curves at the switching events. For example, a small glitch can be seen at $t = 2$ s in active power curve when a reactive power load of 2000 Var was switched on.

FIGURE 3.5: Stand-alone performance: synchronverter active power P_o and load P_{load}

The frequency, shown in Figure 3.7, was well maintained by frequency control loop. Negligible variations in frequency at the instants of reactive power load switching was due to the coupling effect discussed in [145]. At the instant of increased active power load, the synchronverter increased its frequency to meet the increased demand. The maximum rate of change of frequency of 0.04 Hz per second was observed at $t = 5$ s when a load of $3000 + j4000$ VA was added to the

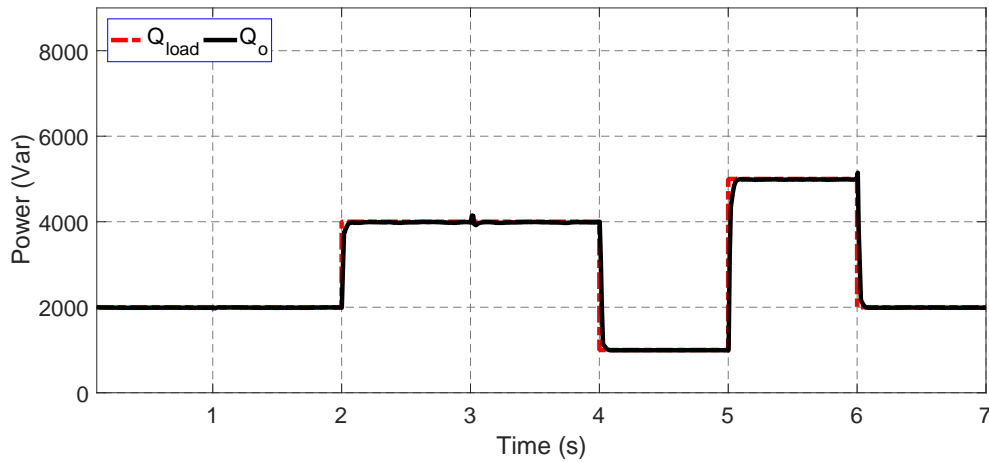


FIGURE 3.6: Stand-alone performance: synchronverter reactive power Q_o and load Q_{load}

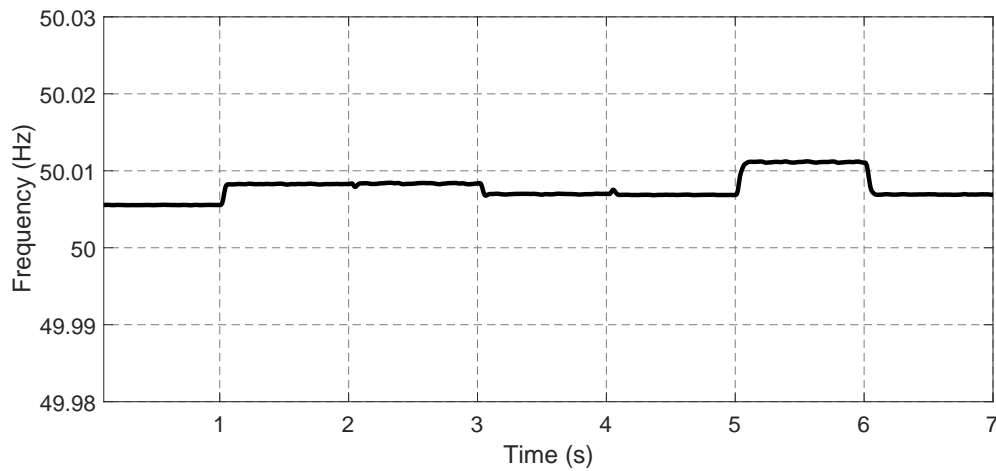


FIGURE 3.7: Stand-alone performance: synchronverter frequency f_o

synchronverter output. This ROCOF is much less than the threshold value of 3 Hz/s defined by IEEE standards [61]. For 60% increase in active power output, the synchronverter frequency was increased by 0.002% of nominal value. The response time for the maximum variation at $t = 5$ s was 83 ms. Similar variations in frequency are reported in [88].

The output phase voltage is shown in Figure 3.8. The transients were observed at the switching instants. The maximum dip was observed at $t = 5$ s when the total load of $3000 + j4000$ VA was switched on. This dip was 5% lower than the steady state value that is less than the threshold value of $\pm 10\%$ defined by IEEE standards [61]. The maximum response time was found to be 108 ms. The

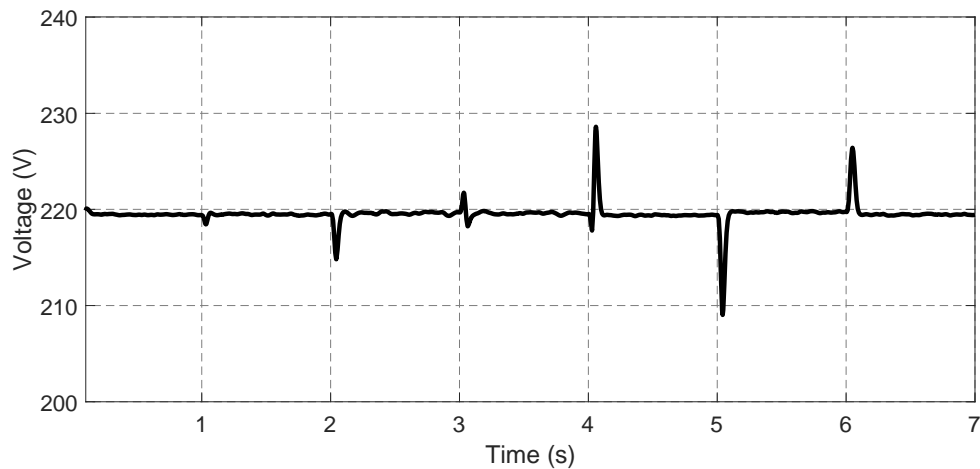


FIGURE 3.8: Stand-alone performance: synchronverter rms phase voltage v_o

maximum rate of rise of voltage was 0.025 V/ms while the rate of change of voltage with respect to reactive power was 2.585 V/kVar.

Results show that the synchronverter supplied active and reactive power as demanded by the local connected load and maintained frequency and voltage close to the rated values. Thus, the synchronverter emulated real synchronous generator successfully in stand-alone mode.

3.4.2 Grid-Connected Performance

After connection with grid, the synchronverter has ability to remain synchronized with grid without the need of dedicated synchronization unit. Therefore, no dedicated synchronization unit is required in this mode. In grid-connected mode, the performance of synchronverter was evaluated with stable grid conditions as well as with variations in grid frequency and voltage magnitude.

3.4.2.1 Grid-Connected Mode with Stable Grid Conditions

In this section, the performance of synchronverter was evaluated with a strong grid i.e., no variations in the grid frequency and voltage. The effect of varying the reference values of active and reactive power was observed. P_r was increased to 8

TABLE 3.3: Variations in active and reactive power reference

Time Instant	P_r	Q_r
$t = 8$ s	8000 W	3000 Var
$t = 9$ s	8000 W	6000 Var
$t = 10$ s	2000 W	6000 Var
$t = 11$ s	2000 W	1000 Var
$t = 12$ s	7000 W	4000 Var

kW at $t = 8$ s and decreased to 2 kW at $t = 10$ s. Q_r was increased to 6 kVar and decreased to 1 kVar at $t = 9$ s and 11 s, respectively. Both P_r and Q_r values were increased to 7 kW and 4 kVar, respectively, at $t = 12$ s. Table 3.3 shows the active and reactive power references at each instant during this operation.

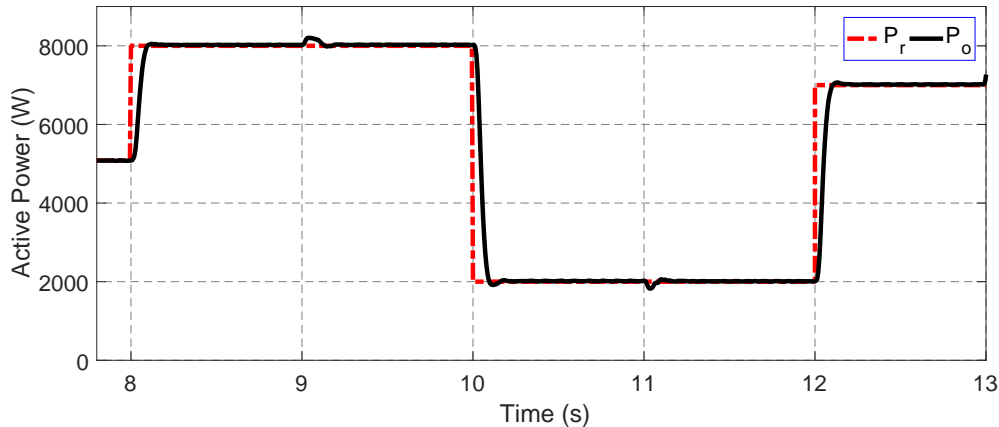


FIGURE 3.9: Grid-connected performance with stable grid conditions: synchronverter active power P_o and active power reference P_r

Figure 3.9 and 3.10 show the synchronverter output active and reactive power along with the corresponding reference values. It was observed that the synchronverter output power followed the reference values very well. The response time of active power for maximum change in P_r at $t = 10$ s was 132 ms while that of reactive power for maximum change in Q_r at $t = 11$ s was 204 ms. Since the time constant of frequency control loop is much smaller than that of voltage control loop, as discussed in Section 3.2.2, the synchronverter varied its active power P_o quicker than reactive power Q_o .

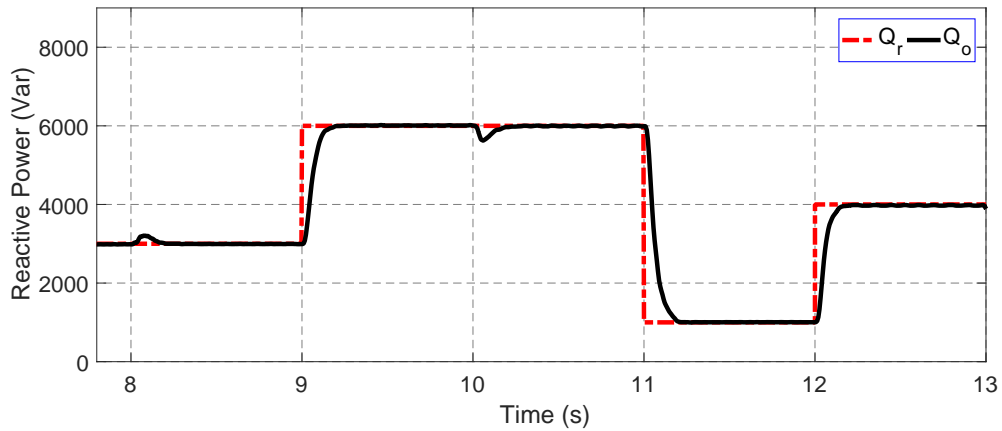


FIGURE 3.10: Grid-connected performance with stable grid conditions: synchronverter reactive power Q_o and reactive power reference Q_r

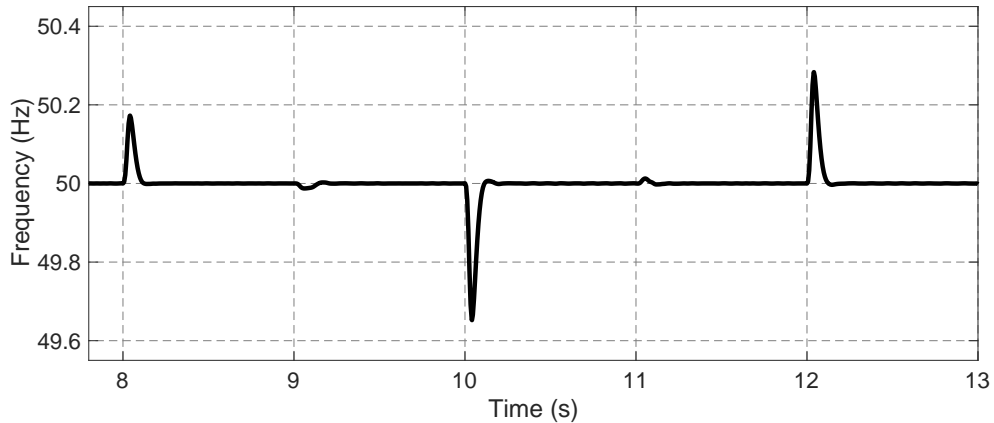


FIGURE 3.11: Grid-connected performance with stable grid conditions: synchronverter frequency f_o

Transients were observed in synchronverter frequency f_o whenever the P_r was changed as shown in Figure 3.11. This behavior was also similar to the real synchronous generators [139]. Highest surge in frequency curve was observed at $t = 10$ s. The frequency was dropped by 0.34 Hz at $t = 10.04$ s and then restored to 50 Hz at $t = 10.13$ s. Although the ROCOF was 8.5 Hz/s, however, the frequency was kept within the permissible limit during the transient.

Negligible transients in f_o for the changes in Q_r were due to the coupling effect between voltage and frequency control loops. This coupling effect between frequency and voltage control loops is due to the inductive line impedance [145]. Figure 3.12

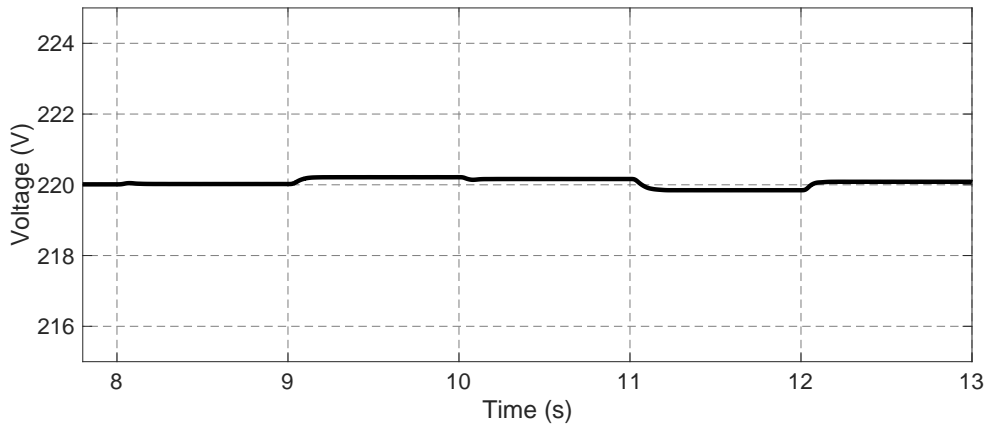


FIGURE 3.12: Grid-connected performance with stable grid conditions: synchronverter rms phase voltage v_o

shows that the synchronverter phase voltage remained close to rated value. The maximum variations in voltage was 0.22 V at $t = 9$ s.

It can be concluded from the results that synchronverter had ability to supply any desired amount of active and reactive power within its power rating. The frequency and voltage were kept at the rated values while supplying power equal to reference values. Therefore, the synchronverter gave desired performance in grid-connected mode without a dedicated synchronization unit.

3.4.2.2 Grid-Connected Performance Following Frequency Event

This part of simulation was performed to further verify the inherent frequency tracking of synchronverter in grid-connected mode. Synchronverter was supply $7000 + j4000$ VA in Q_D -mode discussed in Section 3.2.3 before the frequency event. At $t = 13$ s, the grid frequency was dropped to 49.8 Hz, i.e. by 0.4% and restored to 50 Hz after 0.1 s. Figure 3.13 shows that the synchronverter frequency f_o was slowly changed to 49.8 Hz due to the presence of virtual inertia. The response time was 91 ms whereas the ROCOF was 2.2 Hz/s.

No severe transients were observed in synchronverter output current i_o , shown in Figure 3.14. The maximum current during the event was 1.3 times the normal

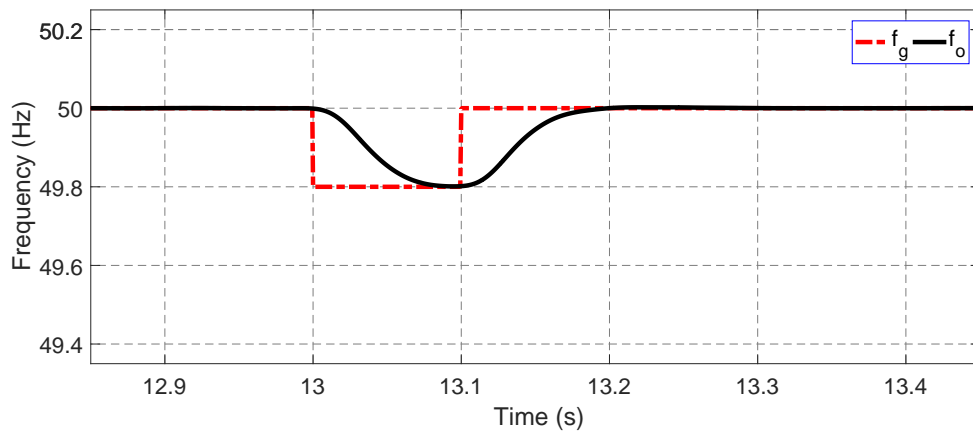


FIGURE 3.13: Grid-connected performance following a frequency event: synchronverter frequency f_o and grid frequency f_g

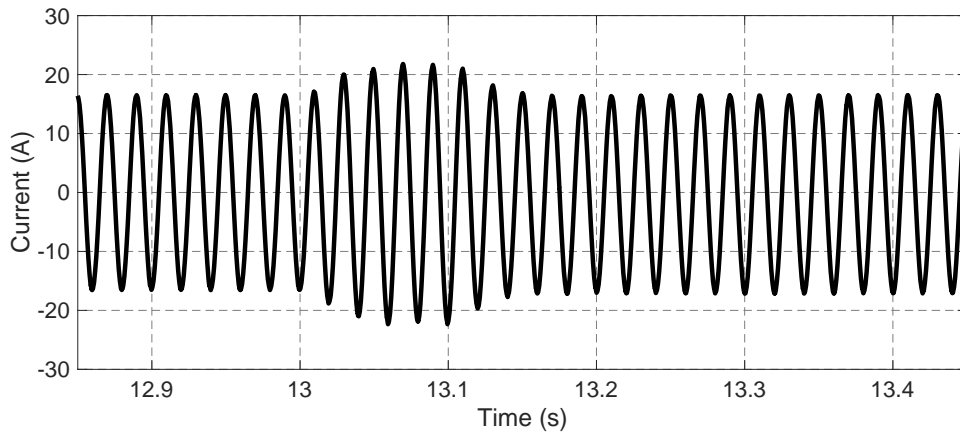


FIGURE 3.14: Grid-connected performance following a frequency event: synchronverter output current i_o

current. This is acceptable as PECs are often designed to withstand excessive short circuit currents for small interval of time [88].

Synchronverter output active power P_o was increased by 29% of the nominal value, as shown in Figure 3.15. By increasing P_o , the synchronverter participated in frequency regulation of the system. Negligible variations were seen in reactive power Q_o , in Figure 3.16, because of the variations in grid voltage during the frequency event. The variations found in Q_o were only $\pm 4.3\%$ of the reference value of 4000 Var. Results show that the synchronverter also provided reactive power support to grid during frequency event.

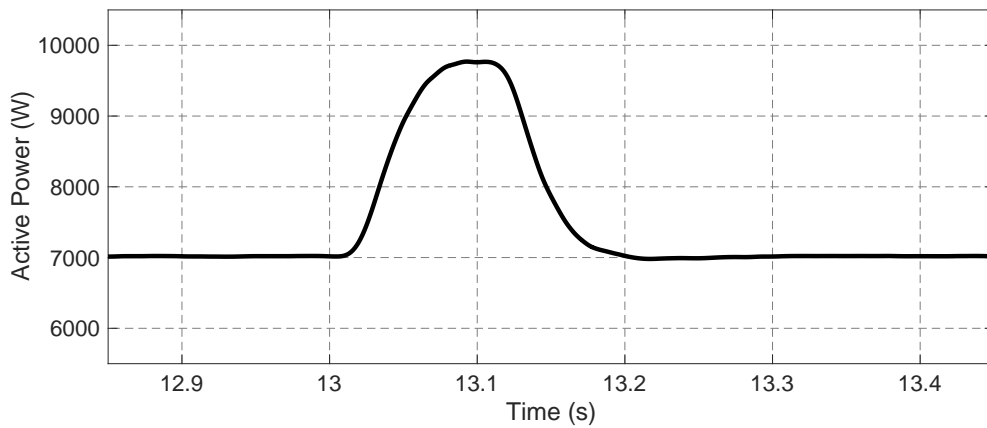


FIGURE 3.15: Grid-connected performance following a frequency event: synchronverter active power P_o

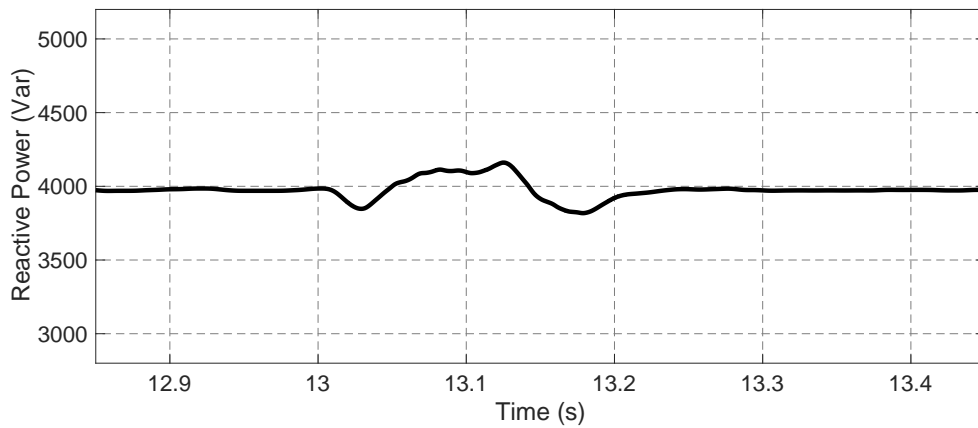


FIGURE 3.16: Grid-connected performance following a frequency event: synchronverter reactive power Q_o

During events of grid frequency fluctuations, the synchronverter tracked and supported the frequency by changing its output active power independent of dedicated synchronization unit. Therefore, synchronverter has ability to remain synchronized with grid while supporting system frequency.

3.4.2.3 Grid-Connected Performance Following Voltage Event

This part of simulations was performed to verify the voltage support capability of synchronverter. Synchronverter was supplying $7000 + j4000$ VA in Q -mode, discussed in Section 3.2.3, before the voltage event. At $t = 13.5$ s, grid voltage

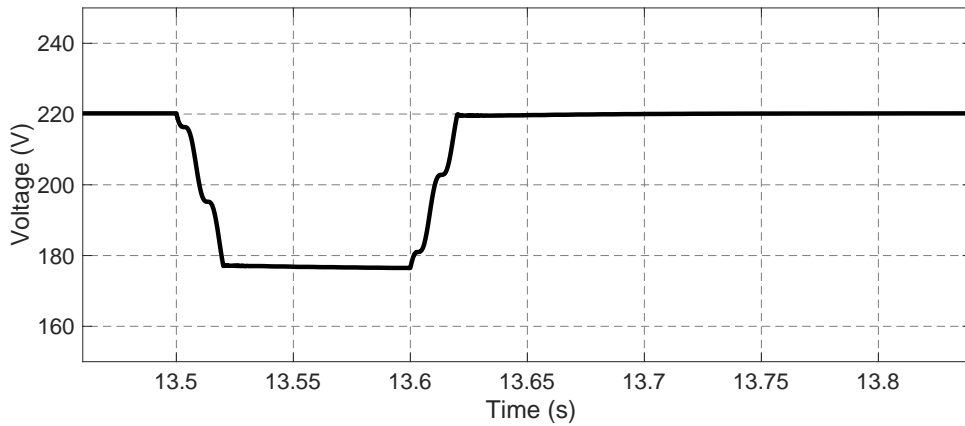


FIGURE 3.17: Grid-connected performance following a voltage event: synchronverter phase voltage v_o

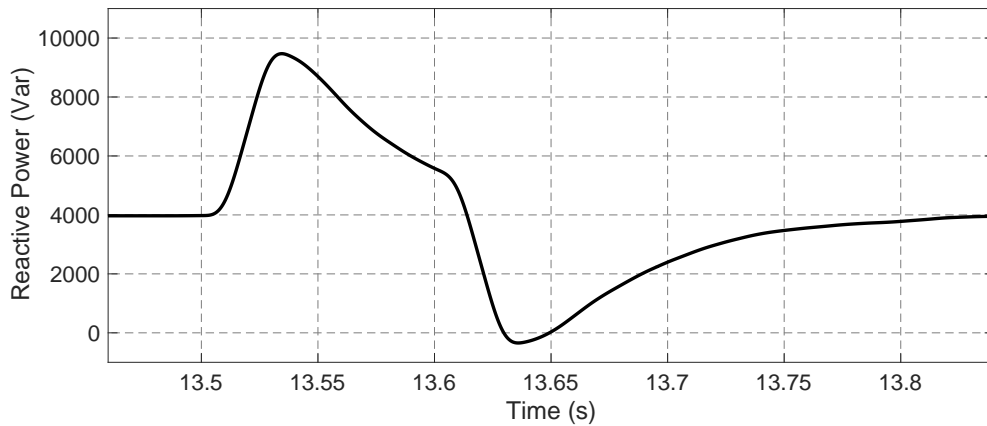


FIGURE 3.18: Grid-connected performance following a voltage event: synchronverter reactive power Q_o

was dropped from 220 V to 176 V, i.e. by 20% and restored to nominal value after 0.1 s.

Figure 3.17 shows variations in synchronverter phase voltage v_o . The synchronverter voltage was reduced following the grid voltage and restored to nominal value after the grid voltage restoration. The response time was 21 ms.

Synchronverter reactive power output Q_o is shown in Figure 3.18. Since the synchronverter was operating in Q -mode, the reactive power Q_o was increased by 50% of the base kVA at the start of the disturbance, i.e. at $t = 13.5$ s and then went to settle down to the reference value Q_r . Similar behavior was observed at

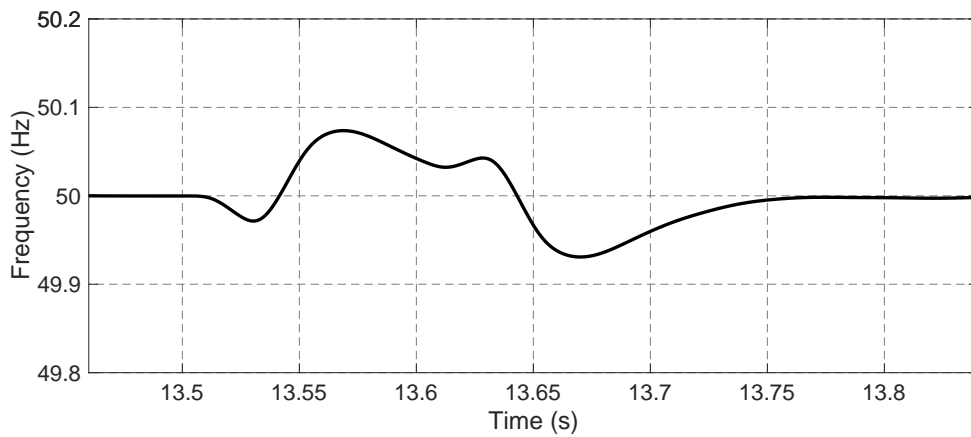


FIGURE 3.19: Grid-connected performance following a voltage event: synchronverter frequency f_o

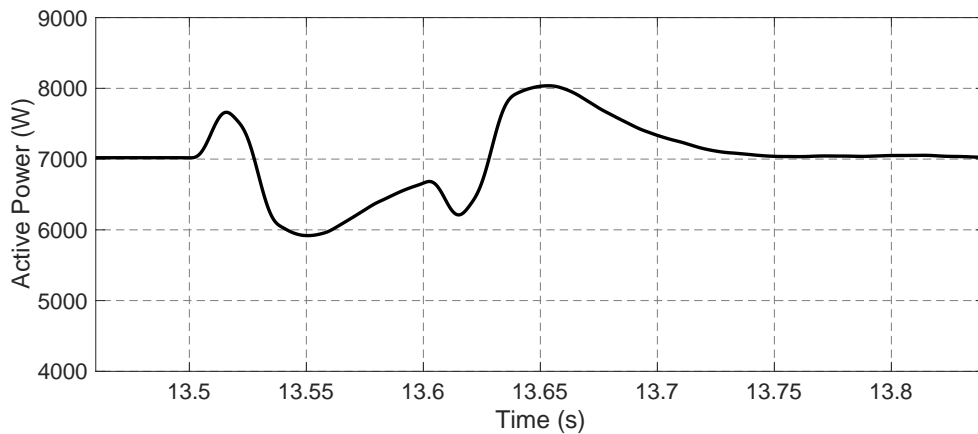


FIGURE 3.20: Grid-connected performance following a voltage event: synchronverter active power P_o

$t = 13.6$ s when the grid voltage was restored. After the grid voltage restoration, Q_o again settled down to the reference value Q_r as shown in Figure 3.18. The response time was 32 ms and the settling time was 242 ms.

Small variations were seen in the frequency f_o and active power output P_o of the synchronverter as shown in Figures 3.19 and 3.20 respectively. This was due to the slight variations in grid frequency during the voltage event. The synchronverter frequency was varied by ± 0.07 Hz i.e. $\pm 0.14\%$ of the nominal value. To counter these variations in f_o , the synchronverter output power P_o was varied by $\mp 10\%$ of the base kVA. When f_o was increased by 0.14%, P_o was reduced by 10% and vice

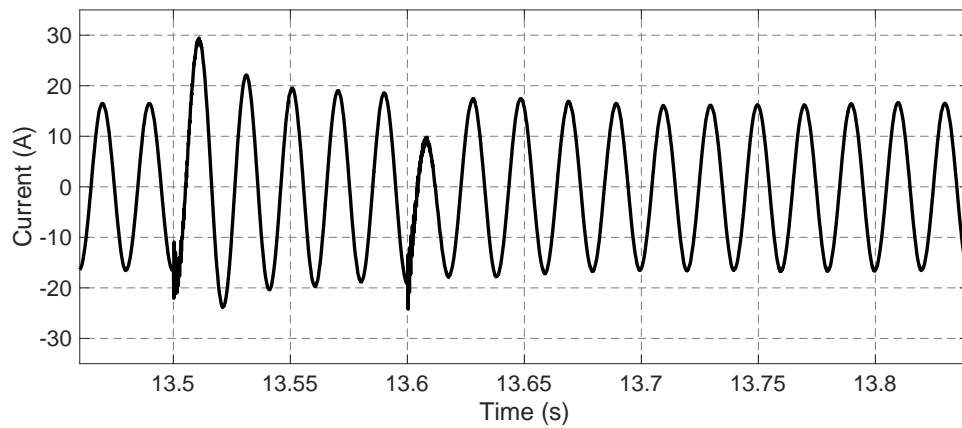


FIGURE 3.21: Grid-connected performance following a voltage event: synchronverter output current i_o

versa as shown in Figure 3.20. In this way the synchronverter supported the grid frequency.

Figure 3.21 shows synchronverter output current i_o . During the voltage event, the maximum current was found to be 1.9 times of the normal current. This is again acceptable as mentioned earlier in previous section.

Results obtained from grid-connected performance prove that the synchronverter exhibited excellent fault-ride through capability during grid dynamics and adjusted its reactive power to support voltage during the grid voltage fluctuations. At the same time, it adjusted its active power to support grid frequency.

3.4.3 Transfer from Grid-Connected to Stand-Alone Mode

This part of simulation was performed to verify the seamless transfer of synchronverter from grid-connected to stand-alone mode. Islanding was done at $t = 14$ s by opening the tie-breaker.

Synchronverter frequency f_o , output phase voltage v_o and current i_o are shown in Figure 3.22, 3.23 and 3.24, respectively. It was observed that the synchronverter output frequency and voltage were not changed dramatically when grid was disconnected while supplying local load. Maximum variations in frequency were only

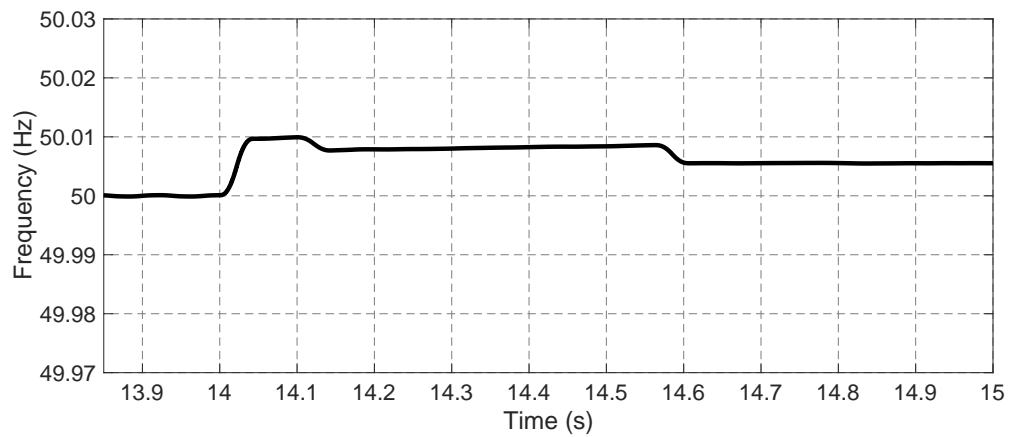


FIGURE 3.22: Transfer from grid-connected to stand-alone mode: synchronverter frequency f_o

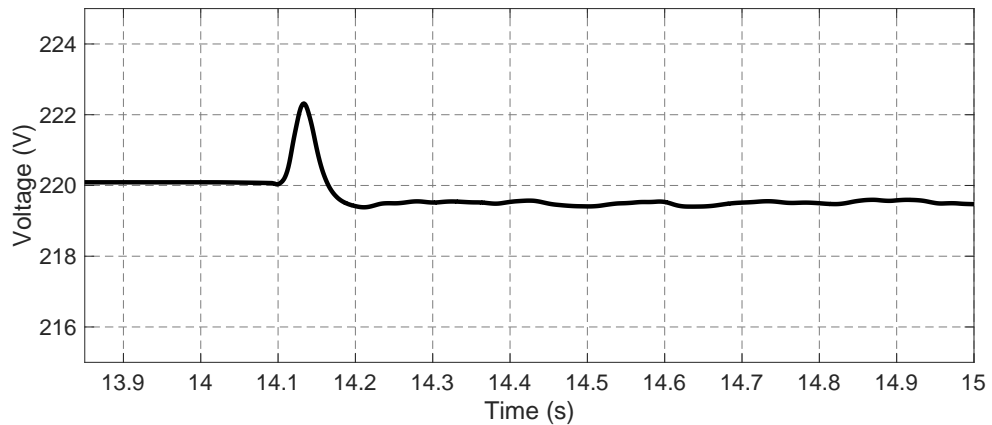


FIGURE 3.23: Transfer from grid-connected to stand-alone mode: synchronverter rms phase voltage v_o

0.01 Hz that is equal to 0.02% of the nominal value at the islanding instant as shown in Figure 3.22. A negligible surge of 0.95% of nominal value was observed in voltage waveform at the islanding instant as shown in Figure 3.23.

Figure 3.24 shows that the synchronverter current was decreased on loss of grid. This was due to the fact the synchronverter was injecting power into the grid. On loss of grid, the synchronverter output power was again restricted by the local demand as discussed in Section 3.4.1. Synchronverter power curves during the transition between stand-alone and grid-connected modes are given in Chapter 4 and Chapter 5.

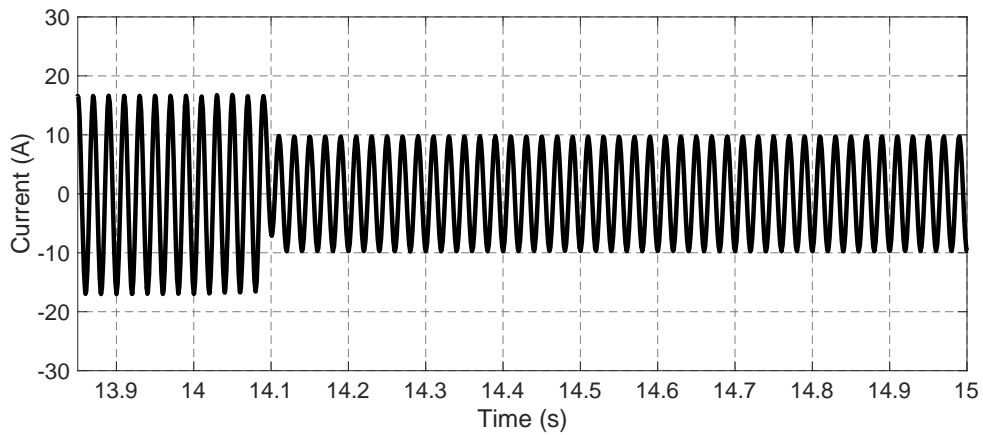


FIGURE 3.24: Transfer from grid-connected to stand-alone mode: synchronverter current i_o

It can be seen from the results that the synchronverter had the inherent feature of seamless transfer from grid-connected to stand-alone mode without making any change in its controller. It offered a smooth transition and therefore, is capable of integrating RERs based grids and DGs into future power grid.

3.5 Summary

In this chapter, synchronverter design is discussed in details using mathematical model of synchronous generator. Later on, the performance of synchronverter is evaluated in both stand-alone and grid-connected mode.

In stand-alone mode, the effect of variations in local connected load on synchronverter performance is evaluated. It was observed that the synchronverter maintained its voltage and frequency irrespective of the variations in the local connected load. Then the grid-connected performance is studied under strong as well as weak grid conditions. Synchronverter supported grid frequency and voltage by varying its active and reactive power. Finally, transfer from grid-connected mode to stand-alone mode is investigated. Synchronverter offered seamless transition from grid-connected to stand-alone mode without any change required in its controller.

From the results, it is clear that the synchronverter has ability to perform like synchronous generator in both operating modes as well as during the transitions between the operating modes. Moreover, in doing so, it doesn't need any PLL-based synchronization unit like other VSMS. Therefore, synchronverter is a strong contender for integrating RERs into future power grid.

Chapter 4

Design and Evaluation of Proposed Auto-Synchronizer

Synchronverter has inherent capability to remain synchronized with grid without any dedicated synchronization unit. Moreover, synchronverter offers seamless transfer from grid-connected to stand-alone mode without any change required in the controller. However, it requires a synchronization unit to track grid phase angle for initial synchronization with grid prior to grid-connection [87].

Due to the complexity, inefficiency, and deteriorating performance of PLL in weak grid, PLL-less synchronization units are proposed in literature. Existing PLL-less synchronizers lack seamless transfer capability except the DRMSV-based synchronizer [102] reported in literature.

This chapter presents the limitations of DRMSV-based synchronizer, designing and advantages of proposed auto-synchronizer and the performance comparison between proposed auto-synchronizer and DRMSV-based synchronizer. Testing of seamless transfer capability of proposed auto-synchronizer is also discussed in this chapter.

An ideal source is assumed at the dc side of synchronverter. All other parameters used in the simulations are same as that used in Chapter 3.

4.1 DRMSV-Based Synchronizer

Figure 4.1 illustrates the schematic diagram of DRMSV-based synchronizer. The RMS value V_d of the difference between v_o and grid voltage v_g is minimized by a Proportional-Integral (PI) controller. When V_d becomes less than the threshold voltage V_{Th} , connection signal is sent to the tie-breaker. The threshold voltage is equal to the few percent of nominal voltage. Threshold value of 12 V is selected in this study.

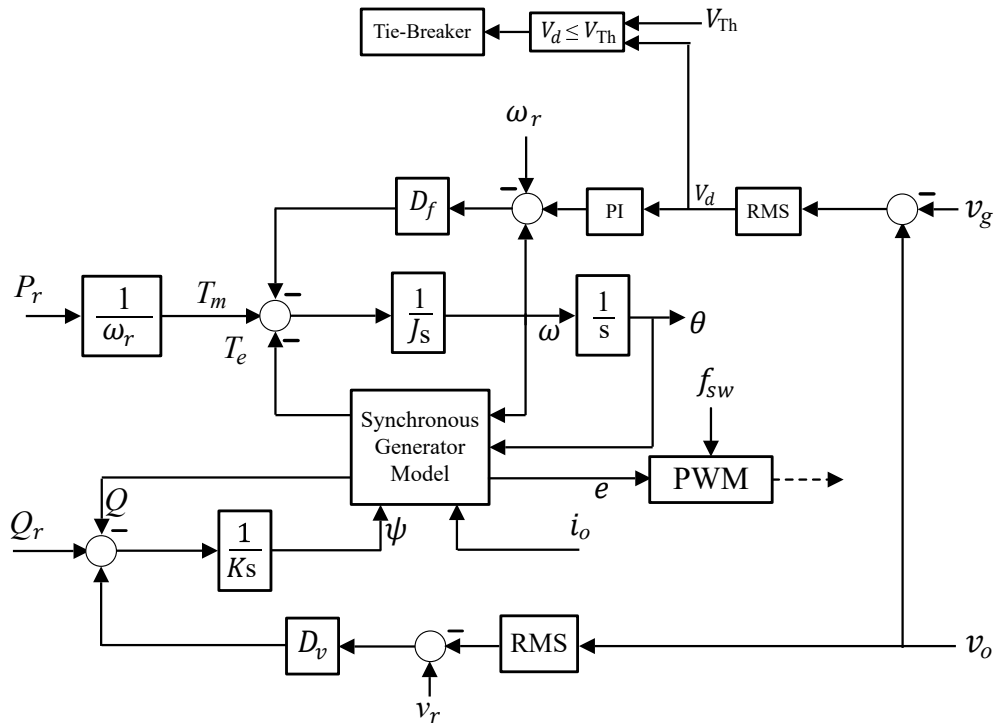


FIGURE 4.1: Schematic diagram of DRMSV-based synchronizer [102]

Although the DRMSV-based approach added the seamless transfer capability in synchronverter. This feature enabled synchronverter to supply critical local load like hospital, military unit, data center or intelligence center during synchronization process. However, this approach has unwanted delays and uncertainties in following scenarios.

- Scenario 1: synchronverter voltage v_o lags grid voltage v_g
- Scenario 2: significant difference between magnitudes of v_o and v_g

These scenarios are explained in details in upcoming sections.

4.1.1 Scenario 1: v_o lags v_g

Figures 4.2 and 4.3 show the performance of DRMSV-based synchronizer depending upon the phase angle of synchronous voltage v_o . When v_o leads v_g , as shown in Figure 4.2, DRMSV-based synchronizer achieve fast synchronization. Since, the RMS value is always positive, the PI controller output remains positive. This results in slowing down the virtual rotor of synchronverter to synchronize with grid. Therefore, V_d decreases in this case and synchronverter synchronizes with grid within few cycles.

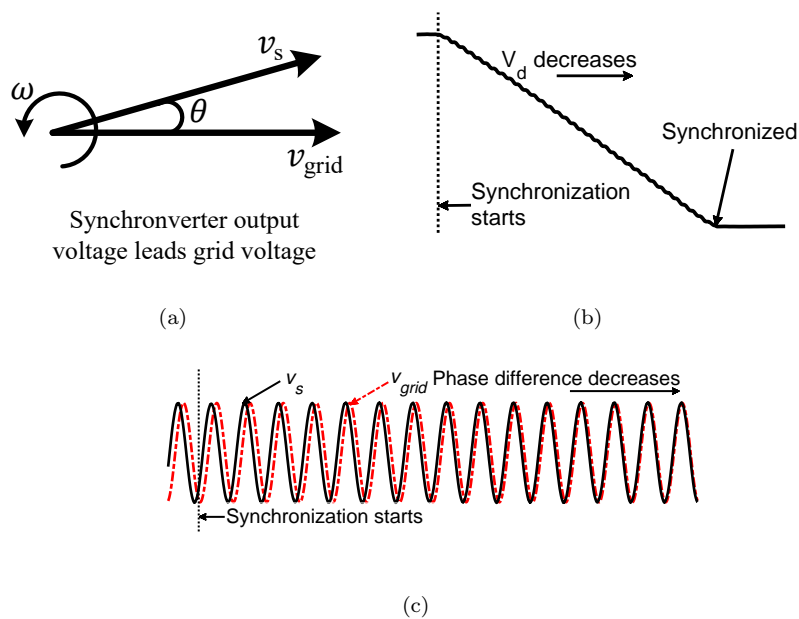


FIGURE 4.2: Performance of DRMSV-based self-synchronization [102] when v_o leads v_g by angle θ

When v_o lags behind v_g , as shown in Figure 4.3, the DRMSV synchronizer results in unwanted delays. To avoid this, synchronverter virtual rotor must speed up to synchronize with grid. However, due to RMS value, the PI input is always positive in this approach. The synchronverter virtual rotor always slows down to synchronize with grid. This leads to increased RMS difference V_d as well as phase difference as shown in Figure 4.3. In this way the phase difference first increases to

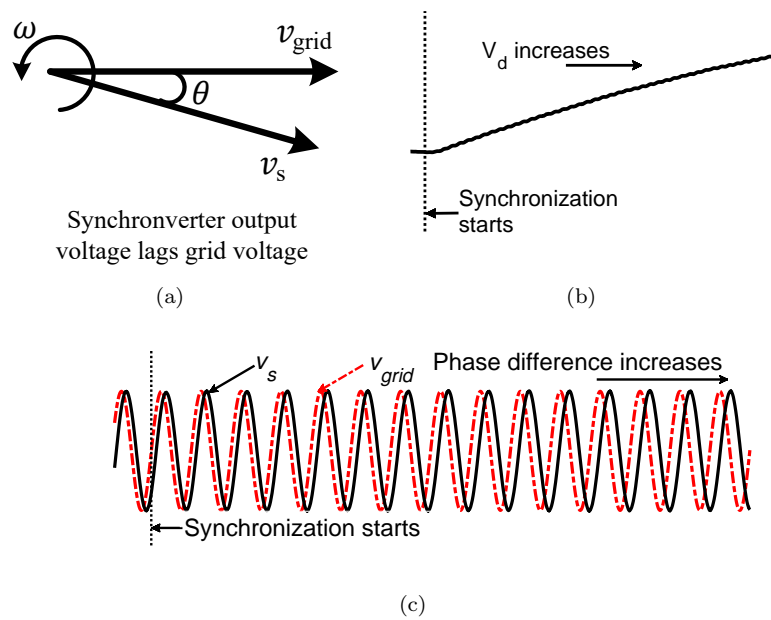


FIGURE 4.3: Performance of DRMSV-based self-synchronization [102] when v_o lags v_g by angle θ

180° and then decreases to 0° . Therefore, the DRMSV synchronizer [102] results in unwanted delays in synchronization in this scenario.

4.1.2 Scenario 2: Significant Difference Between $|v_o|$ & $|v_g|$

Figure 4.4 shows the performance of DRMSV-based approach depending upon the difference between $|v_o|$ and $|v_g|$. Figure 4.4(a) shows v_o and v_g when the grid voltage magnitude becomes 110% of the nominal value. Figure 4.4(b) shows both voltages for the case $|v_g|$ drops to 90% of the nominal value. Since the DRMSV-based synchronizer controls only the virtual speed of synchronverter, the difference between $|v_o|$ and $|v_g|$ remains constant. This can be seen in Figures 4.4(a) and 4.4(b).

Figure 4.4(c) shows that the error V_d varies periodically depending upon the phase difference between v_o and v_g . The smallest value of V_d ($= |v_o - v_g|$) corresponds to 0° phase difference. Similarly, the largest value of V_d ($=$ twice of $|v_o|$) occurs at 180° phase difference. Since, V_d never goes below V_{Th} , the synchronverter is unable to synchronize with the grid in this scenario.

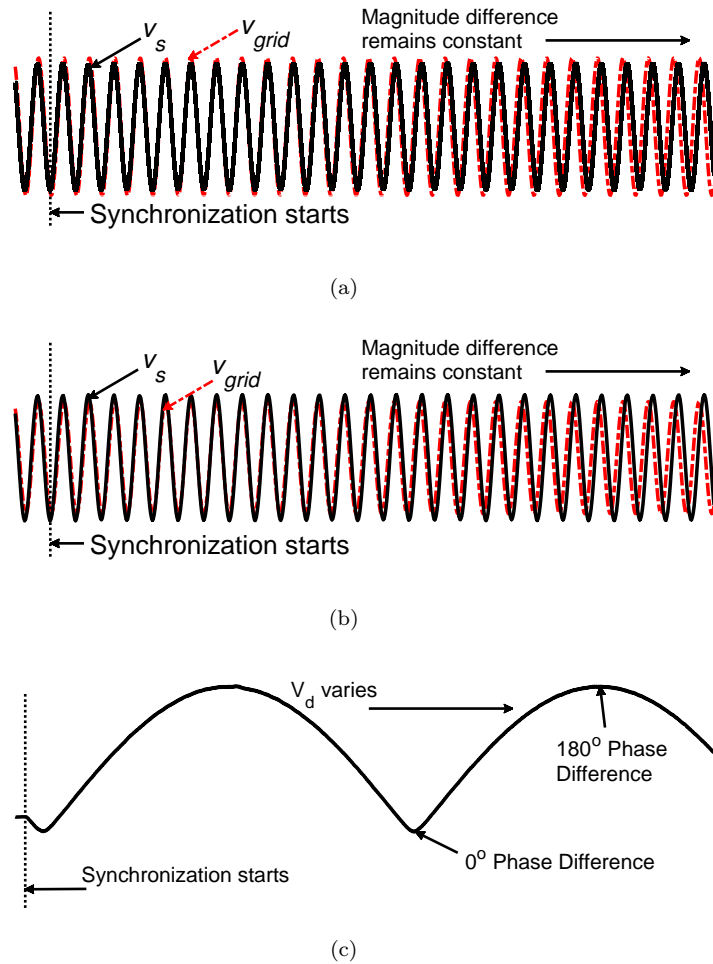


FIGURE 4.4: Performance of DRMSV-based self-synchronization [102] when;
 (a) v_g becomes 110% of nominal value, (b) v_g drops to 90% of nominal value,
 (c) RMS difference V_d between v_o and v_g for both cases

Although, the problem of failed synchronization can be solved by increasing V_{Th} . However, the increased V_{Th} will increase surge current at breaker closure. This surge current can cause unequal stress in transformer windings and can damage its insulation system [146].

4.2 Design of Proposed Auto-Synchronizer

The main objective is to realize the seamless transfer of synchronverter from stand-alone mode to grid-connected mode without shutting down the local connected load. For this, the phase and magnitude difference between the synchronverter output voltage v_o and grid voltage v_g is to be minimized. An enhanced, PLL-less

control loop shown in Figure 3.3. Applying simple mathematics on F_1 yields:

$$\begin{aligned} F_1 &= V_o \sin(\omega_r t + \theta_o) \sin(\omega_r t) \\ &= \frac{1}{2} V_o [\cos(\theta_o) - \cos(2\omega_r t + \theta_o)] \end{aligned} \quad (4.4)$$

Similarly,

$$\begin{aligned} F_2 &= V_o \sin(\omega_r t + \theta_o) \cos(\omega_r t) \\ &= \frac{1}{2} V_o [\sin(\theta_o) + \sin(2\omega_r t + \theta_o)] \end{aligned} \quad (4.5)$$

By taking average of F_1 and F_2 over one cycle of fundamental frequency, factors $\cos(2\omega_r t + \theta_o)$ and $\sin(2\omega_r t + \theta_o)$ become zero.

$$\overline{F_1} = \frac{1}{2} V_o \cos(\theta_o) \quad (4.6)$$

$$\overline{F_2} = \frac{1}{2} V_o \sin(\theta_o) \quad (4.7)$$

Now, θ_o can be calculated by following equation:

$$\theta_o = \tan^{-1} \left(\frac{\overline{F_2}}{\overline{F_1}} \right) \quad (4.8)$$

Similarly, θ_g of the grid voltage is calculated, assuming grid frequency equal to the nominal value. The difference between θ_o and θ_g is sent to the PI controller with gains denoted by K_f and I_f in Table 4.1. The input to the PI controller is positive when v_o leads v_g i.e., $\theta_o - \theta_g > 0$, and is negative when v_o lags v_g i.e., $\theta_o - \theta_g < 0$. The PI controller has the job to drive its input to 0. The output of this PI controller ω_s is used to adjust ω_r during synchronization process as shown in Figure 4.5.

Depending upon the sign of ω_s , the synchronverter virtual rotor speeds up or slows down to achieve fast synchronization. When v_o leads v_g , ω_s decreases ω_r . In this way, synchronverter virtual rotor slows down to synchronize with grid. Similarly, when v_o lags v_g , ω_s increases ω_r due to which virtual rotor speeds up to synchronize with grid. Thus, fast synchronization is achieved independent of the phase of the

synchronverter voltage with respect to grid. Therefore, the problem of unwanted delays associated with DRMSV-based approach is addressed by proposed auto-synchronizer.

To minimize the effect of significant difference between $|v_o|$ and $|v_g|$ another PI controller with gains K_v and I_v is used. This PI controller has also the job of driving its input to 0. The output of this PI controller v_s is used to adjust v_r during synchronization process as shown in Figure 4.5.

When $|v_g|$ is higher than $|v_o|$, v_s increases the reference voltage v_r of the voltage control loop and vice versa. In this way, the synchronverter voltage magnitude follows the grid voltage magnitude to drive V_d below threshold voltage V_{Th} . Thus, the proposed auto-synchronizer gives the promising solution of self-synchronization in both scenarios discussed in Sections 4.1.1 and 4.1.2.

It is worth to be noted that unlike DRMSV-based approach, V_d is not fed to the PI controller to achieve synchronization. Instead, it is only used as criteria for tie-breaker closure. In proposed auto-synchronizer, V_d always decreases when the phase and magnitude difference decreases. Equations (4.1) – (4.8) are similar to Costas loop [147, 148] as they are the fundamentals of sinusoidal signals.

During synchronization, the controller is fed with the actual output current. No need to achieve synchronization by driving this current to zero as in virtual impedance based synchronization approach [88, 116]. In proposed synchronizer, the synchronization will be achieved while supplying actual load current. Therefore, the synchronverter is able to supply uninterrupted power to the local connected load all the time. Also, the proposed synchronizer has no computational burden like tuning of complex parameters for the estimation of phase angles.

Further, as discussed earlier, the proposed synchronizer acts only during synchronization process. After tie-breaker closure, the proposed synchronizer is eliminated from the main controller at grid-connection. This is represented by switches S shown in Figure 4.5. Therefore, the proposed synchronizer has no effect on the synchronverter dynamic performance and system stability in grid-connected mode.

TABLE 4.1: Synchronizer parameters used in simulations

Parameters	Symbols	Values
Proportional gain	K_f	0.2
Integral gain	I_f	3.2
Proportional gain	K_v	0.1
Integral gain	I_v	1.8
Threshold voltage	V_{Th}	12 V

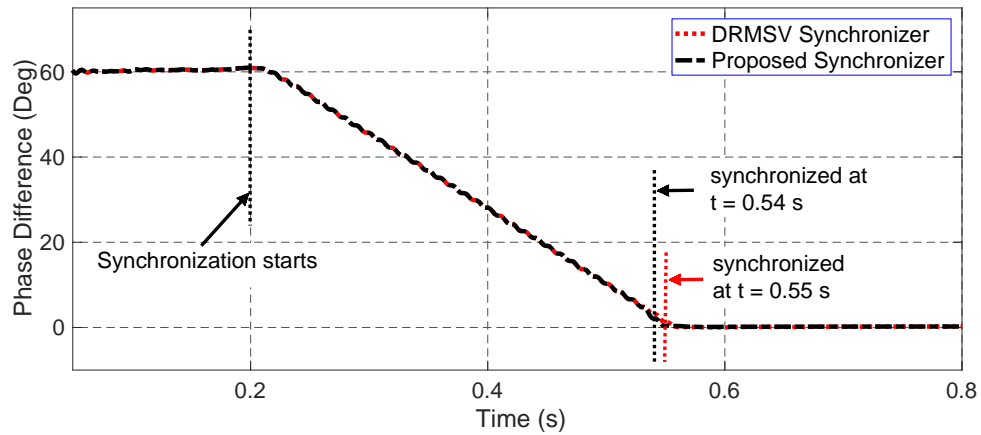
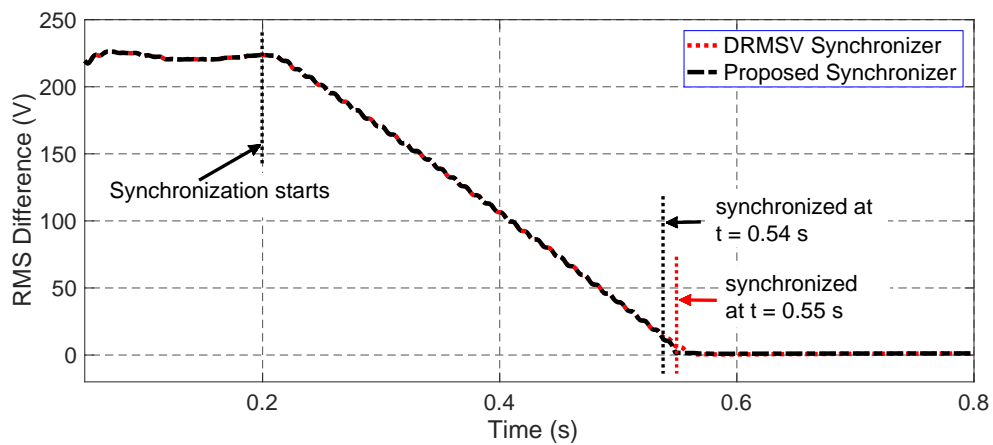
Synchronizer parameters used in the simulations are tabulated in Table 4.1. The PI gains tabulated in Table 4.1 are obtained by trial-and-error method.

4.3 Simulation Results and Discussions

The proposed auto-synchronizer was validated and compared with DRMSV-based synchronizer using simulations performed in MATLAB/Simulink. Tables 3.1 and 4.1 show the parameters used in the simulations. In all the cases, the synchronization process was initiated at $t = 0.2$ s. Proposed auto-synchronizer was tested and compared with DRMSV-based synchronizer for both scenarios, discussed in Sections 4.1.1 and 4.1.2. Results obtained from simulations are discussed in Sections 4.3.1 to 4.3.4. The seamless transfer capability during synchronization process is verified in Section 4.3.5.

4.3.1 Case-I: Grid Synchronization when v_o Led v_g

In this part of simulations, the proposed auto-synchronizer was compared with DRMSV synchronizer [102] when v_o led v_g . Simulations were started at $t = 0$ s with a local load connected at the output terminal. Synchronization process was initiated at $t = 0.2$ s. The initial phase difference between v_o and v_g was equal to 60° as shown in Figure 4.6. This phase difference resulted in RMS difference of 224 V, as shown in Figure 4.7 at the start of synchronization process.

FIGURE 4.6: Case-I: phase difference between v_o and v_g during synchronizationFIGURE 4.7: Case-I: RMS difference V_d between v_o and v_g during synchronization

With DRMSV synchronizer, the corrective value ω_s based on this 224 V RMS difference was fed to reference angular speed ω_r via PI controller as shown in Figure 4.1. Due to this ω_r was reduced to 311 rad/s during the synchronization process. The output frequency f_o of the synchronverter was equal to 49.5 Hz during the synchronization process as shown in Figure 4.8. All this indicated that the virtual rotor of synchronverter was slowed down to synchronize with grid. The PI controller of the DRMSV synchronizer drove the RMS difference to zero. Synchronization was achieved at $t = 0.55$ s as indicated in Figures 4.6 to 4.8.

With proposed auto-synchronizer, the corrective value ω_s based on 60° phase difference was fed to reference angular speed ω_r via PI controller as shown in Figure

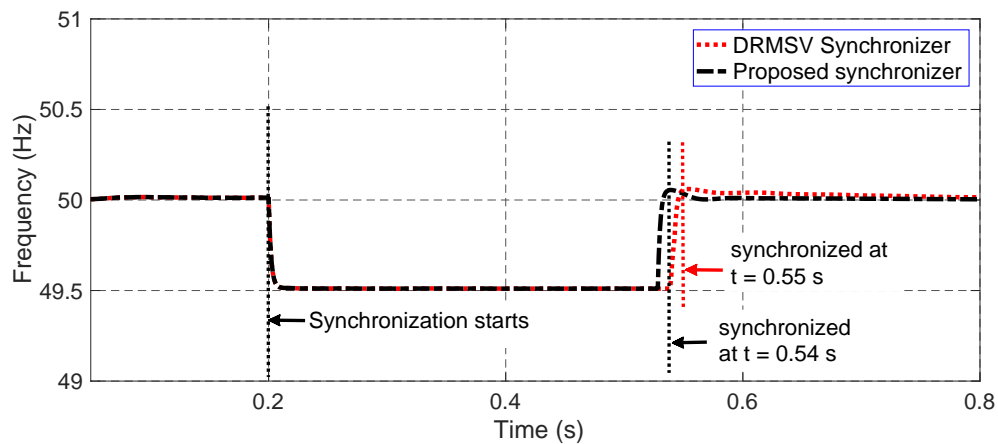


FIGURE 4.8: Case-I: synchronverter frequency f_o during synchronization

4.5. Due to this ω_r was reduced to 311 rad/s during the synchronization process. The output frequency was equal to 49.5 Hz similar to that of DRMSV synchronizer. The PI controller drove the angle difference to zero. Synchronization was achieved at $t = 0.54$ s as indicated in Figures 4.6 to 4.8.

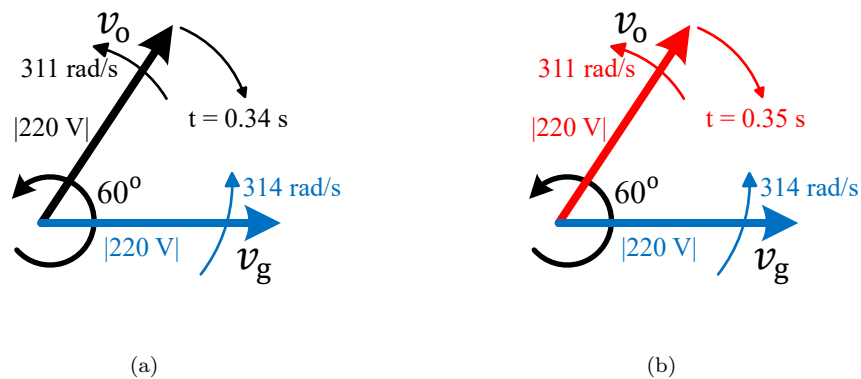


FIGURE 4.9: Case-I: phasor representation of synchronization process with (a) proposed auto-synchronizer, (b) DRMSV-based synchronizer

Although the working of both synchronizers was different, however, their performance was found similar in Case-I. Both synchronizers took almost same time to synchronize the synchronverter with grid. Figure 4.9 illustrates the phasor representation of the synchronization process in Case-I. In both Figures 4.9(a) and 4.9(b) phasor v_o leading v_g by 60° is rotating at a slower speed of 311 rad/s than v_g . It takes almost 0.34 s to synchronize with v_g . Table 4.2 presents the summary of Case-1 in tabular form.

TABLE 4.2: Comparison of proposed synchronizer with DRMSV synchronizer during synchronization process in Case-I

Metrics	Proposed Synchronizer	DRMSV-based Synchronizer
Initial phase difference ($\theta_o - \theta_g$)	60°	60°
Initial RMS difference (V_d)	224 V	224 V
Error signals	$(\theta_o - \theta_g)$ and $(v_o - v_g)$	V_d
Actions taken by synchronizer	ω_r reduced	ω_r reduced
Angular speed ω_o	311 rad/s	311 rad/s
Output voltage v_o	220 V	220 V
Synchronization	Achieved	Achieved
Time elapsed in synchronization	0.34 s	0.35 s
Improvement	Nil	
Remarks	Performance of both synchronizers were similar in this case	

4.3.2 Case-II: Grid Synchronization when v_o Lagged v_g

In this part of simulations, the proposed synchronizer was compared with DRMSV synchronizer [102] when v_o lagged v_g . Similar to the Case-I, the synchronization was initiated at $t = 0.2$ s. The initial phase difference between v_o and v_g was equal to -45° as shown in Figure 4.10. This phase difference resulted in RMS difference of 165 V, as shown in Figure 4.11 at the start of synchronization process.

Similar to Case-I, with DRMSV synchronizer, the reference angular speed ω_r of the synchronverter was again reduced to 311 rad/s during the synchronization process. Due to this the output frequency f_o of the synchronverter was again equal to 49.5 Hz for synchronizing with grid as shown in Figure 4.12. Since the synchronverter voltage was already lagging in this case, the reduction in ω_r resulted in further delays in achieving synchronization. In this case, the phase difference first increased to 180° and then decreased to 0° as shown in Figure 4.10.

Due to the phase difference $\theta_o - \theta_g$, the RMS difference V_d between v_o and v_g first increased to 422 V i.e. at 180° phase difference and then decreased below the threshold value at 0° phase difference as shown in Figure 4.11. Synchronization

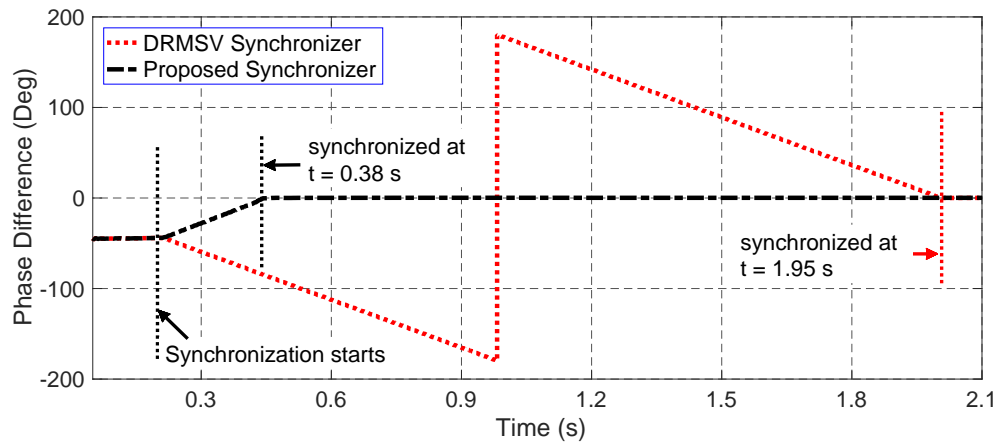


FIGURE 4.10: Case-II: phase difference between v_o and v_g during synchronization

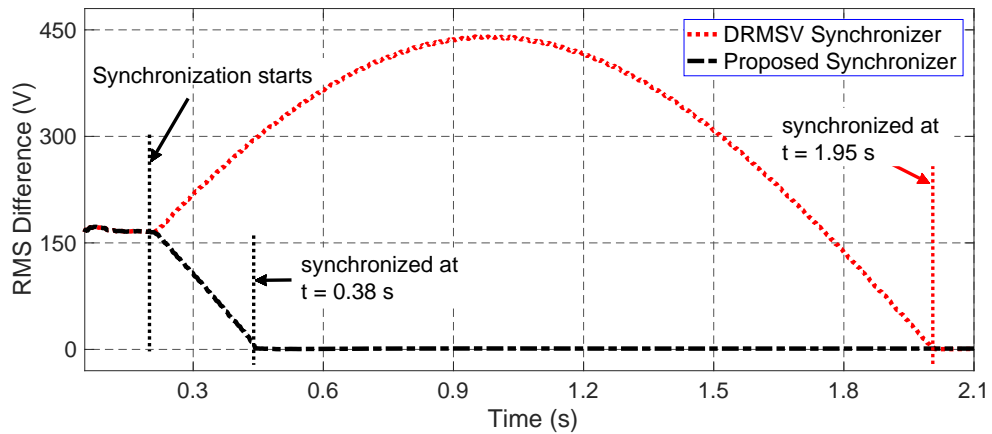


FIGURE 4.11: Case-II: RMS difference V_d between v_o and v_g during synchronization

with DRMSV synchronizer was achieved at $t = 1.95$ s as shown in Figures 4.10 to 4.12.

Since the error signal to be minimized in proposed auto-synchronizer was $\theta_o - \theta_g$, therefore, the proposed synchronizer increased the reference angular speed ω_r to 317 rad/s to synchronize with grid. Due to this the synchronverter frequency f_o became 50.5 Hz during the synchronization process as shown in Figure 4.12. In this case, the virtual rotor sped up to synchronize with grid.

With the proposed synchronizer, the synchronization was achieved at $t = 0.38$ s. The proposed synchronizer reduced the time elapsed in achieving synchronization

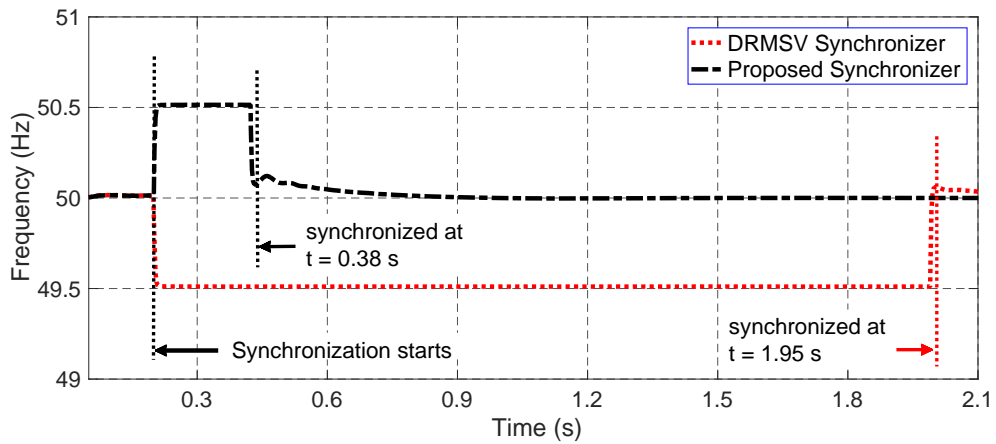


FIGURE 4.12: Case-II: synchronverter frequency f_o during synchronization

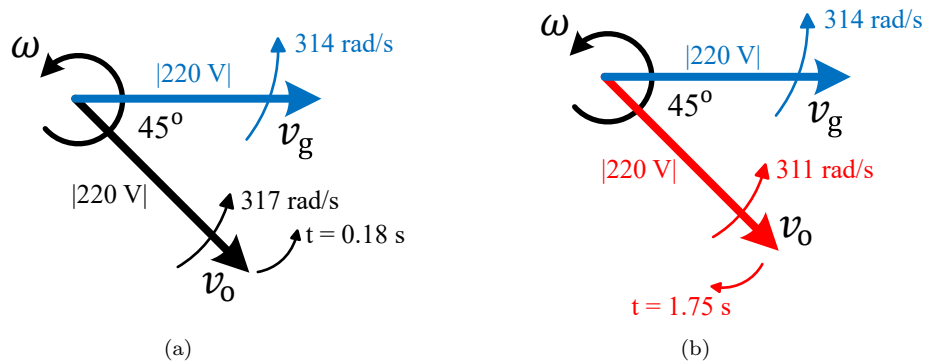


FIGURE 4.13: Case-II: phasor representation of synchronization process with (a) proposed auto-synchronizer, (b) DRMSV-based synchronizer

by 89.71%. Therefore, the proposed synchronizer addressed the issues of unwanted delays associated with DRMSV synchronizer.

Figure 4.13 illustrates the phasor representation of the synchronization process in Case-II in which phasor v_o is lagging behind phasor v_g by 45° . Figure 4.13(a) presents the synchronization process with proposed synchronizer. The phasor v_o is rotating at faster speed of 317 rad/s to catch the phasor v_g . It takes 0.18 s to synchronize with v_g . Figure 4.13(b) presents the synchronization process with DRMSV synchronizer. The phasor v_o is rotating slower at the speed of 311 rad/s. It takes 1.57 s more than the proposed synchronizer to achieve synchronization. Time elapsed in synchronization process is 1.75 s i.e. 89.71% higher than that of proposed synchronizer.

TABLE 4.3: Comparison of proposed synchronizer with DRMSV synchronizer during synchronization process in Case-II

Metrics	Proposed Synchronizer	DRMSV-based Synchronizer
Initial phase difference ($\theta_o - \theta_g$)	-45°	-45°
Initial RMS difference (V_d)	165 V	165 V
Error signals	$(\theta_o - \theta_g)$ and $(v_o - v_g)$	V_d
Actions taken by synchronizer	ω_r increased	ω_r reduced
Angular speed ω_o	317 rad/s	311 rad/s
Output voltage v_o	220 V	220 V
Synchronization	Achieved	Achieved
Time elapsed in synchronization	0.18 s	1.75 s
Improvement	Time elapsed in synchronization was reduced by 89.71% by the proposed synchronizer	
Remarks	Proposed synchronizer addressed the unwanted delays issue associated with DRMSV synchronizer	

Table 4.3 presents the summary of Case-II in tabular form. It can be concluded from the results obtained from Case-I and Case-II that the proposed synchronizer provided a fast synchronization with grid independent of the lagging or leading phase angle of synchronverter voltage.

4.3.3 Case-III: Grid Synchronization when $|v_g| = 90\%$ of V_n

In this case, the grid voltage magnitude was kept to 90% of the nominal value. The synchronization was initiated at $t = 0.2$ s. Figure 4.14 shows synchronverter output voltage v_o during synchronization with both approaches. The initial phase difference between v_o and v_g was 60° , similar to that of Case-I, as shown in Figure 4.15.

It was observed that the magnitude and phase difference between v_o and v_g resulted in initial RMS difference V_d of 212 V at the start of synchronization process as shown in Figure 4.16. With DRMSV synchronizer, the error signal was V_d ,

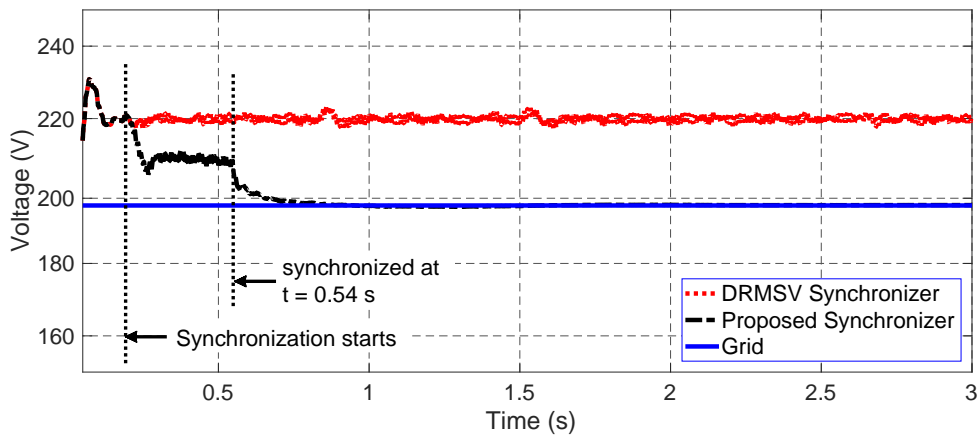


FIGURE 4.14: Case-III: synchronverter phase voltage v_o and grid voltage v_g during synchronization

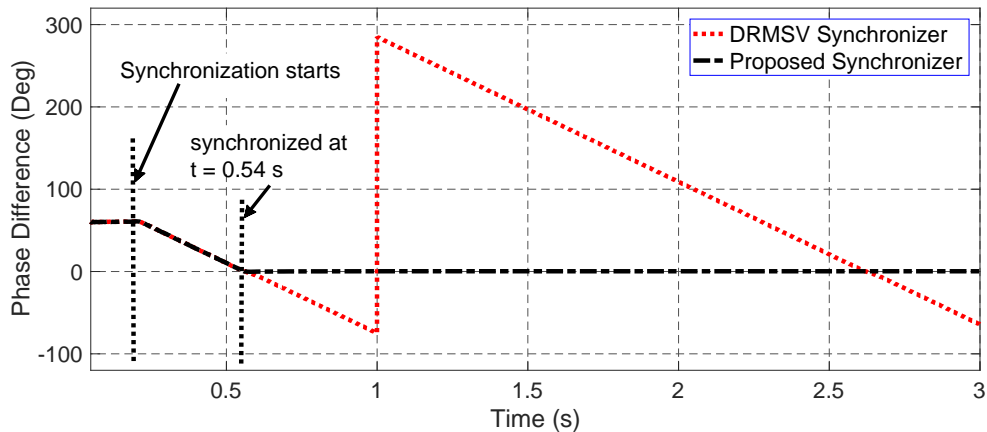


FIGURE 4.15: Case-III: phase difference between v_o and v_g during synchronization

therefore, the only action taken in this case was the reduction in the reference angular speed ω_r similar to that of Case-I and Case-II. The difference in voltage magnitude was not addressed by DRMSV synchronizer at all. The phase difference started decreasing at the start of synchronization process and became zero at $t = 0.54$ s, as shown in Figure 4.15. Although both v_o and v_g were in phase at $t = 0.54$ s, however, the synchronization was not achieved due to the magnitude difference. Therefore, the phase difference varied periodically as seen in the Figure 4.15.

Based on the variations in phase difference discussed above, the RMS difference V_d between v_o and v_g also varied periodically. The minimum value of V_d was 22

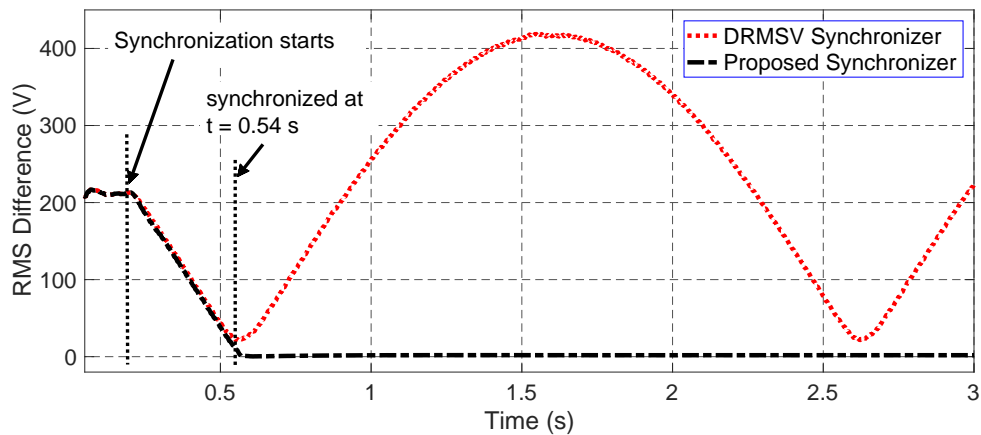


FIGURE 4.16: Case-III: RMS difference V_d between v_o and v_g during synchronization

V at $t = 0.54$ s corresponding to 0° phase difference while the maximum value of 422 V was at $t = 1.6$ s corresponding to 180° phase difference between v_o and v_g . Since, V_d never went below the threshold voltage V_{Th} , the DRMSV synchronizer failed to synchronize the synchronverter with grid.

The proposed synchronizer observed both error signals i.e., the phase difference as well as the magnitude difference between v_o and v_g . As a result, it reduced the reference angular speed ω_r as well as the reference voltage v_r of the voltage control loop shown in Figure 4.5. The virtual rotor of synchronverter was slowed down to 311 rad/s and the output frequency f_o became 49.5 Hz during synchronization process, similar to Case-I. At the same time the synchronverter output voltage v_o was reduced to 209 V, as shown in Figure 4.14, to synchronize the synchronverter with grid.

With proposed synchronizer, both phase and magnitude differences between v_o and v_g were reduced during synchronization process. The RMS difference V_d went below the threshold voltage V_{Th} and the synchronization was achieved at $t = 0.54$ s as shown in Figures 4.14 to 4.16.

Figure 4.17 illustrates the phasor representation of the synchronization process in Case-III in which phasor v_o is leading phasor v_g by 60° and the magnitude of v_g is 198 V. Figure 4.17(a) presents the synchronization process with proposed

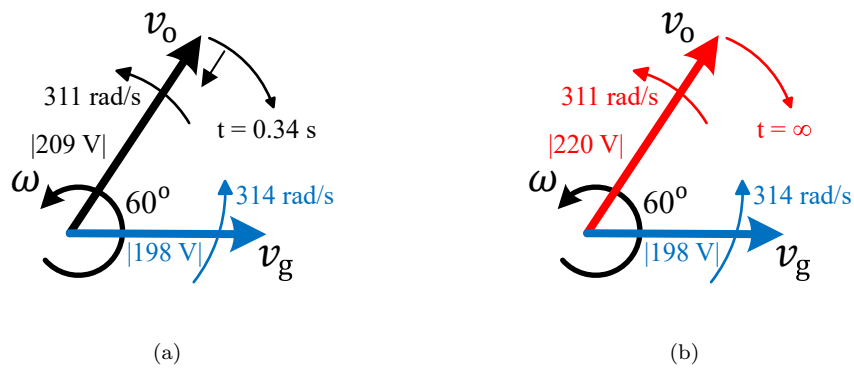


FIGURE 4.17: Case-III: phasor representation of synchronization process with (a) proposed auto-synchronizer, (b) DRMSV-based synchronizer

TABLE 4.4: Comparison of proposed synchronizer with DRMSV synchronizer during synchronization process in Case-III

Metrics	Proposed Synchronizer	DRMSV-based Synchronizer
Initial voltage magnitude difference ($v_o - v_g$)	22 V	22 V
Initial phase difference ($\theta_o - \theta_g$)	60°	60°
Initial RMS difference (V_d)	212 V	212 V
Error signals	$(\theta_o - \theta_g)$ and $(v_o - v_g)$	V_d
Actions taken by synchronizer	ω_r reduced and v_r reduced	ω_r reduced
Angular speed ω_o	311 rad/s	311 rad/s
Output voltage v_o	209 V	220 V
Synchronization	Achieved	Failed
Time elapsed in synchronization	0.34 s	∞
Improvement	Proposed synchronizer synchronized the synchronverter while DRMSV synchronizer failed	
Remarks	Proposed synchronizer addressed the uncertainties issue associated with DRMSV synchronizer	

synchronizer. The phasor v_o is rotating at slower speed of 311 rad/s to catch the phasor v_g . The magnitude of v_o is also reduced to 209 V to synchronize with v_g . It takes 0.34 s to synchronize with v_g .

Figure 4.17(b) presents the synchronization process with DRMSV synchronizer.

The phasor v_o is rotating at slower speed of 311 rad/s to catch the phasor v_g . However, the magnitude of v_o is higher than that of v_g . Due to this difference both phasors can not be synchronized. Therefore, an infinite time is required to achieve synchronization.

Table 4.4 presents the summary of Case-III in tabular form. It can be concluded from the results of this section that the proposed synchronizer has addressed the limitations and uncertainties in synchronization associated with DRMSV synchronizer.

4.3.4 Case-IV: Grid Synchronization when $|v_g| = 110\%$ of V_n

In this case, the grid voltage magnitude was kept to 110% of the nominal value. The synchronization was initiated at $t = 0.2$ s. Figure 4.18 shows synchronverter output voltage v_o during synchronization with both approaches. The initial phase difference between v_o and v_g was 60° , similar to that of Case-I and Case-III, as shown in Figure 4.19.

It was observed that the magnitude and phase difference between v_o and v_g resulted in initial RMS difference V_d of 234 V at the start of synchronization process as shown in Figure 4.20. With DRMSV synchronizer, the error signal was V_d , therefore, the only action taken in this case was the reduction in the reference angular speed ω_r similar to that of Case-I to Case-III. Similar to Case-III, the phase difference started decreasing at the start of synchronization process and became zero at $t = 0.54$ s, as shown in Figure 4.19. Since the magnitude difference between v_o and v_g was not reduced by DRMSV synchronizer, it again failed to synchronize the synchronverter with grid. Both phase difference and the RMS difference varied periodically in a similar fashion as they varied in Case-III.

The proposed synchronizer again observed both error signals i.e., the phase difference as well as the magnitude difference between v_o and v_g . Based on these error signals, it reduced the reference angular speed ω_r and increased the reference

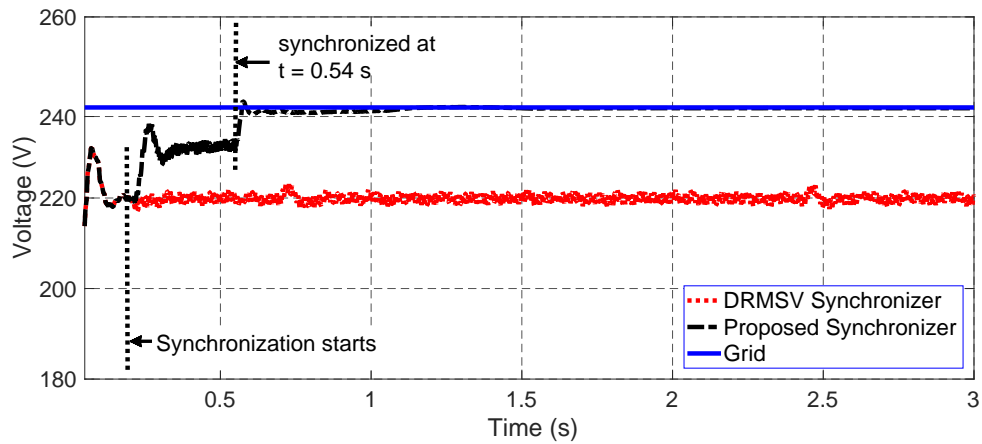


FIGURE 4.18: Case-IV: synchronverter phase voltage v_o and grid voltage v_g during synchronization

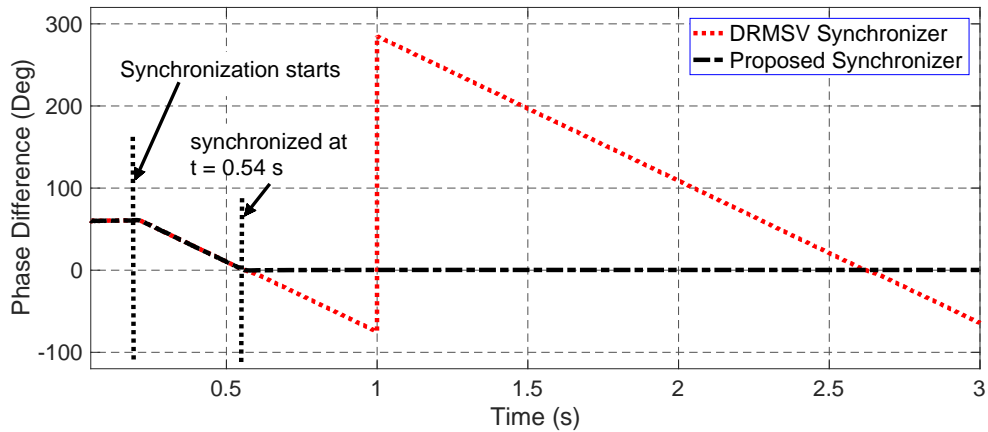


FIGURE 4.19: Case-IV: phase difference between v_o and v_g during synchronization

voltage v_r of the voltage control loop. The virtual rotor of synchronverter was slowed down to 311 rad/s and the output frequency f_o became 49.5 Hz during synchronization process, similar to Case-I. At the same time the synchronverter output voltage v_o was increased to 231 V, as shown in Figure 4.18, to synchronize the synchronverter with grid.

With proposed synchronizer, both phase and magnitude differences between v_o and v_g were reduced during synchronization process. The RMS difference V_d went below the threshold voltage V_{Th} and the synchronization was achieved at $t = 0.54$ s as shown in Figures 4.18 to 4.20.

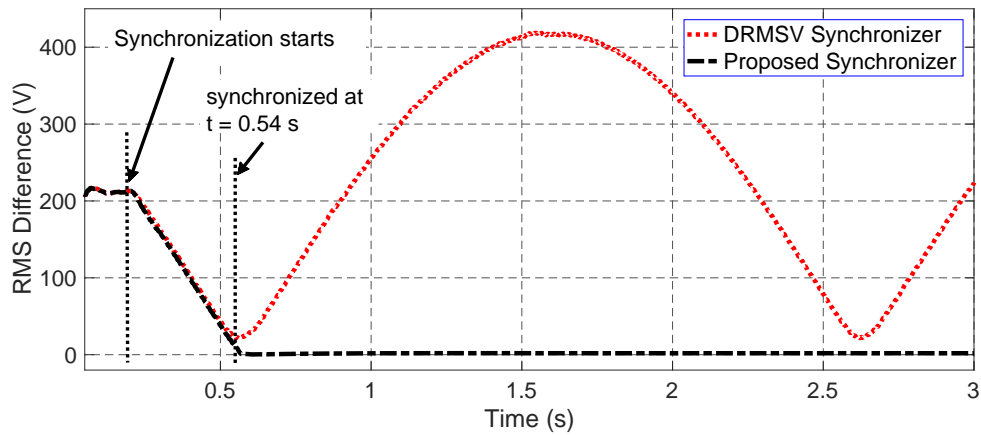


FIGURE 4.20: Case-IV: RMS difference V_d between v_o and v_g during synchronization

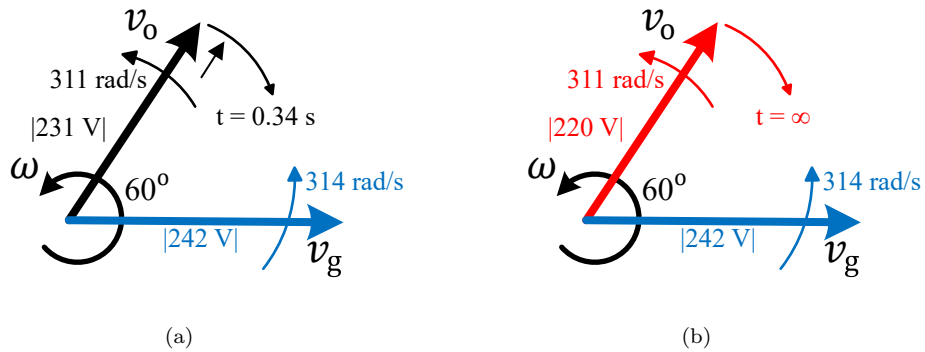


FIGURE 4.21: Case-IV: phasor representation of synchronization process with (a) proposed auto-synchronizer, (b) DRMSV-based synchronizer

Figure 4.21 illustrates the phasor representation of the synchronization process in Case-IV in which phasor v_o is leading phasor v_g by 60° and the magnitude of v_g is 242 V. Figure 4.21(a) presents the synchronization process with proposed synchronizer. The phasor v_o is rotating at slower speed of 311 rad/s to catch the phasor v_g . The magnitude of v_o is also increased to 231 V to synchronize with v_g . It takes 0.34 s to synchronize with v_g .

Figure 4.21(b) presents the synchronization process with DRMSV synchronizer. The phasor v_o is rotating at slower speed of 311 rad/s to catch the phasor v_g . However, the magnitude of v_o is lower than that of v_g . Due to this difference both phasors can not be synchronized. Therefore, an infinite time is required to achieve synchronization.

TABLE 4.5: Comparison of proposed synchronizer with DRMSV synchronizer during synchronization process in Case-IV

Metrics	Proposed Synchronizer	DRMSV-based Synchronizer
Initial voltage magnitude difference ($v_o - v_g$)	-22 V	-22 V
Initial phase difference ($\theta_o - \theta_g$)	60°	60°
Initial RMS difference (V_d)	234 V	234 V
Error signals	$(\theta_o - \theta_g)$ and $(v_o - v_g)$	V_d
Actions taken by synchronizer	ω_r reduced and v_r increased	ω_r reduced
Angular speed ω_o	311 rad/s	311 rad/s
Output voltage v_o	231 V	220 V
Synchronization	Achieved	Failed
Time elapsed in synchronization	0.34 s	∞
Improvement	Proposed synchronizer synchronized the synchronverter while DRMSV synchronizer failed	
Remarks	Proposed synchronizer addressed the uncertainties issue associated with DRMSV synchronizer	

Table 4.5 presents the summary of Case-IV in tabular form. Results obtained from Case-III and Case-IV show that the proposed synchronizer provided a fast, reliable, and promising solution of synchronverter initial synchronization with grid independent of significant magnitude difference between synchronverter and grid voltages. It has successfully addressed the uncertainties issues associated with DRMSV synchronizer.

4.3.5 Seamless Transfer Capability

As discussed in Section 4.2, the main objective of synchronizer designing was to realize the seamless transfer of synchronverter from stand-alone mode to grid-connected mode without shutting down the local connected load. DRMSV-based synchronizer has the seamless transfer capability. This feature should be retained by the proposed synchronizer.

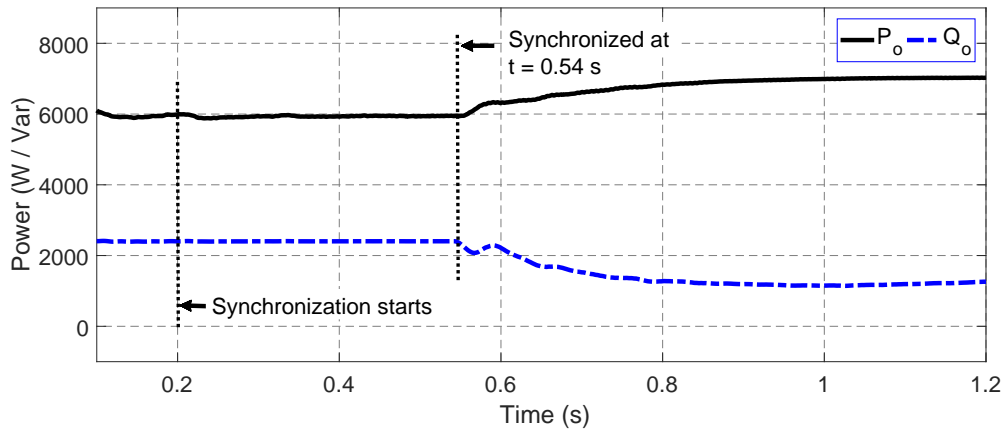


FIGURE 4.22: Synchronverter active and reactive power outputs P_o and Q_o , respectively in Case-I

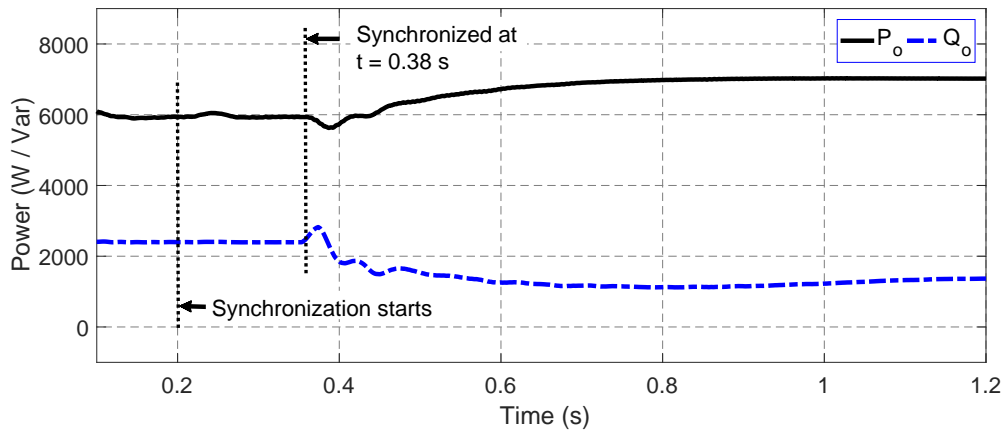


FIGURE 4.23: Synchronverter active and reactive power outputs P_o and Q_o , respectively in Case-II

The seamless transfer capability of the proposed synchronizer was verified in all the simulation cases (Case-I to Case-IV) discussed in Sections 4.3.1 to 4.3.4. Figure 4.22 to 4.25 show the synchronverter active power P_o and reactive power Q_o during the synchronization process.

In Case-I, the synchronverter was supplying a local load of $6000 + j2500$ VA before the start of the synchronization process. Figure 4.22 shows that the same load was supplied during the synchronization process due to proposed synchronizer. After the grid connection, the output powers P_o and Q_o tracked the reference values of 7000 W and 1000 Var, respectively, as discussed in the Section 3.4.2.1.

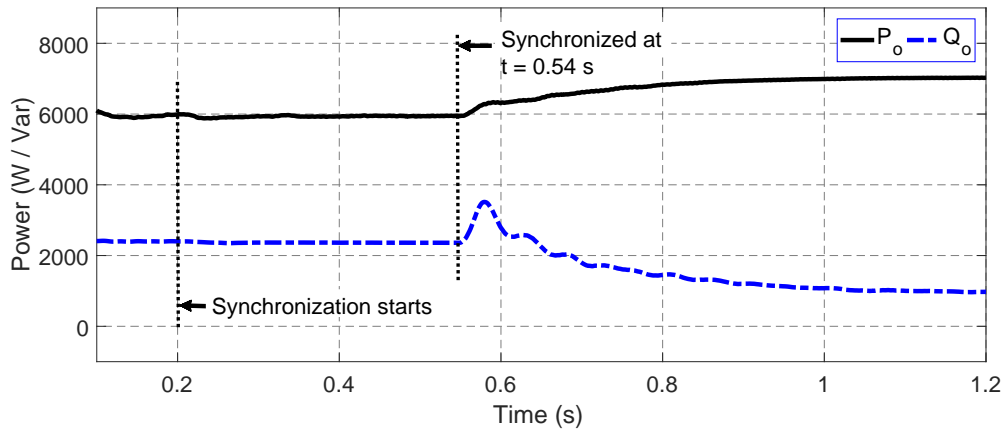


FIGURE 4.24: Synchronverter active and reactive power outputs P_o and Q_o , respectively in Case-III

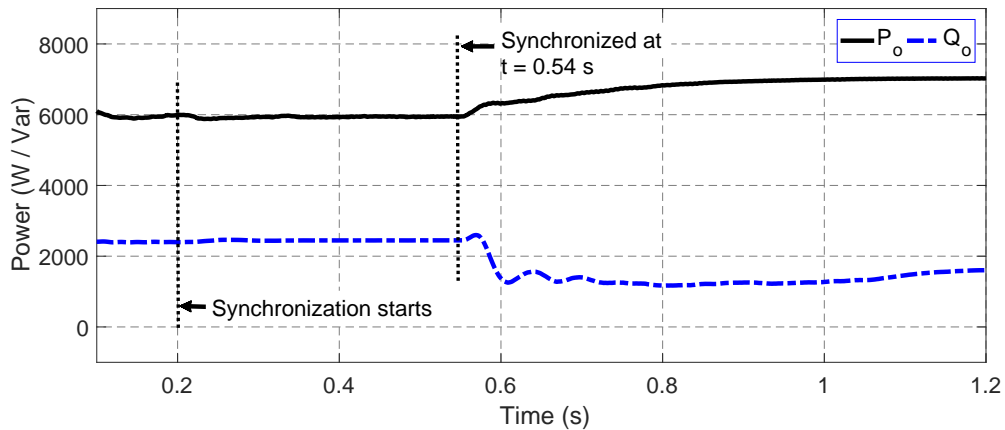


FIGURE 4.25: Synchronverter active and reactive power outputs P_o and Q_o , respectively in Case-IV

Figure 4.23 shows the active and reactive power of synchronverter during synchronization process in Case-II. Same results were obtained in this case too. The synchronverter was able to supply the load of $6000 + j2500$ VA during synchronization process. After synchronization, reference values were followed by the synchronverter similar to Case-I.

Similarly, in Case-III and Case-IV, the synchronverter supplied 6000 W and 2500 var during synchronization process, as shown in Figure 4.24. After grid connection, reference values were followed by the synchronverter similar to Case-I and Case-II.

It is clear from the results that with proposed synchronizer, the synchronverter was

able to supply power to the local connected load during synchronization process in each case. Therefore, the research objective of enabling seamless transfer capability in synchronverter is achieved successfully.

4.4 Summary

In this chapter an enhanced, PLL-less auto-synchronizer is proposed and compared with DRMSV synchronizer under adverse grid conditions. Results obtained by simulations showed that the proposed auto-synchronizer can improve the speed of synchronization process upto 99%. It has successfully addressed the uncertainties and unwanted delays associated with the DRMSV synchronizer reported in [102] while retaining the feature of seamless transfer capability. Therefore, the proposed auto-synchronizer:

- Ensured fast and promising synchronization with grid independent of the local voltage phase angle lagging or leading the grid phase.
- Ensured fast and promising synchronization with grid independent of the deviation of grid voltage magnitude from the nominal value.
- Ensured uninterrupted power supply to local load during synchronization process

Hence the primary objective of this research has been achieved.

Chapter 5

Solar Power Plant Integration into Power Grid

Almost all the literature about synchronverter assume an ideal source at the dc side of synchronverter. Chapters 3 and 4 discussed design of synchronverter and the proposed auto-synchronizer, respectively, also assuming an ideal source at dc bus. Ideal source means an infinite power can be drawn or supplied to the dc side at any time. This is not true practically. Since the motivation of this research is the integration of Solar Power Plant (SPP) into power grid, the designed synchronizer should be validated with non-ideal dc source. Also, the performance of synchronverter should be investigated with Solar Power Plant connected to it at the dc side.

This chapter presents the extension of the designed synchronverter of Chapter 3 to integrate 250 kW SPP into power grid. Performance of synchronverter with intermittent nature of PV panels is investigated in detail and the proposed auto-synchronizer of Chapter 4 is implemented on synchronverter having SPP at the dc bus.

Simulations are performed to test the validity of proposed auto-synchronizer and investigate the synchronverter performance with non-ideal source at dc bus.

5.1 Design of Complete System

The schematic diagram of the complete system under investigation is shown in Figure 5.1. The electrical part is similar to that of Figure 3.2 except the source at dc bus. Instead of an ideal dc source, an SPP of 250 kW rating is connected via MPPT-controlled DC-DC boost converter. Additional measurement units are added; to measure the voltage and current of SPP, and the voltage at dc bus of synchronverter.

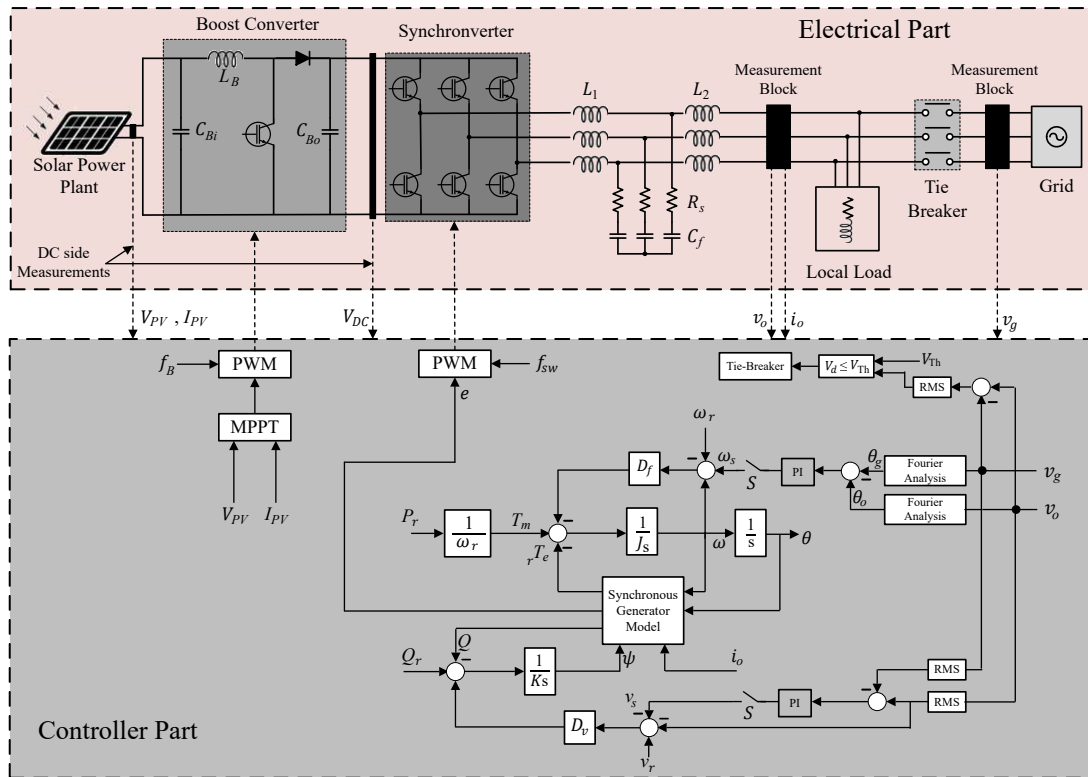


FIGURE 5.1: Schematic diagram of complete model under investigation

The controller part, shown in Figure 5.1, is same as depicted in Figure 4.5 except the control of DC-DC boost converter. Here, the boost converter is controlled by incremental conductance algorithm [149, 150] to track the maximum power point (MPP) of SPP according to the operating conditions.

The detailed designing of synchronverter and proposed auto-synchronizer is already discussed in Chapter 3 and 4, respectively. Same procedure is followed here to extend the model to 250 kW rating. Since, boost converter was not required

TABLE 5.1: Parameters used in simulations

Parameters	Symbols	Values
Nominal DC Voltage	V_{DC}	800 V
Damping Coefficient	D_f	506.6
Nominal Line Voltage	V_L	381 V
Virtual Inertia	J	1.0132
Nominal Power	P_n	250 kW
Voltage Droop Coefficient	D_v	16070
Switching Frequency	f_{sw}	8 kHz
Integrator Gain	K	100970
Nominal Frequency	f_n	50 Hz
Filter Capacitor	C_f	100 μ F
Filter Inductor	L_1	0.330 mH
Filter Inductor	L_2	56 μ H
Series Resistor	R_s	100 m Ω
Threshold voltage	V_{Th}	12 V
Voltage Loop Time Constant	τ_v	0.02 s
Frequency Loop Time Constant	τ_f	0.002 s
Proportional gain	K_f	0.2
Integral gain	I_f	3.2
Proportional gain	K_v	0.1
Integral gain	I_v	1.8

with ideal dc source in Chapter 3, its designing is elaborated in this chapter. Parameter values of synchronverter, proposed auto-synchronizer and LCL filter are tabulated in Table 5.1.

5.1.1 Solar Power Plant

Solar Power Plant (SPP) used in this study is constructed by using built-in PV modules "1Soltech 1STH-355-WH" in MATLAB/Simulink. SPP is composed of

84 parallel strings of these modules having 9 series-connected modules per string. The module specifications are tabulated in Table 5.2.

TABLE 5.2: Specifications of PV module used in SPP

Specification	Value
Maximum Power	334.905 W
Open Circuit Voltage	49.9 V
Voltage at MPP	41.5 V
Short Circuit Current	9 A
Current at MPP	8.07 A

Ambient temperature of 25°C is considered in this study and is kept constant. However, the Irradiance level is varied to study the synchronverter performance with intermittent nature of SPP.

5.1.2 DC-DC Boost Converter

The DC-DC boost converter design is found in [151, 152]. The inductor L_B value is selected using following equation:

$$L_B = \frac{V_{PV,max} D_{max}}{f_B \Delta I_{PV}} \quad (5.1)$$

Where, $V_{PV,max}$ is the maximum output voltage of SPP, D_{max} is the maximum duty cycle, and f_B is the switching frequency of boost converter switch, ΔI_{PV} is the ripple content in output current of SPP. In this study, 1% ripple is assumed. Input capacitor C_{Bi} value is calculated by following equation:

$$C_{Bi} = \frac{\Delta I_{PV}}{f_B \Delta V_{PV}} \quad (5.2)$$

Where ΔV_{PV} is the ripple content in the output voltage of SPP. 1.2% ripple is assumed in output voltage in this study. The value of output capacitor C_{Bo} is

TABLE 5.3: Parameters of boost converter

Parameters	Symbols	Values
Input Capacitor	C_{Bi}	150 μ F
Output Capacitor	C_{Bo}	1100 μ F
Inductor	L_B	3 mH
Switching Frequency	F_B	10 kHz
Maximum Duty Cycle	D_{max}	0.55

selected using the following equation:

$$C_{Bo} = \frac{I_{DC} D_{max}}{f_B \Delta V_{DC}} \quad (5.3)$$

Where, I_{DC} is the output current of the boost converter and ΔV_{DC} is the ripple value in the output voltage of boost converter. In this study, 2% ripple is considered in V_{DC} . Boost converter parameters are tabulated in Table 5.3.

5.2 Simulation Results and Discussions

All the simulations in this chapter were performed to investigate the performance of synchronverter and the validation of proposed auto-synchronizer with a Solar Power Plant connected at the dc side of synchronverter. Like Chapter 3, simulations were performed in MATLAB 9.2/Simulink using SimPowerSystem library. Solver and the tolerance level were same as those of simulations performed in previous chapters.

In Section 5.2.1, stand-alone performance was investigated with variations in the local connected load. In Section 5.2.2, validation of the proposed synchronizer was tested. In Section 5.2.3, grid-connected performance with intermittent nature of SPP was studied. In Section 5.2.4 and 5.2.5, grid-connected performance following a frequency and voltage event, respectively, was investigated. Finally, in Section 5.2.6, seamless transfer of synchronverter from grid-connected to stand-alone mode was tested.

TABLE 5.4: Variations in local load connected to synchronverter with SPP at the dc bus

Time Instant	P_{load}	Q_{load}
$t = 0$ s	80 kW	40 kVar
$t = 1$ s	120 kW	40 kVar
$t = 2$ s	120 kW	80 kVar
$t = 3$ s	100 kW	80 kVar
$t = 4$ s	100 kW	20 kVar
$t = 5$ s	160 kW	100 kVar
$t = 6$ s	80 kW	40 kVar

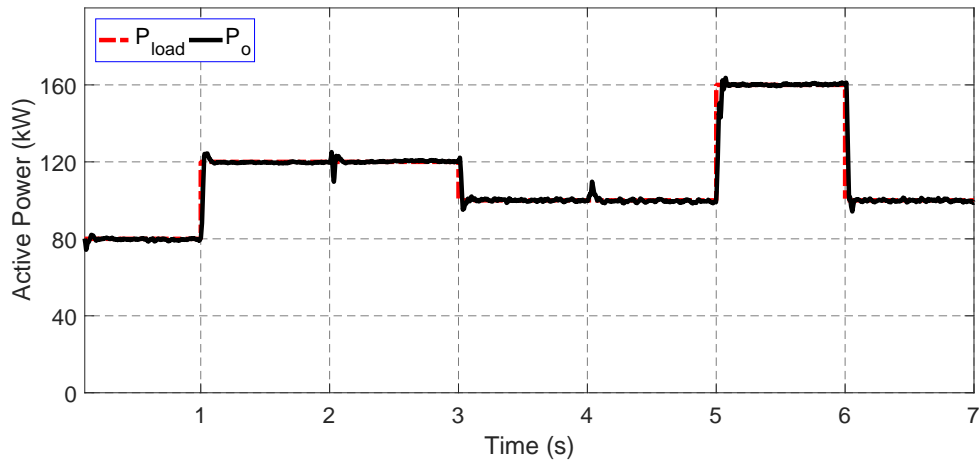
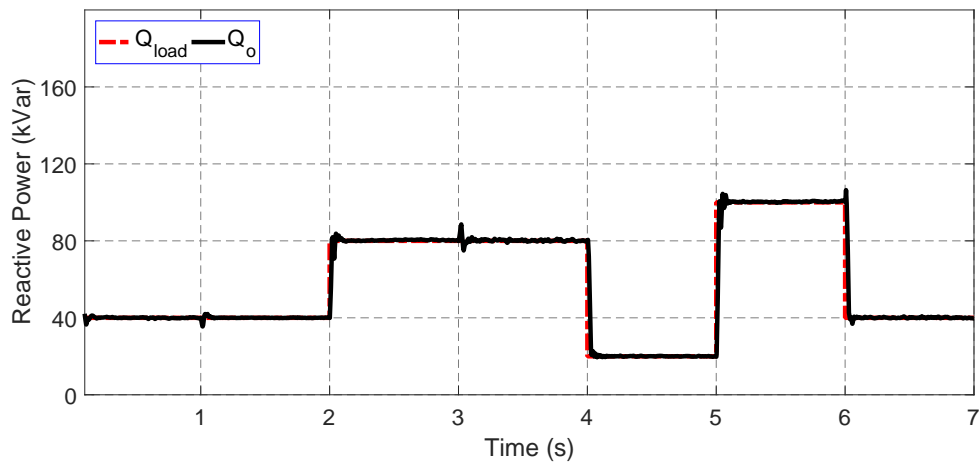
5.2.1 Stand-Alone Performance

As discussed in Section 3.4.1, one of the research objectives is the study of stand-alone performance of synchronverter with variations in local connected load. In this part, this performance was again evaluated with a non-ideal source, i.e., SPP, connected at the dc bus.

The simulations were started at $t = 0$ s with a local load of $80 + j40$ kVA connected at the ac side of synchronverter. Active and reactive loads were varied, similar to that done in Chapter 3, to study the effect of changes in operating conditions on synchronverter performance.

A load of 40 kW was switched-on at $t = 1$ s. Similarly, a load of 40 kVar was switched-on at $t = 2$ s. The total resistive load was changed to 100 kW at $t = 3$ s and the total inductive load was changed to 20 kVar at $t = 4$ s. Total load on synchronverter was increased to $160 + j100$ kVA at $t = 5$ s and decreased to $80 + j40$ kVA at $t = 6$ s. Table 5.4 shows the active and reactive power load connected to synchronverter at each instant during stand-alone operation.

Similar to the results of Chapter 3, the active and reactive power output of the synchronverter was equal to the power demanded by the local load as shown in Figures 5.2 and 5.3, respectively. For the maximum active power change of 60 kW at $t = 5$ s, the response time was 83 ms. Similarly, for the maximum reactive

FIGURE 5.2: Stand-alone performance: synchronverter active power P_o FIGURE 5.3: Stand-alone performance: synchronverter reactive power Q_o

power change of 80 kVAR at $t = 5$ s, the response time was also 83 ms. Transients were also seen in power curves at the switching events as discussed in Chapter 3.

The frequency, shown in Figure 5.4, was again well maintained by frequency control loop. Negligible variations in frequency at the instants of reactive power load switching was due to the coupling effect discussed in [145]. At the instant of increased active power load, the synchronverter increased its frequency to meet the increased demand. The maximum rate of change of frequency of 0.714 Hz per second was observed at $t = 5$ s when a load of $60 + j80$ kVA was added to the synchronverter output. This ROCOF is again much less than the threshold value of 3 Hz/s defined by IEEE standards [61]. For 60% increase in active power

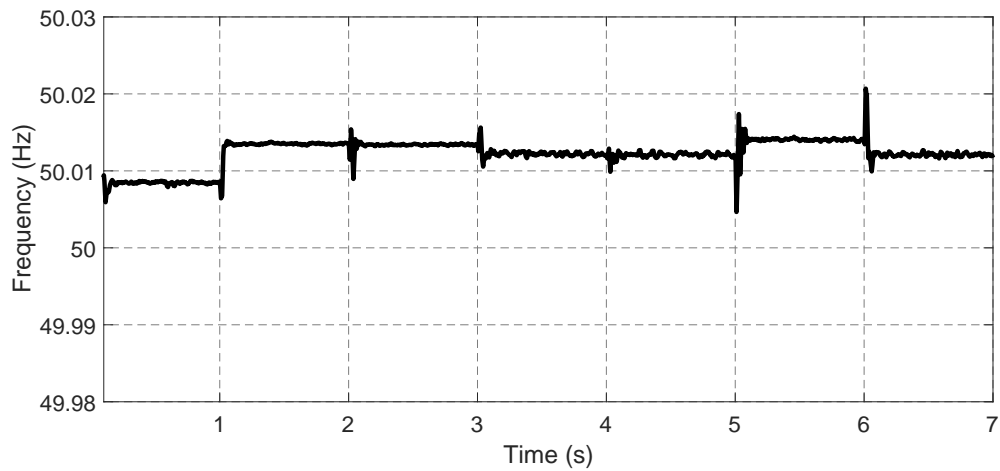


FIGURE 5.4: Stand-alone performance: synchronverter frequency f_o

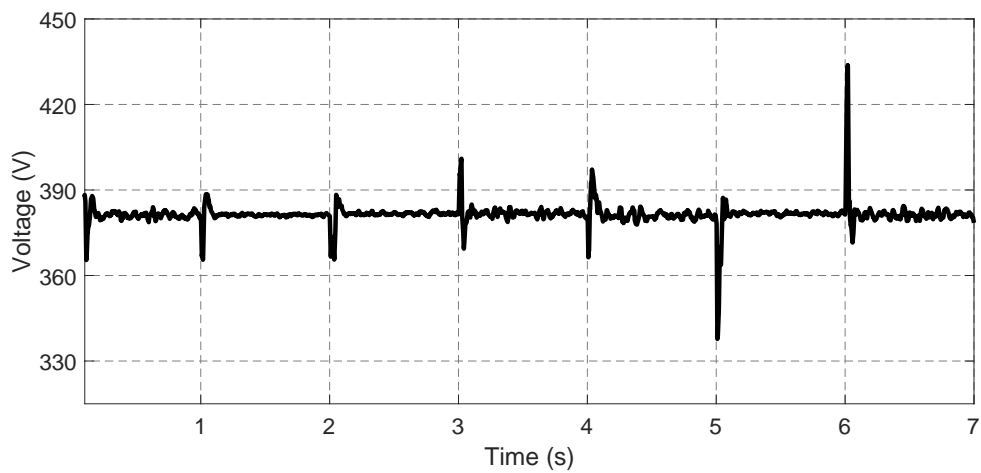


FIGURE 5.5: Stand-alone performance: synchronverter line voltage v_o

output, the synchronverter frequency was increased by 0.004% of nominal value. The response time for the maximum variation at $t = 5$ s was 83 ms.

The output voltage is shown in Figure 5.5. The transients were observed at the switching instants. The maximum surge was observed at $t = 6$ s when the total load of $80 + j60$ kVA was switched off. This surge was 13.8% higher than the steady state value that was less than the threshold value of $\pm 15\%$ surge voltage defined by IEEE standards [61]. The maximum response time was found to be 68 ms that was much less than the response time in case of ideal source. The maximum rate of rise of voltage was 1.52 V/ms while the rate of change of voltage with respect to reactive power was 0.3125 V/kVar.

TABLE 5.5: Comparison of stand-alone performance of synchronverter with different dc sources

Observations & Measurements	Ideal Source	SPP
Response time for frequency	83 ms	83 ms
Response time for voltage	108 ms	68 ms
Max. ROCOF (df/dt)	0.04 Hz/s	0.741 Hz/s
$\Delta f/\Delta P$	0.333 Hz/MW	0.033 Hz/MW
Max. Rate of Rise of Voltage (dV/dt)	0.025 V/ms	1.52 V/ms
$\Delta V/\Delta Q$	2.585 V/kVar	0.3125 V/kVar
Steady-state oscillations	No	Yes
Coupling effect	Yes	Yes

The stand-alone performance of synchronverter with both ideal and non-ideal source at dc bus is compared in Table 5.5. Results have shown that synchronverter performance was a bit different with SPP as compared to that of ideal source. Due to higher ratings, the performance with SPP was better than that of ideal source of lower ratings. However, the ROCOF and the rate of rise of voltage was higher in case of non-ideal source. Also, the steady-state oscillations were observed in results obtained in case of synchronverter operating with SPP at the dc bus.

It can be concluded that synchronverter mimics synchronous generator and maintains its frequency and voltage in stand-alone mode irrespective of the nature of source connected at the dc bus.

5.2.2 Synchronization with Grid

In this section, the application of the proposed synchronizer for synchronverter with SPP at dc bus was verified. Simulations were started at $t = 0$ s with a local load of $150 + j30$ kVA connected at the ac side of synchronverter. Synchronization process was initiated at $t = 0.2$ s. The initial phase difference between v_o and v_g was equal to 45° . This phase difference resulted in RMS difference of 165 V at the start of synchronization process similar to Case-II discussed in Chapter 2.

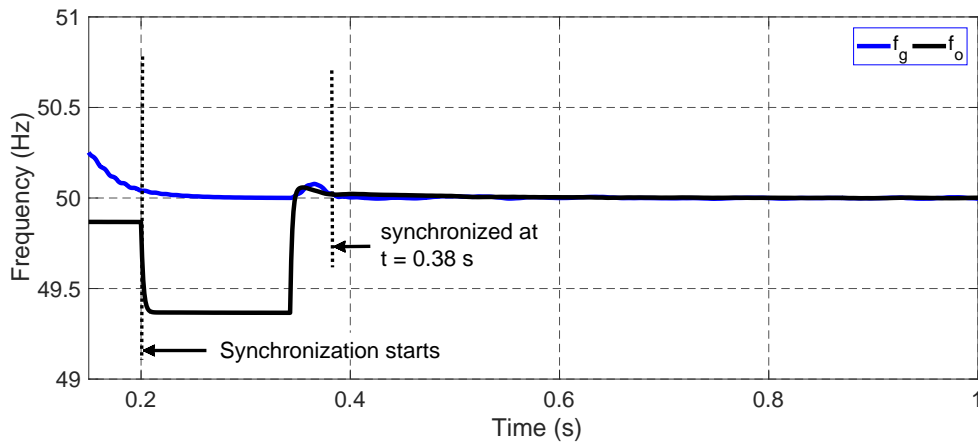


FIGURE 5.6: Grid synchronization with proposed synchronizer: synchronverter frequency f_o

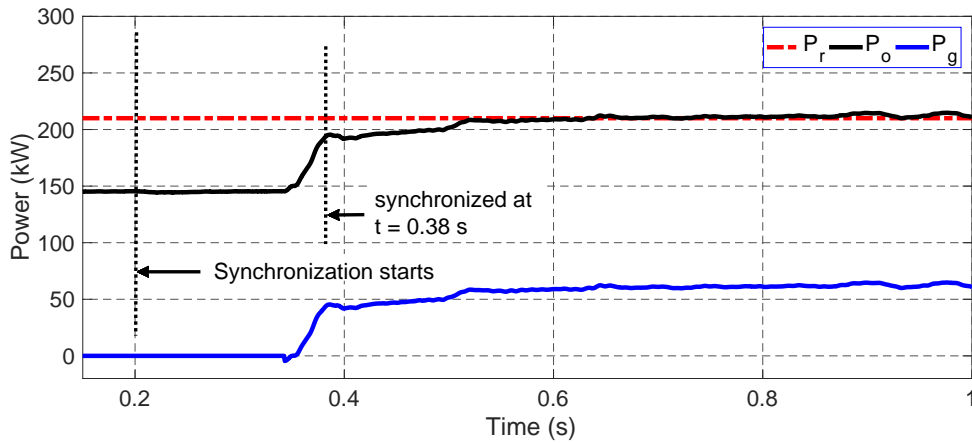


FIGURE 5.7: Grid synchronization with proposed synchronizer: active power reference P_r , synchronverter active power P_o , and active power exchanged with grid P_g

Figure 5.6 shows that the proposed synchronizer reduced the reference frequency of synchronverter. Due to this, the virtual rotor slowed down to angular speed of 311 rad/s to synchronize with grid. Synchronization was achieved at $t = 0.38$ s. Time elapsed in synchronization process was 0.18 s, similar to that of Case-II with ideal source at dc bus. After grid connection, the proposed synchronizer was removed from the controller, and the frequency was restored to the nominal value.

Figures 5.7 and 5.8 show that the proposed synchronizer enabled synchronverter to supply uninterrupted power to local load during synchronization process. During the process, P_r was set to 210 kW and Q_r was 60 kVar. After grid connection, the

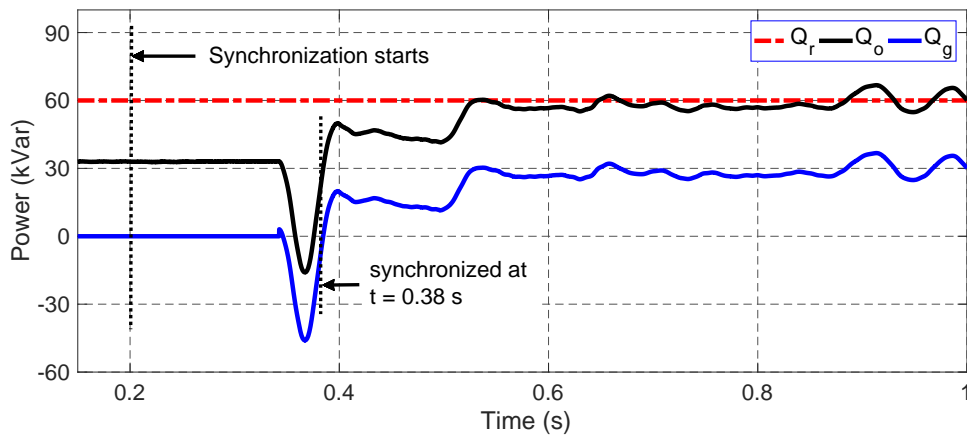


FIGURE 5.8: Grid synchronization with proposed synchronizer: reactive power reference Q_r , synchronverter reactive power Q_o , and reactive power exchanged with grid Q_g

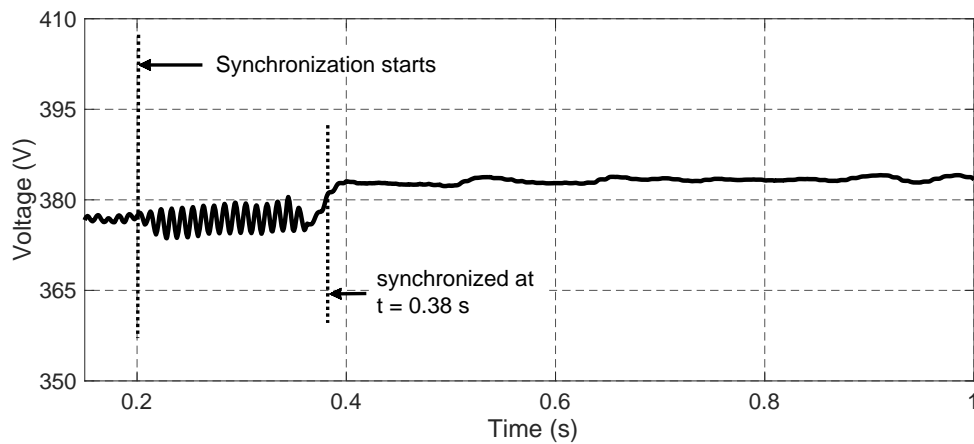


FIGURE 5.9: Grid synchronization with proposed synchronizer: synchronverter line voltage v_o

synchronverter tracked the power reference values and injected additional power i.e., $60 + j30$ kVA, into the grid. The active and reactive power injected into the grid is shown by P_g and Q_g in Figures 5.7 and 5.8, respectively.

Synchronverter output voltage v_o is shown in Figure 5.9. No surge was observed in v_o at the instant of grid connection. Although, steady-state oscillations were observed in v_o during synchronization process, however, they were only $\pm 0.6\%$ of the nominal value.

Results show that the proposed synchronizer is equally valid for synchronverter

having non-ideal source at its dc side. The proposed synchronizer enabled the seamless transfer of synchronverter from stand-alone to grid-connected mode without interrupting supply to local connected load.

5.2.3 Grid-Connected Mode with Variable Irradiance

This part of simulations was performed to investigate the performance of synchronverter with intermittent nature of SPP. Simulations were started at $t = 0$ s with synchronverter supplying local load of $150 + j30$ kVA in stand-alone mode. Synchronization was started at $t = 0.2$ s and synchronverter was synchronized with grid at $t = 0.38$ s. The duration from $t = 0$ s to $t = 0.85$ s is not shown in results of this part of simulations as this is already illustrated in results of Section 5.2.2. After grid connection, the synchronverter active and reactive power outputs were set at 210 kW and 60 kVar, respectively.

TABLE 5.6: Irradiance Level in W/m^2

Irradiance Level	1000	800	400	400	1000
Time in seconds	2	4	5	8	9

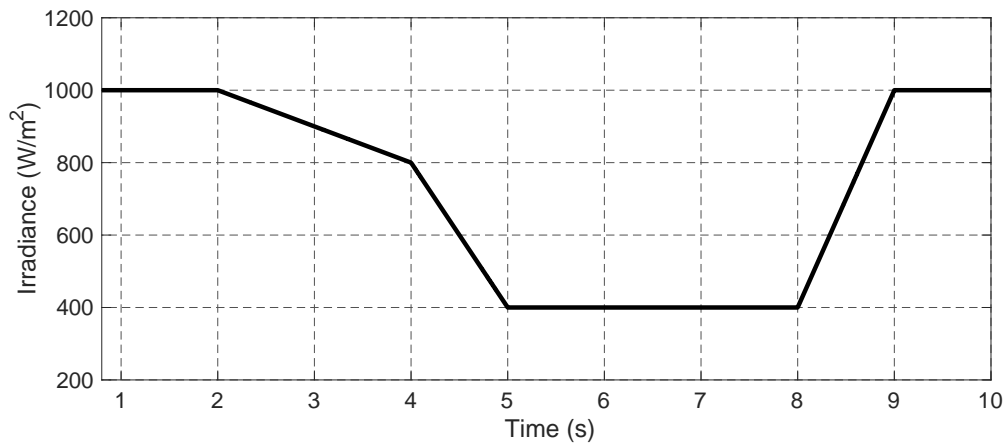


FIGURE 5.10: Grid-connected performance with variable Irradiance level: Irradiance level

Irradiance level was set at $1000 \text{ W}/\text{m}^2$ initially. From $t = 2$ s, the irradiance level was varied as tabulated in table 5.6. Variations in Irradiance level are shown in

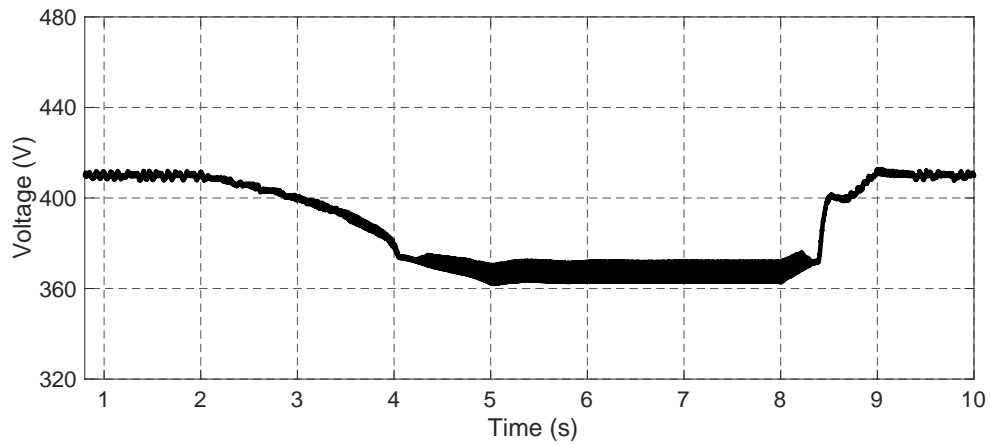


FIGURE 5.11: Grid-connected performance with variable Irradiance level: SPP voltage V_{PV}

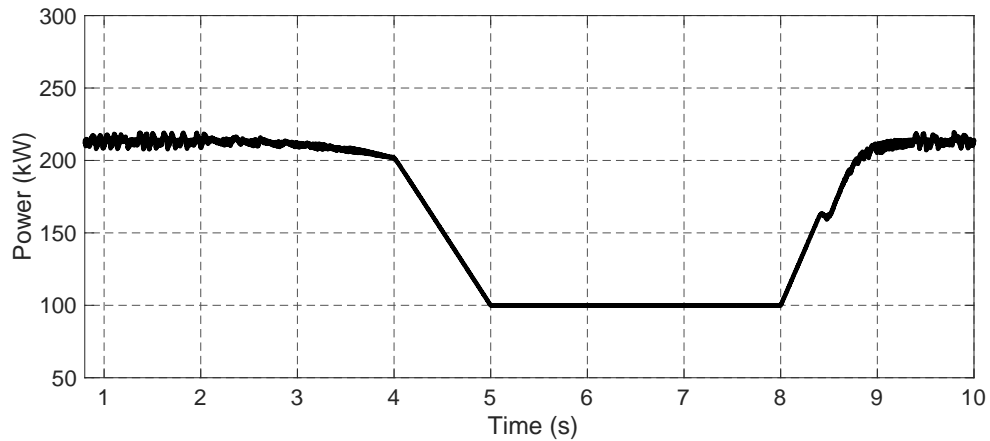


FIGURE 5.12: Grid-connected performance with variable Irradiance level: SPP power P_{PV}

Figure 5.10. Effect of variations in irradiance level on SPP voltage and power can be observed in Figures 5.11 and 5.12, respectively. Both V_{PV} and P_{PV} were changed with the variations in irradiance level. With 60% reduction in irradiance level, the SPP power was reduced by 52.38%. Oscillations were observed in V_{PV} when the irradiance level was 400 W/m^2 . These oscillations were $\pm 1.18\%$ of the steady-state voltage level.

Synchronverter output active power P_o , shown in Figure 5.13, followed the same pattern as that of SPP power. In case of ideal source, in Chapter 3, P_o was equal to the reference value P_r due to availability of infinite power at the dc side. However,

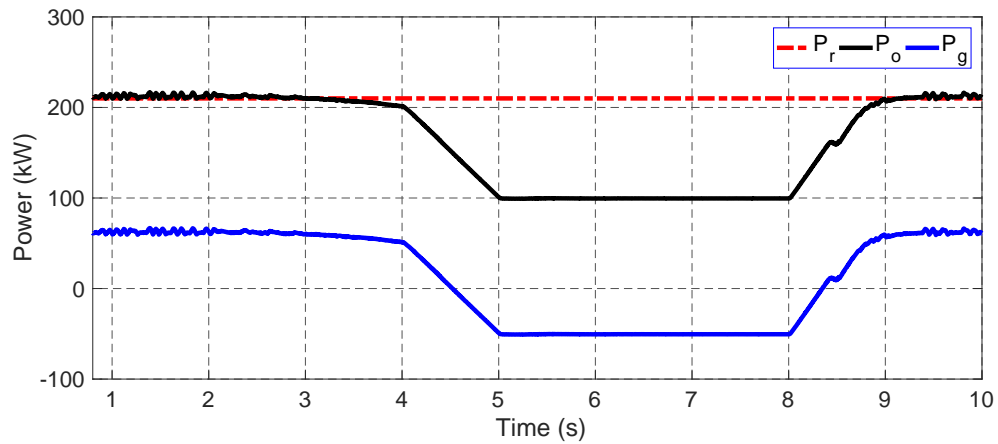


FIGURE 5.13: Grid-connected performance with variable Irradiance level: active power reference P_r , synchronverter active power P_o , and active power exchanged with grid P_g

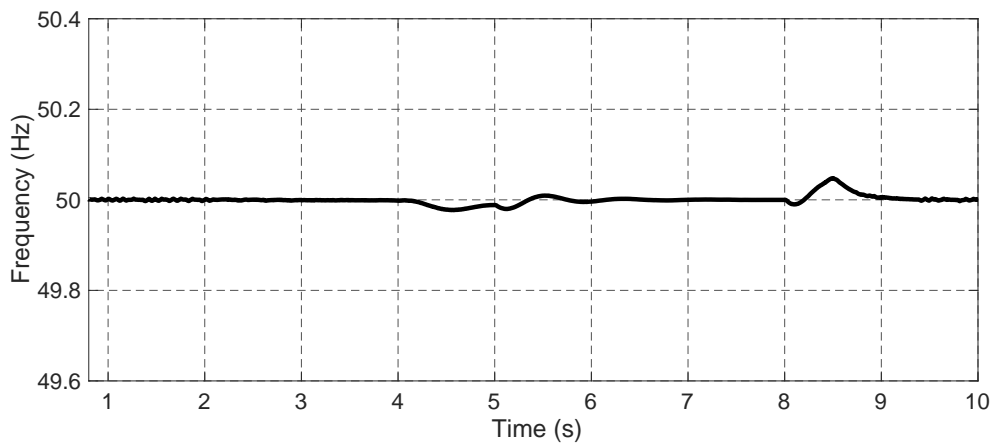


FIGURE 5.14: Grid-connected performance with variable Irradiance level: synchronverter frequency f_o

with SPP, the available power was limited, therefore, P_o was deviated from P_r . The output power P_o was also reduced by 52% due to the reduced SPP power.

The power P_g shown in Figure 5.13 is the power exchange with the grid. Before $t = 4$ s, the synchronverter was injecting 60 kW into the grid. At $t = 5$ s, since the SPP power reduced to 100 kW, the synchronverter was unable to supply local load. In this case, 50 kW was supplied by grid to meet the local load as shown by -50 kW in Figure 5.13 between $t = 5$ s to $t = 8$ s.

Even with variations in the dc side power, the synchronverter kept its frequency

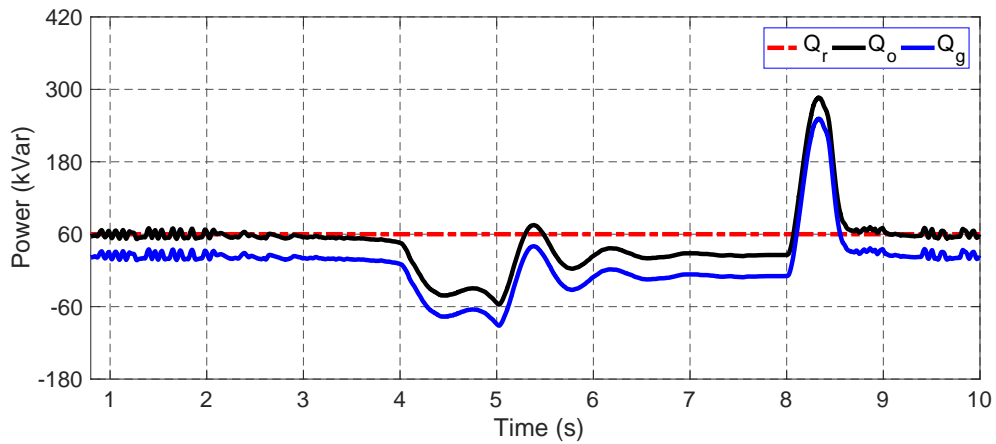


FIGURE 5.15: Grid-connected performance with variable Irradiance level: reactive power reference Q_r , synchronverter reactive power Q_o , and reactive power exchanged with grid Q_g

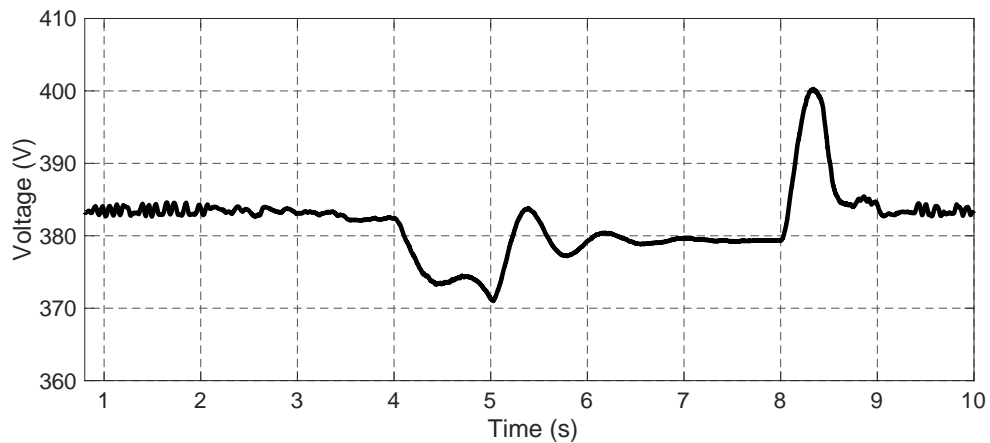


FIGURE 5.16: Grid-connected performance with variable Irradiance level: synchronverter line voltage v_o

f_o at the nominal value with negligible variations, as shown in Figure 5.14. The maximum variation observed in frequency was of 0.05 Hz at $t = 8.5$ s. The response time of the transient in frequency was 1.396 s. The maximum ROCOF observed was 0.15 Hz/s that is much less than the threshold level defined by IEEE standards. It can be concluded that the frequency control loop of synchronverter worked exceptionally to keep the frequency at the nominal value.

Synchronverter reactive power Q_o and output voltage v_o are shown in Figures 5.15 and 5.16, respectively. It is mentioned in Section 3.2.2 that the frequency control loop responds much faster than the voltage control loop to the grid dynamics.

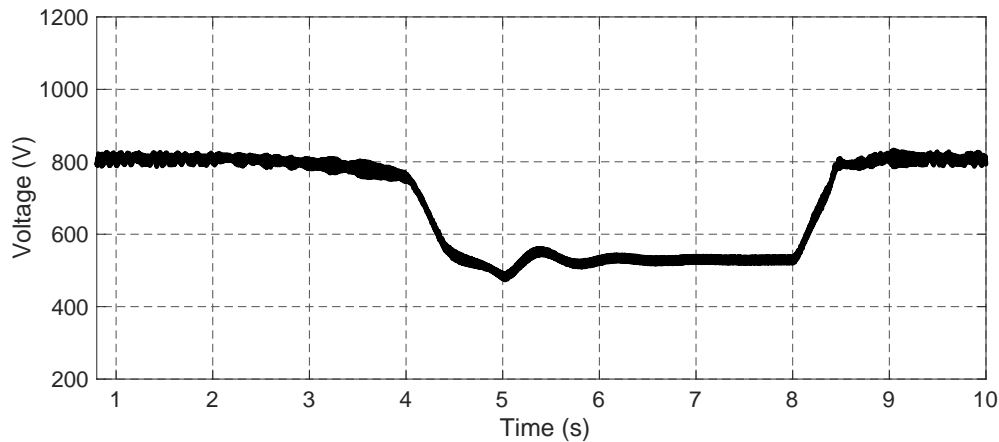


FIGURE 5.17: Grid-connected performance with variable Irradiance level: dc-bus voltage V_{DC}

For this reason, the voltage response was slower to the irradiance variation. The response time of voltage was 1.24 s. Between $t = 5$ s to $t = 8$ s, the voltage of the synchronverter was set to steady-state value of 380 V at which the reactive power output was lesser than the reference value Q_r . A surge of 4.98% was observed at $t = 8.34$ s that is less than the threshold level of $\pm 10\%$ defined in IEEE standards. The rate of rise of voltage was 0.06 V/ms.

DC bus voltage V_{DC} is shown in Figure 5.17. Since, the maximum duty cycle of boost converter was set to 0.55, V_{DC} went below the nominal value during lower Irradiance level due to lower voltage extraction from the SPP. Therefore, a sophisticated control is required here to maintain the dc link voltage. By applying dc-bus voltage regulation proposed in [96], the output voltage of synchronverter can be improved further.

The performance of synchronverter with intermittent nature of SPP was found satisfactory. Synchronverter kept its frequency at the nominal value irrespective of the drastic changes in power of SPP. However, the voltage regulation was a bit slower and can be improved by regulating the dc link voltage. One major difference from ideal source, discussed in Section 3.4.2.1, was found that the synchronverter was unable to track the reference values of active and reactive power due to the finite source of power at the dc bus.

5.2.4 Grid-Connected Mode Following Frequency Event

This part of simulations was performed to verify the inherent frequency tracking of synchronverter with SPP at the dc bus. Simulations were started at $t = 0$ s with synchronverter supplying local load in stand-alone mode. Synchronization was started at $t = 0.2$ s and synchronverter was synchronized with grid at $t = 0.38$ s, as in Sections 5.2.2. After grid connection, the synchronverter active and reactive power outputs were set at 210 kW and 60 kVar, respectively. The synchronverter was operating in Q_D -mode discussed in Section 3.2.3.

Grid frequency was dropped by 0.25 Hz i.e. 0.5% at $t = 2$ s and was restored to nominal value at $t = 2.2$ s. Synchronverter frequency f_o and grid frequency f_g are shown in Figure 5.18. It was observed that f_o was slowly reduced to 49.75 Hz due to inertia of the virtual rotor. The response time was 222 ms and the ROCOF was 1.04 Hz/s. Similar results were obtained in Chapter 3 with ideal source at dc side. However, due to finite source of power at dc bus in this Chapter, the response time is higher than that of Chapter 3.

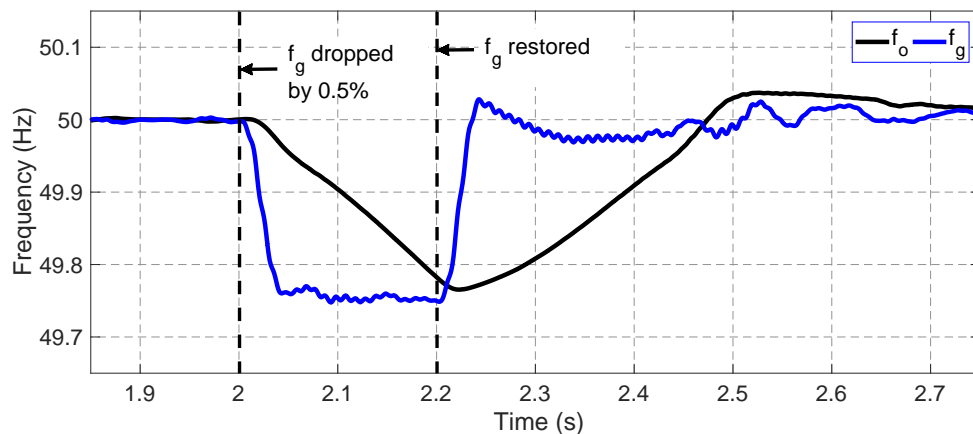


FIGURE 5.18: Grid-connected performance following frequency event: grid frequency f_g and synchronverter frequency f_o

Since, the proposed synchronizer was removed from the synchronverter after grid connection, as discussed in Section 5.2.2, synchronverter successfully tracked the grid frequency in grid-connected mode without the requirement of any dedicated synchronization unit.

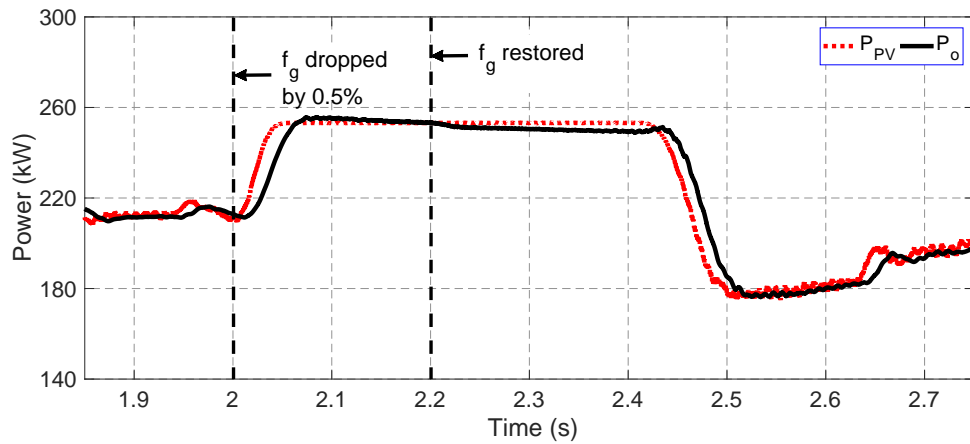


FIGURE 5.19: Grid-connected performance following frequency event: synchronverter active power P_o and SPP power P_{PV}

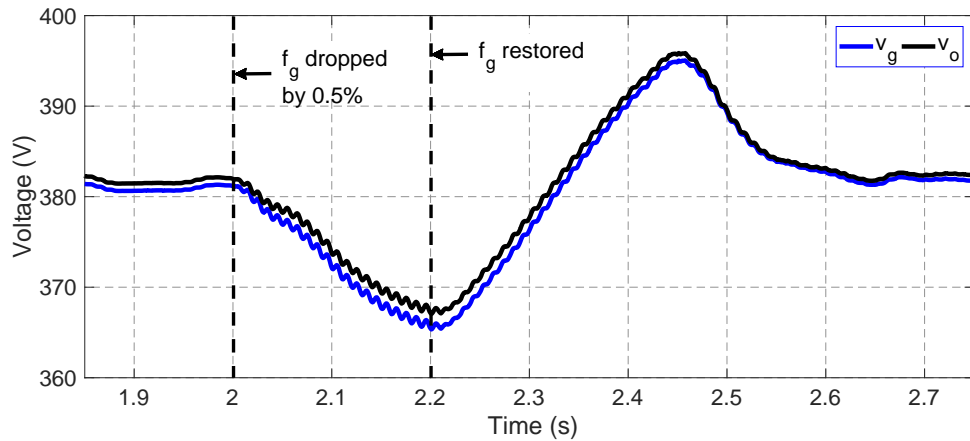


FIGURE 5.20: Grid-connected performance following frequency event: grid line voltage v_g and synchronverter line voltage v_o

Synchronverter active power output P_o and SPP power P_{PV} are shown in figure 5.19. It can be seen in figure that the synchronverter increased its P_o , to the maximum available P_{PV} at the dc side, to support frequency. The higher the reserve available at dc side, the greater the support synchronverter can provide to the grid frequency. This can also be verified from the results obtained in Chapter 3 where an ideal source was connected at dc side. The infinite power was available there.

To further improve the inertial response of synchronverter, ESS can be connected at the dc side. In this way the total reserved inertia will be increased.

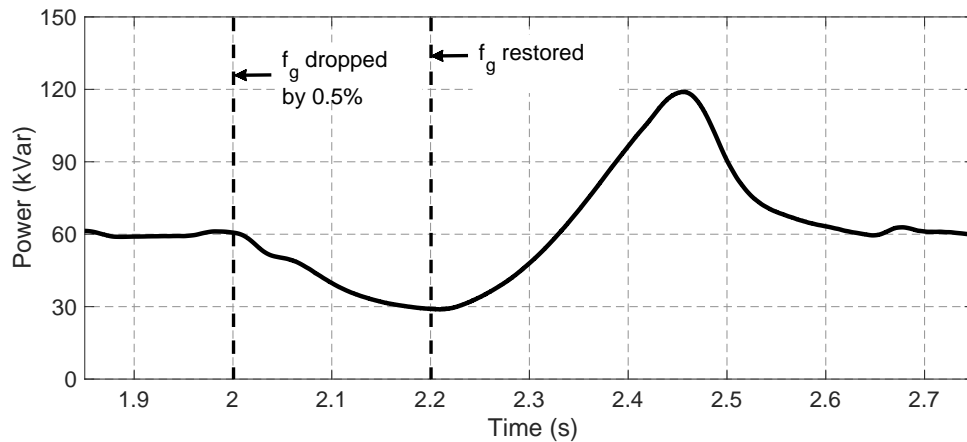


FIGURE 5.21: Grid-connected performance following frequency event: synchronverter reactive power Q_o

Synchronverter output voltage v_o and grid voltage v_g is shown in Figure 5.20. The response is similar to that obtained in case of ideal source in Chapter 3. However, here v_g is more deviated from the nominal value due to 0.5% reduction in the frequency. The voltage was fluctuated by $\pm 8.06\%$ of the nominal value. This is less than the permissible range of $\pm 10\%$ set by the grid codes [61].

Synchronverter reactive power Q_o is shown in Figure 5.21. The reactive power was increased by 100% of the reference value of 60 kVar when the voltage was increased by 8.06% of the nominal value. It can be concluded from the results obtained in this section that the synchronverter can track and support the grid frequency without any dedicated synchronization unit. By adding ESS at the dc side, this inertial response can be improved further.

5.2.5 Grid-Connected Mode Following Voltage Event

This part of simulations was performed to verify the voltage support capability of synchronverter in grid-connected mode during a voltage event. Simulations were started at $t = 0$ s with synchronverter supplying local load in stand-alone mode. Synchronization was started at $t = 0.2$ s and synchronverter was synchronized with grid at $t = 0.38$ s, as in Sections 5.2.2. After grid connection, the synchronverter

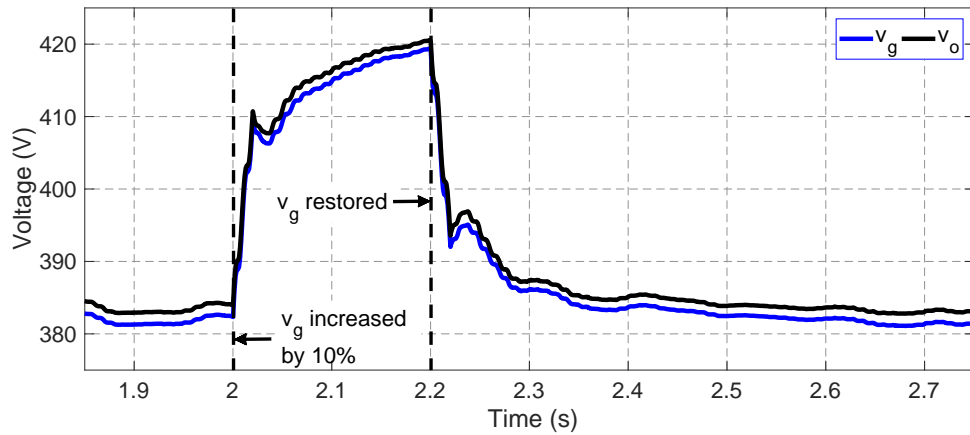


FIGURE 5.22: Grid-connected performance following voltage event: grid line voltage v_g and synchronverter line voltage v_o

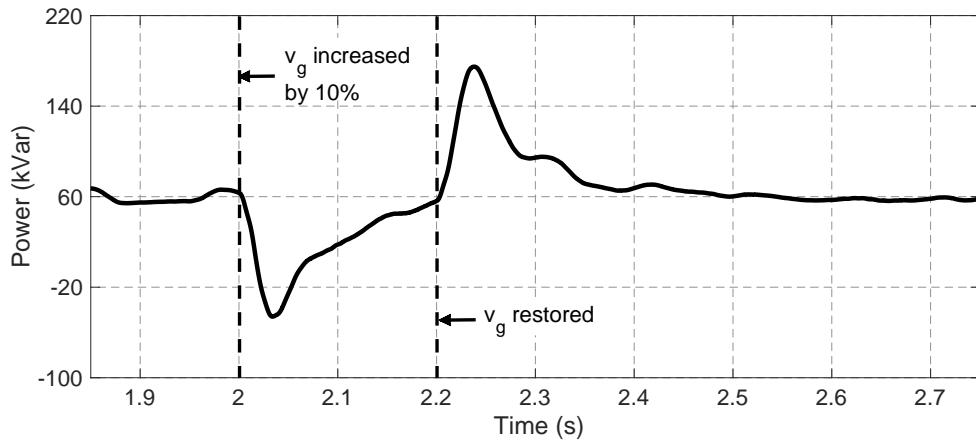


FIGURE 5.23: Grid-connected performance following voltage event: synchronverter reactive power Q_o

active and reactive power outputs were set at 210 kW and 60 kVar, respectively. The synchronverter was operating in Q -mode discussed in Section 3.2.3.

Grid voltage was increased by 10% at $t = 2$ s and was restored to nominal value at $t = 2.2$ s. It was observed that the synchronverter voltage followed the grid voltage as shown in Figure 5.22. Since the synchronverter was operating in Q -mode, as the result of 10% increase in grid voltage, the synchronverter decreased its reactive power Q_o by 200% of the reference value at the start of the disturbance i.e. at $t = 2$ s and then settled it down to the reference value Q_r of 60 kVar as shown in Figure 5.23. After the grid voltage restoration, Q_o again settled down to the

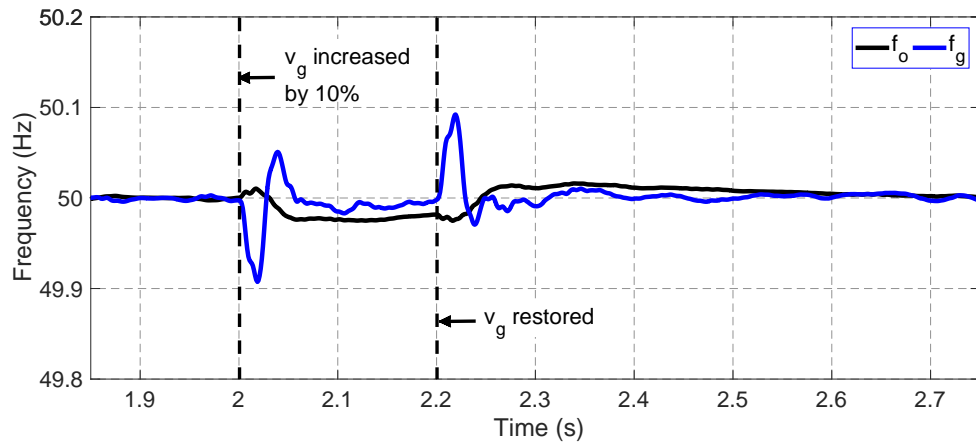


FIGURE 5.24: Grid-connected performance following voltage event: grid frequency f_g and synchronverter frequency f_o

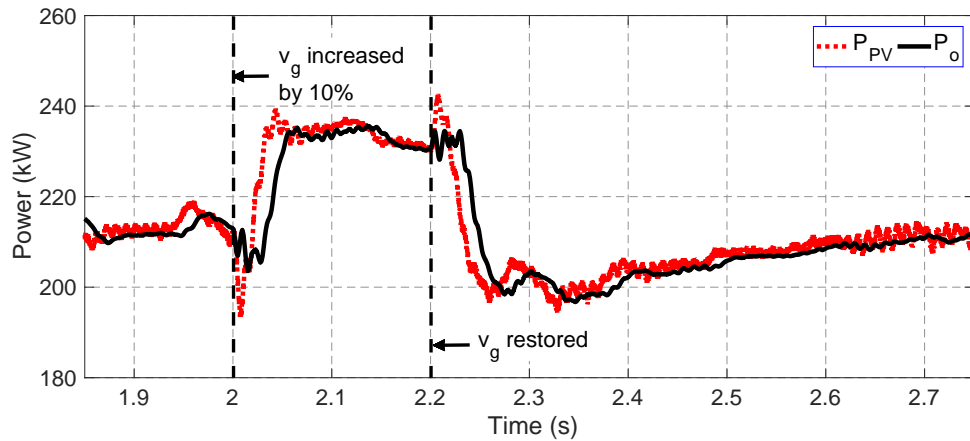


FIGURE 5.25: Grid-connected performance following voltage event: synchronverter active power P_o and SPP power P_{PV}

reference value Q_r . The response time was 35 ms and the settling time was 293 ms. Both the response time and settling time were a bit higher than that obtained with ideal source in Chapter 3 due to the limited power available at dc bus.

It can be seen from the results that in case of grid voltage deviated more than 10% of the nominal value, the synchronverter voltage would follow the grid voltage until the protective relays disconnect the grid. At loss of grid, the synchronverter performance will be the same as discussed in Section 5.2.6.

Synchronverter frequency f_o and grid frequency f_g is shown in Figure 5.24. Due to the virtual inertia possessed by the synchronverter, f_o was varied slowly due to

the variations in f_g . The maximum change in frequency was 0.02 Hz i.e. 0.04% of the nominal value.

Figure 5.25 shows synchronverter output active power P_o and SPP power P_{PV} during the voltage event. It was observed that both P_o and P_{PV} had similar response than that of the case with ideal dc source. For the $\pm 0.04\%$ variation in frequency, the output power P_o was varied by $\mp 10.16\%$ of the rated value that is about $\mp 12\%$ of the reference value P_r .

5.2.6 Transfer from Grid-Connected to Stand-Alone Mode

Synchronverter offers seamless transfer from grid-connected to stand-alone mode without any change required in its controller. To verify this for synchronverter having SPP at the dc side, this part of simulations was performed.

Simulations were started at $t = 0$ s with synchronverter supplying local load of $150 + j30$ in stand-alone mode. Synchronization was started at $t = 0.2$ s and synchronverter was synchronized with grid at $t = 0.38$ s by slowing down its virtual rotor using the proposed synchronizer, as in Sections 5.2.2. After grid connection, the synchronverter active and reactive power outputs were set at 210 kW and 60 kVar, respectively.

Before the islanding event, the synchronverter was supplying the local load and feeding $60 + j30$ kVA into the grid. Islanding was done at $t = 2$ s by opening the tie-breaker shown in Figure 5.1. It was observed that the synchronverter kept its frequency f_o , shown in Figure 5.26, at the desired level on loss of grid mains. On the loss of grid, the frequency f_o was increased by 0.06 Hz at $t = 2$ s.

Synchronverter active power output P_o , and SPP power P_{PV} are shown in Figure 5.27. It can be seen that synchronverter continued to supply the local load, on loss of grid, without any change required in its controller. The power P_g also shown in figure is the power exchange between synchronverter and grid during the operation. During grid-connected mode, the synchronverter injected 60 kW into

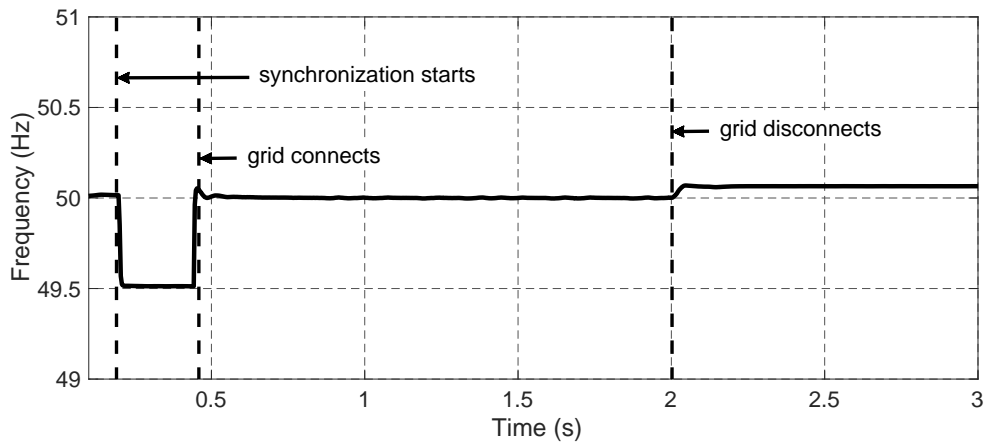


FIGURE 5.26: Transfer from grid-connected to stand-alone mode: synchronverter frequency f_o

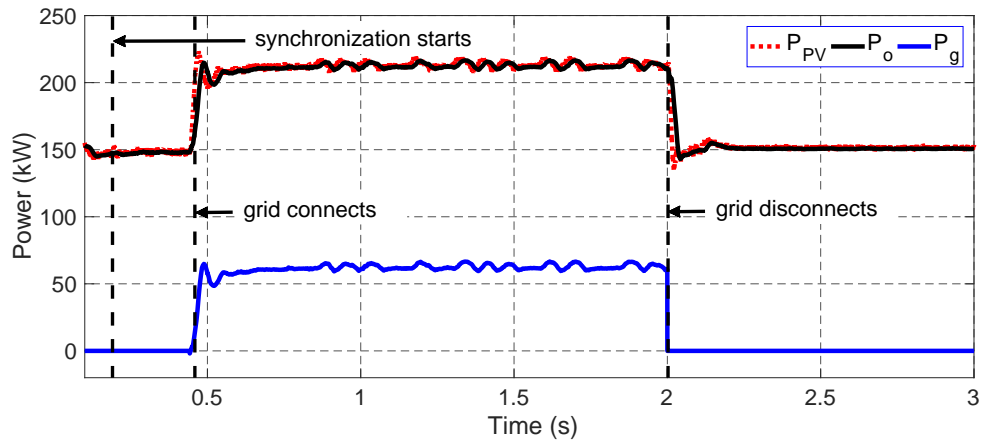


FIGURE 5.27: Transfer from grid-connected to stand-alone mode: synchronverter active power P_o and active power exchanged with grid P_g

the grid. At $t = 2$ s, the synchronverter output was equal to the connected load irrespective of the reference value P_r . Due to the reduced P_o at islanding instant, the frequency f_o was increased by 0.06 Hz.

The synchronverter output voltage v_o , shown in Figure 5.28, was not changed dramatically during transfer from grid-connected to stand-alone mode. A surge of 10% was observed at the islanding instant for the time of 30 ms that is equal to only one and half cycles of fundamental waveform.

Synchronverter reactive power output Q_o is shown in Figure 5.29. It can be seen that synchronverter continued to supply the local load, on loss of grid, without

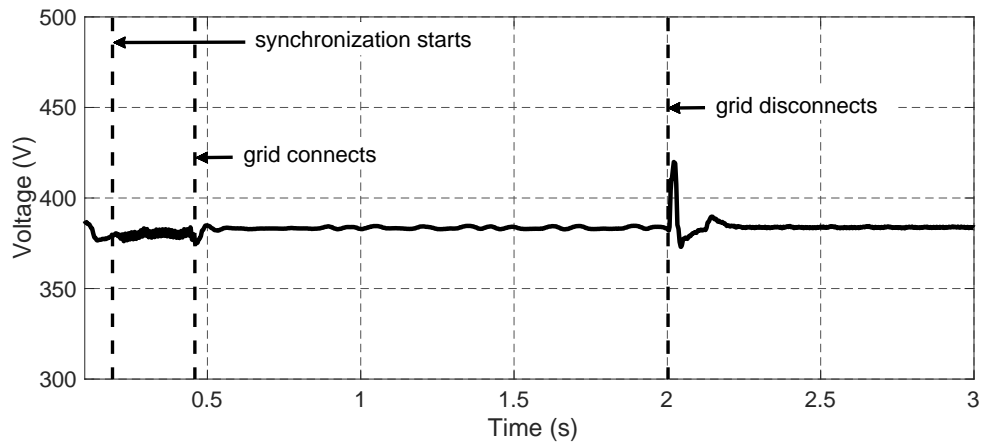


FIGURE 5.28: Transfer from grid-connected to stand-alone mode: synchronverter line voltage v_o

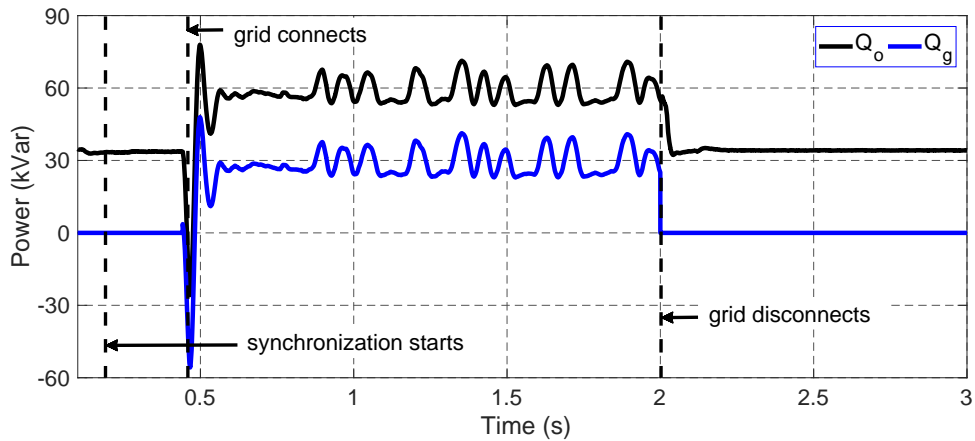


FIGURE 5.29: Transfer from grid-connected to stand-alone mode: synchronverter reactive power Q_o and reactive power exchanged with grid Q_g

any change required in its controller. The power Q_g also shown in figure is the reactive power exchange between synchronverter and grid during the operation. During grid-connected mode, the synchronverter injected 30 kVar into the grid. At $t = 2$ s, the synchronverter output was equal to the connected load irrespective of the reference value Q_r .

Results obtained in this part of simulations have shown that the synchronverter has ability to switch its mode of operation from grid-connected to stand-alone without any change required in the controller circuit. The results obtained were similar to that of the case of ideal source at dc bus in Chapter 3. However, the

surge in voltage v_o at the islanding instant was higher than that of Chapter 3 due to the higher ratings of the system.

5.3 Summary

In this chapter, the synchronverter design presented in Chapter 3 is successfully extended to integrate 250 kW Solar Power Plant (SPP) into power grid. All the scenarios of Chapter 3 are re-simulated to investigate the performance of synchronverter with SPP at the dc bus. Results obtained in this chapter are compared with those obtained in Chapter 3. In most of the cases the results were similar to that obtained with ideal source. In stand-alone mode, the results were better due to the higher ratings of the system. Synchronverter maintained its frequency and voltage irrespective of the nature of source at the dc bus.

The validity of the proposed synchronizer, presented in Chapter 4, is also verified for the extended system. It was found that the proposed synchronizer is equally valid for synchronverter having an intermittent natured source at dc bus.

Later on, the performance of synchronverter was investigated with intermittent input power, with fluctuating grid dynamics and with loss of grid mains. One of the major difference found was the availability of limited power at the dc side. With ideal source at dc bus, the synchronverter can draw infinite power to track the reference values all the time. However, with SPP at the dc bus, the output power can deviate from the reference values particularly with low irradiance levels. To further improve the performance of synchronverter with SPP, the dc bus voltage regulation is suggested.

Chapter 6

Conclusions and Future

Directions

Synchronverter is the best replication of synchronous generator in future power grid. It has inherent capability to remain synchronized with grid without any dedicated synchronization unit. However, for seamless transfer from stand-alone to grid-connected mode, the synchronverter requires a synchronizer to track grid phase prior to grid connection. As stated in research objective 1, in this research, an enhanced, PLL-less, auto-synchronizer for the synchronverter is proposed that offers: (a) fast and promising synchronization with grid independent of the grid phase angle lagging or leading the local voltage phase angle, (b) fast and promising synchronization with grid independent of the deviation of grid voltage magnitude from the nominal value, and (c) uninterrupted power supply to local load during synchronization process. Therefore, the proposed synchronizer addressed the problem found in existing PLL-less synchronizers. The performance of proposed synchronizer is compared with existing DRMSV-based synchronizer. Results obtained from comparison have shown that the proposed synchronizer addressed the limitations and uncertainties of DRMSV-based synchronizer, enabled the synchronverter to supply power to the local load during synchronization process, and improved the synchronization speed upto 99% under certain grid conditions.

As stated in research objective 2, the effect of variations in connected load on synchronverter performance in stand-alone mode is investigated in detail. It is found that synchronverter has capability to mimic synchronous generator by keeping its frequency and voltage within the permissible range defined by grid codes. It is also found that the higher the ratings of the system, better will be the performance of synchronverter.

As stated in research objective 3, in this study, the performance of synchronverter with SPP connected at the dc bus is investigated and compared with its performance with ideal dc source. It is found that the performances in both the cases are similar except few differences. One major difference is the availability of finite power at the dc bus. In case of ideal source, synchronverter can draw infinite power at any instant to keep its output equal to the reference values irrespective of the operating conditions. However, with SPP, the output power can deviate from the reference value because of the finite source of power. The performance and inertial dynamics of synchronverter can be improved further by connecting ESS at the dc bus. By connecting ESS at dc bus, virtual inertia will be increased and performance will be more similar to that of the ideal source at dc bus.

6.1 Future Directions

Findings of this research on the synchronverter performance in various modes of operation show promising solutions to stabilize the future power grid. This research can be extended in various directions in future as highlighted below:

- In this study MPPT-controlled solar power plant is integrated into power grid. Due to this conventional MPPT approach, the output voltage of the boost converter deviated from the nominal value under low irradiation level condition. A sophisticated control of dc bus is required that incorporates the intermittent nature of SPP, and regulates dc bus voltage irrespective of the operating conditions. Several DC link voltage algorithms have been proposed in literature that can be applied to further investigate the performance

of synchronverter with non-ideal source at dc bus with variable dc voltage scenarios.

- This research considered a solar power plant without any parallel-connected energy storage device at the dc side of synchronverter. ESD in parallel with RERs has positive impact in inertia emulation. In this way, the energy reserve at dc side can be increased and more energy can be drawn or supplied to dc bus. This will increase the overall virtual inertia of the system. The work presented here can be extended to a system including an ESD at the dc side.
- This work is based solely on simulations. It can be validated with experimental setup in future. In this study, synchronizer for three-phase synchronverter is proposed. In future, the proposed auto-synchronizer can be tested for single-phase synchronverter. Experimental setup of single-phase synchronverter can also be designed to validate the proposed auto-synchronizer.
- Issues like; required storage capacity calculations of ESD, charging and discharging algorithm and the effect of state-of-charge of ESD on synchronverter performance need to be explored in the future.
- This study focused on single synchronverter unit operating in stand-alone or grid-connected mode. It can be extended to multiple parallel operating synchronverters in a hybrid microgrid. Similarly, the validity of proposed auto-synchronizer can be tested for multiple parallel operating units.
- The control parameters of synchronverter used in this research are not fully optimized. There are several optimization approaches proposed in literature to get better inertial, dynamic and steady-state response from synchronverter. These algorithms can also be applied on synchronverter presented in this study.
- Most of the stability analyses of synchronverter presented in literature assume ideal source at the dc bus. Small-signal model of the complete system

including SPP, discussed in this study, can be developed. Stability analysis can be performed using small-signal model including the uncertainties in operating conditions of SPP.

- There are some additional windings termed as damper windings in the rotor of synchronous machines. These windings suppress the hunting and helps to synchronize the CSG with grid after disturbances. These damper windings can be included mathematically in synchronverter model presented in this study.

Future directions of this research are not limited to the afore-mentioned points. There is no limit of the knowledge and above all those who know, there is One Who truly knows.

Bibliography

- [1] D. Tan and D. Novosel, “Energy challenge, power electronics & systems PEAS technology and grid modernization,” *CPSS Transactions on Power Electronics and Applications*, vol. 2, no. 1, pp. 3–11, 2017.
- [2] T. Kerdphol, F. S. Rahman, and Y. Mitani, “Virtual inertia control application to enhance frequency stability of interconnected power systems with high renewable energy penetration,” *Energies*, vol. 11, no. 981, pp. 1–16, 2018.
- [3] W. U. Tareen, S. Mekhilef, M. S. Mahmoudian, and B. Horan, “Active power filter (APF) for mitigation of power quality issues in grid integration of wind and photovoltaic energy conversion system,” *Renewable and Sustainable Energy Reviews*, vol. 70, pp. 635–655, 2017.
- [4] N. Saxena, I. Hussain, B. Singh, and A. L. Vyas, “Implementation of grid integrated PV-battery system for residential and electrical vehicle applications,” *IEEE Transactions on Industrial Electronics*, vol. 65, no. 8, pp. 6592–6601, 2018.
- [5] X. Ding, G. Huang, Y. Xu, and J. Guo, “A multi-objective optimization model for a non-traditional energy system in beijing under climate change conditions,” *Energies*, vol. 12, no. 1692, pp. 1–21, 2019.
- [6] S. Dong and Y. C. Chen, “Analysis of feasible synchronverter pole-placement region to facilitate parameter tuning,” *IEEE Transactions on Energy Conversion*, vol. 36, no. 4, pp. 2782–2793, 2021.

- [7] K. Sakimoto, Y. Miura, and T. Ise, "Stabilization of a power system including inverter-type distributed generators by a virtual synchronous generator," *Electrical Engineering in Japan*, vol. 187, no. 3, pp. 7–17, 2014.
- [8] M. Jabeen, M. Umar, M. Zahid, M. U. Rehman, R. Batool, and K. Zaman, "Socio-economic prospects of solar technology utilization in Abbottabad, Pakistan," *Renewable and Sustainable Energy Reviews*, vol. 39, pp. 1164–1172, 2014.
- [9] "Energy resources, National Transmission and Dispatch Company (NTDC)," 2018, Accessed on 29-11-2021. [Online]. Available: <https://ntdc.gov.pk/energy>
- [10] "Annual report 2020-21, National Electric Power Regulatory Authority (NEPRA)," 2021, Accessed on 29-11-2021. [Online]. Available: <https://nepra.org.pk/publications/Annual%20Reports/Annual%20Report%202020-21.pdf>
- [11] "Current status of solar PV power projects," 2021, Accessed on 29-11-2021. [Online]. Available: <https://www.aedb.org/ae-technologies/solar-power/solar-current-status>
- [12] A. A. Khosa, T. Rashid, N. U. H. Shah, M. Usman, and M. S. Khalil, "Performance analysis based on probabilistic modelling of Quaid-e-Azam solar park (QASP) Pakistan," *Energy Strategy Reviews*, vol. 29, pp. 1–10, 2020.
- [13] U. Tamrakar, D. Shrestha, M. Maharjan, and B. P. Bhattarai, "Virtual inertia: Current trends and future directions," *Applied Sciences*, vol. 7, no. 7, pp. 1–29, 2017.
- [14] D. Liu, Q. C. Zhong, Y. Wang, and G. Liu, "Modeling and control of a V2G charging station based on synchronverter technology," *CSEE Journal of Power and Energy Systems*, vol. 4, no. 3, pp. 326–338, 2018.

-
- [15] Q. C. Zhong, “Virtual synchronous machines: A unified interface for grid integration,” *IEEE Power Electronics Magazine*, vol. 3, no. 4, pp. 18–27, 2016.
- [16] C. Yuan, P. Xie, D. Yang, and X. Xiao, “Transient stability analysis of islanded AC microgrids with a significant share of virtual synchronous generators,” *Energies*, vol. 11, no. 1, pp. 1–19, 2018.
- [17] R. Shi and X. Zhang, “VSG-based dynamic frequency support control for autonomous PV-diesel microgrids,” *Energies*, vol. 11, no. 7, pp. 1–16, 2018.
- [18] S. S. Refaat, H. A. Rub, A. P. Sanfilippo, and A. Mohamed, “Impact of grid-tied large-scale photovoltaic system on dynamic voltage stability of electric power grids,” *IET Renewable Power Generation*, vol. 12, no. 2, pp. 157–164, 2018.
- [19] X. Liang, “Emerging power quality challenges due to integration of renewable energy sources,” *IEEE Transactions on Industry Applications*, vol. 53, no. 2, pp. 855–866, 2017.
- [20] J. Fang, H. Li, Y. Tang, and F. Blaabjerg, “On the inertia of future more-electronics power systems,” *IEEE Journal of Emerging and Selected Topics in Power Electronics*, vol. 7, no. 4, pp. 2130–2146, 2019.
- [21] Q. C. Zhong and G. Weiss, “Synchronverters: Inverters that mimic synchronous generators,” *IEEE Transactions on Industrial Electronics*, vol. 58, no. 4, pp. 1259–1267, 2011.
- [22] U. Tamrakar, D. Galipeau, R. Tonkoski, and I. Tamrakar, “Improving transient stability of photovoltaic-hydro microgrids using virtual synchronous machines,” in *IEEE Eindhoven PowerTech*, Eindhoven, July 2015, pp. 1–6.
- [23] S. D’Arco, J. A. Suul, and O. B. Fosso, “Control system tuning and stability analysis of virtual synchronous machines,” in *IEEE Energy Conversion Congress and Exposition*, Denver, September 2013, pp. 2664–2671.

- [24] Q. C. Zhong, Z. Ma, W. L. Ming, and G. C. Konstantopoulos, “Grid-friendly wind power systems based on the synchronverter technology,” *Energy Conversion and Management*, vol. 89, pp. 719–726, 2015.
- [25] S. D’Arco and J. A. Suul, “Virtual synchronous machines - classification of implementations and analysis of equivalence to droop controllers for microgrids,” in *IEEE Grenoble Conference PowerTech*, Grenoble, June 2013, pp. 1–7.
- [26] H. Beck and R. Hesse, “Virtual synchronous machine,” in *9th International Conference on Electrical Power Quality and Utilisation (EPQU)*, Barcelona, October 2007, pp. 1–6.
- [27] Y. Chen, R. Hesse, D. Turschner, and H. Beck, “Comparison of methods for implementing virtual synchronous machine on inverters,” *Renewable Energy & Power Quality Journal*, vol. 1, no. 10, pp. 734–739, 2012.
- [28] Y. Hirase, K. Abe, K. Sugimoto, and Y. Shindo, “A grid-connected inverter with virtual synchronous generator model of algebraic type,” *Electrical Engineering in Japan (English translation of Denki Gakkai Ronbunshi)*, vol. 184, no. 4, pp. 10–21, 2013.
- [29] R. Shi, X. Zhang, C. Hu, and H. Xu, “Self-tuning virtual synchronous generator control for improving frequency stability in autonomous photovoltaic-diesel microgrids,” *Journal of Modern Power Systems and Clean Energy*, vol. 6, no. 3, pp. 482–494, 2018.
- [30] P. Rodriguez, I. Candela, and A. Luna, “Control of PV generation systems using the synchronous power controller,” in *IEEE Energy Conversion Congress and Exposition*, Denver, September 2013, pp. 993–998.
- [31] T. Loix, S. D. Breucker, P. Vanassche, J. V. den Keybus, J. Driesen, and K. Visscher, “Layout and performance of the power electronic converter platform for the VSYNC project,” in *IEEE Bucharest PowerTech*, Bucharest, June 2009, pp. 1–8.

- [32] Q. C. Zhong, G. C. Konstantopoulos, B. Ren, and M. Krstic, "Improved synchronverters with bounded frequency and voltage for smart grid integration," *IEEE Transactions on Smart Grid*, vol. 9, no. 2, pp. 786–796, 2018.
- [33] S. Dong, Y. Chi, and Y. Li, "Active voltage feedback control for hybrid multiterminal HVDC system adopting improved synchronverters," *IEEE Transactions on Power Delivery*, vol. 31, no. 2, pp. 445–455, 2016.
- [34] H. Bevrani, T. Ise, and Y. Miura, "Virtual synchronous generators: A survey and new perspectives," *International Journal of Electrical Power and Energy Systems*, vol. 54, pp. 244–254, 2014.
- [35] R. Hesse, D. Turschner, and H. Beck, "Micro grid stabilization using the virtual synchronous machine (VISMA)," in *International Conference on Renewable Energies and Power Quality ICREPQ'11*, Valencia, April 2009, pp. 1–6.
- [36] C. Pelczar, "Mobile virtual synchronous machine for vehicle-to-grid applications," PhD dissertation, Clausthal University of Technology, 2012.
- [37] C. Pelczar, M. Stubbe, H. P. Beck, and O. Zirn, "FPGA current controller for the virtual synchronous machine," in *International Exhibition and Conference for Power Electronics, Intelligent Motion, Renewable Energy and Energy Management PCIM*, Nuremberg, May 2012, pp. 138–145.
- [38] J. Machaowski, J. Bialek, and J. R. Bumby, *Power system dynamics stability and control*, 3rd ed. Wiley, 2012.
- [39] Y. Chen, R. Hesse, D. Turschner, and H. Beck, "Dynamic properties of the virtual synchronous machine (VISMA)," *Renewable Energy & Power Quality Journal*, vol. 1, no. 9, pp. 755–759, 2011.
- [40] T. Dewenter, W. Heins, B. Werther, A. K. Hartmann, C. Bohn, and H. Beck, "Parameter optimization of a virtual synchronous machine in a microgrid," *International Journal of Power and Energy Systems*, vol. 36, pp. 1–17, 2016.

- [41] Y. Chen, R. Hesse, D. Turschner, and H. Beck, "Investigation of the virtual synchronous machine in the island mode," in *3rd IEEE PES Innovative Smart Grid Technologies Europe (ISGT Europe)*, Berlin, October 2012, pp. 1–6.
- [42] H. A. Alsiraji and R. El-Shatshat, "Comprehensive assessment of virtual synchronous machine based voltage source converter controllers," *IET Generation, Transmission and Distribution*, vol. 11, no. 7, pp. 1762–1769, 2017.
- [43] Y. Hirase, K. Abe, K. Sugimoto, K. Sakimotor, H. Bevrani, and T. Ise, "A novel control approach for virtual synchronous generators to suppress frequency and voltage fluctuations in microgrids," *Applied Energy*, vol. 210, pp. 699–710, 2018.
- [44] O. Mo, S. D'Arco, and J. A. Suul, "Evaluation of virtual synchronous machines with dynamic or quasi-stationary machine models," *IEEE Transactions on Industrial Electronics*, vol. 64, no. 7, pp. 5952–5962, 2017.
- [45] T. Shintai, Y. Miura, and T. Ise, "Oscillation damping of a distributed generator using a virtual synchronous generator," *IEEE Transactions on Power Delivery*, vol. 29, no. 2, pp. 668–676, 2014.
- [46] K. Sakimoto, Y. Miura, and T. Ise, "Characteristics of parallel operation of inverter-type distributed generators operated by a virtual synchronous generator," *Electrical Engineering in Japan*, vol. 192, no. 4, pp. 9–19, 2015.
- [47] S. D'Arco and J. A. Suul, "Equivalence of virtual synchronous machines and frequency-droops for converter-based microgrids," *IEEE Transactions on Smart Grid*, vol. 5, no. 1, pp. 394–395, 2014.
- [48] J. Alipoor, Y. Miura, and T. Ise, "Power system stabilization using virtual synchronous generator with alternating moment of inertia," *IEEE Journal of Emerging and Selected Topics in Power Electronics*, vol. 3, no. 2, pp. 451–458, 2015.

- [49] J. Liu, D. Yang, W. Yao, R. Fang, H. Zhao, and B. Wang, "PV-based virtual synchronous generator with variable inertia to enhance power system transient stability utilizing the energy storage system," *Protection and Control of Modern Power Systems*, vol. 2, no. 39, pp. 1–8, 2017.
- [50] A. Miguel, L. Torres, L. A. C. Lopes, L. A. Moran, C. Espinoza, and R. Jose, "Self-tuning virtual synchronous machine: A control strategy for energy storage systems to support dynamic frequency control," *IEEE Transactions on Energy Conversion*, vol. 29, no. 4, pp. 833–840, 2014.
- [51] M. Guan, W. Pan, J. Zhang, Q. Hao, J. Cheng, and X. Zheng, "Synchronous generator emulation control strategy for voltage source converter (VSC) stations," *IEEE Transactions on Power Systems*, vol. 30, no. 6, pp. 3093–3101, 2015.
- [52] C. Rodriguez, G. Candela, D. Rocabert, and R. Teodorescu, "Virtual controller of electromechanical characteristics for static power converters," US patent US20140067138 A1, 2012.
- [53] W. Zhang, D. Remon, and P. Rodriguez, "Frequency support characteristics of gridinteractive power converters based on the synchronous power controller," *IET Renewable Power Generation*, vol. 11, no. 4, pp. 470–479, 2017.
- [54] W. Zhang, A. M. Cantarellas, J. Rocabert, A. Luna, and P. Rodriguez, "Synchronous power controller with flexible droop characteristics for renewable power generation systems," *IEEE Transactions on Sustainable Energy*, vol. 7, no. 4, pp. 1572–1582, 2016.
- [55] W. Zhang, D. Remon, I. Candela, A. Luna, and P. Rodriguez, "Grid-connected converters with virtual electromechanical characteristics: Experimental verification," *CSEE Journal of Power and Energy Systems*, vol. 3, no. 3, pp. 286–295, 2017.

- [56] S. D'Arco, J. A. Suul, and O. B. Fosso, "A virtual synchronous machine implementation for distributed control of power converters in smartgrids," *Electric Power Systems Research*, vol. 122, pp. 180–197, 2015.
- [57] J. A. Suul, S. D'Arco, and G. Guidi, "Virtual synchronous machine-based control of a single-phase bi-directional battery charger for providing vehicle-to-grid services," *IEEE Transactions on Industry Applications*, vol. 52, no. 4, pp. 3234–3244, 2016.
- [58] S. D'Arco, J. A. Suul, and O. B. Fosso, "Small-signal modeling and parametric sensitivity of a virtual synchronous machine in islanded operation," *International Journal of Electrical Power and Energy Systems*, vol. 72, pp. 3–15, 2015.
- [59] B. Zhang, X. Yan, D. Li, X. Zhang, J. Han, and X. Xiao, "Stable operation and small-signal analysis of multiple parallel DG inverters based on a virtual synchronous generator scheme," *Energies*, vol. 11, no. 1, pp. 1–22, 2018.
- [60] C.-K. Nguyen, T.-T. Nguyen, H.-J. Yoo, and H.-M. Kim, "Improving transient response of power converter in a stand-alone microgrid using virtual synchronous generator," *Energies*, vol. 11, no. 1, pp. 1–27, 2018.
- [61] IEEE, *application guide for IEEE Std 1547, IEEE standard for interconnecting distributed resources with electric power systems*. Institute of Electrical and Electronics Engineering, 2009.
- [62] K. Shi, H. Ye, P. Xu, D. Zhao, and L. Jiao, "Low-voltage ride through control strategy of virtual synchronous generator based on the analysis of excitation state," *IET Generation, Transmission and Distribution*, vol. 12, no. 9, pp. 2165–2172, 2018.
- [63] M. P. V. Wesenbeeck, S. W. H. de Hann, P. Varela, and K. Visscher, "Grid tied converter with virtual kinetic storage," in *IEEE Bucharest PowerTech*, Bucharest, July 2009, pp. 1–7.

- [64] M. Torres and L. A. C. Lopes, "Virtual synchronous generator control in autonomous wind-diesel power systems," in *IEEE Electrical Power and Energy Conference (EPEC)*, Montreal, October 2009, pp. 1–6.
- [65] V. Karapanos, S. de Hann, and K. Zwetsloot, "Real time simulation of a power system with VSG hardware in the loop," in *37th Annual Conference of the IEEE Industrial Electronics Society*, Melbourne, November 2011, pp. 3748–3754.
- [66] M. Albu, M. Calin, D. Federenciuc, and J. Diaz, "The measurement layer of the virtual synchronous generator operation in the field test," in *IEEE International Workshop on Applied Measurements for Power Systems (AMPS)*, Aachen, September 2011, pp. 85–89.
- [67] S. Wang, J. Hu, X. Yuan, and L. Sun, "On inertial dynamics of virtual-synchronous-controlled DFIG-based wind turbines," *IEEE Transactions on Energy Conversion*, vol. 30, no. 4, pp. 1691–1702, 2015.
- [68] S. Wang, J. Hu, and X. Yuan, "Virtual synchronous control for grid-connected DFIG-based wind turbines," *IEEE Journal of Emerging and Selected Topics in Power Electronics*, vol. 3, no. 4, pp. 932–944, 2015.
- [69] "Network operation of the first virtual synchronous machine system of china southern power grid," 2017, Accessed on 18-02-2021. [Online]. Available: http://www.csg.cn/xwzx/2017/gsyw/201702/t20170222_151669.html
- [70] "Virtual synchronous generator demonstration projects puts into operation," 2017, Accessed on 18-02-2021. [Online]. Available: http://paper.people.com.cn/zgnyb/html/2017-01/02/content_1740630.html
- [71] K. M. Cheema, "A comprehensive review of virtual synchronous generator," *Electrical Power and Energy Systems*, vol. 120, pp. 1–10, 2020.
- [72] J. Liu, Y. Miura, H. Bevrani, and T. Ise, "Enhanced virtual synchronous generator control for parallel inverters in microgrids," *IEEE Transactions on Smart Grid*, vol. 8, no. 5, pp. 2268–2277, 2017.

- [73] H. Wu, X. Ruan, D. Yang, X. Chen, W. Zhao, Z. Lv, and Q. C. Zhong, "Small-signal modeling and parameters design for virtual synchronous generators," *IEEE Transactions on Industrial Electronics*, vol. 63, no. 7, pp. 4292–4303, 2016.
- [74] G. Yao, Z. Lu, Y. Wang, M. Benbouzid, and L. Moreau, "A virtual synchronous generator based hierarchical control scheme of distributed generation systems," *Energies*, vol. 10, no. 12, pp. 1–23, 2017.
- [75] D. Chen, Y. Xu, and A. Q. Huang, "Integration of DC microgrids as virtual synchronous machines into the AC grid," *IEEE Transactions on Industrial Electronics*, vol. 64, no. 9, pp. 7455–7466, 2017.
- [76] J. Liu, Y. Miura, and T. Ise, "Comparison of dynamic characteristics between virtual synchronous generator and droop control in inverter-based distributed generators," *IEEE Transactions on Power Electronics*, vol. 31, no. 5, pp. 3600–3611, 2016.
- [77] K. Y. Yap, C. R. Sarimuthu, and J. M.-Y. Lim, "Virtual inertia-based inverters for mitigating frequency instability in grid-connected renewable energy system: A review," *Applied Sciences*, vol. 9, no. 24, pp. 1–29, 2019.
- [78] M. Ashabani and Y. A. R. I. Mohamed, "Integrating VSCs to weak grids by nonlinear power damping controller with self-synchronization capability," *IEEE Transactions on Power Systems*, vol. 29, no. 2, pp. 805–814, 2014.
- [79] B. Li, L. Zhou, X. Yu, C. Zheng, and J. Liu, "Improved power decoupling control strategy based on virtual synchronous generator," *IET Power Electronics*, vol. 10, no. 4, pp. 462–470, 2017.
- [80] I. Serban and C. P. Ion, "Microgrid control based on a grid-forming inverter operating as virtual synchronous generator with enhanced dynamic response capability," *Electrical Power and Energy Systems*, vol. 89, pp. 94–105, 2017.
- [81] Y. Ma, W. Cao, L. Yang, F. Wang, and L. M. Tolbert, "Virtual synchronous generator control of full converter wind turbines with short term energy

- storage,” *IEEE Transactions on Industrial Electronics*, vol. 64, no. 11, pp. 8821–8831, 2017.
- [82] J. Fang, Y. Tang, H. Li, and X. Li, “A battery/ultracapacitor hybrid energy storage system for implementing the power management of virtual synchronous generators,” *IEEE Transactions on Power Electronics*, vol. 33, no. 4, pp. 2820–2824, 2018.
- [83] C. Gao, X. Liu, and H. Chen, “Research on the control strategy of distributed energy resources inverter based on improved virtual synchronous generator,” *Scientific Reports*, vol. 7, no. 9025, pp. 1–12, 2017.
- [84] B. Gao, C. Xia, N. Chen, K. Cheema, L. Yang, and C. Li, “Virtual synchronous generator based auxiliary damping control design for the power system with renewable generation,” *Energies*, vol. 10, no. 8, pp. 1–21, 2017.
- [85] M. Ashabani and Y. A. R. I. Mohamed, “New family of microgrid control and management strategies in smart distribution grids; analysis, comparison and testing,” *IEEE Transactions on Power Systems*, vol. 29, no. 5, pp. 2257–2269, 2014.
- [86] K. R. Vasudevan, V. K. Ramachandaramurthy, T. S. Babu, and A. Pouryekta, “Synchronverter: A comprehensive review of modifications, stability assessment, applications and future perspectives,” *IEEE Access*, vol. 8, pp. 131 565–131 589, 2020.
- [87] M. Naeem, M. Ashraf, and U. A. Khan, “A robust auto-synchronizer for synchronverter,” *Computers and Electrical Engineering*, vol. 98, pp. 1–12, 2022.
- [88] Q. C. Zhong, P.-L. P. Nguyen, Z. Ma, and W. Sheng, “Self-synchronised synchronverters: Inverters without a dedicated synchronisation unit,” *IEEE Transactions on Power Electronics*, vol. 29, no. 2, pp. 617–630, 2014.
- [89] E. T. Montalvo, V. M. Sanchez, and J. M. Ramirez, “Synchronverter assessment for the frequency regulation of control areas encompassing renewable

- distributed generation,” *International Journal of Hydrogen Energy*, vol. 46, no. 51, pp. 26 138–26 151, 2021.
- [90] Q. Tan, Z. Lv, B. Xu, W. Jiang, X. Ai, and Q. C. Zhong, “A novel three-phase four-wire grid-connected synchronverter that mimics synchronous generators,” *Journal of Power Electronics*, vol. 16, no. 6, pp. 2221–2230, 2016.
- [91] R. Rosso, S. Engelken, and M. Liserre, “Robust stability analysis of LCL filter based synchronverter under different grid conditions,” *IEEE Transactions on Power Electronics*, vol. 34, no. 6, pp. 5842–5853, 2019.
- [92] Z. Shuai, Y. Hu, Y. Peng, C. Tu, and Z. J. Shen, “Dynamic stability analysis of synchronverter-dominated microgrid based on bifurcation theory,” *IEEE Transactions on Industrial Electronics*, vol. 64, no. 9, pp. 7467–7477, 2017.
- [93] R. Rosso, S. Engelken, and M. Liserre, “Robust stability analysis of synchronverters operating in parallel,” *IEEE Transactions on Power Electronics*, vol. 34, no. 11, pp. 11 309–11 319, 2019.
- [94] C. Li, J. Xu, and C. Zhao, “A coherency-based equivalence method for MMC inverters using virtual synchronous generator control,” *IEEE Transactions on Power Delivery*, vol. 31, no. 3, pp. 1369–1378, 2016.
- [95] J. Zakis, E. Makovenko, H. Zeng, O. Husev, and L. Kutt, “qZS inverter as synchronverter in small-scale micro-grid,” *Elektronika Ir Elektrotechnika*, vol. 24, no. 2, pp. 58–62, 2018.
- [96] M. Ashabani and Y. A. R. I. Mohamed, “Novel comprehensive control framework for incorporating VSCs to smart power grids using bidirectional synchronous-VSC,” *IEEE Transactions on Power Systems*, vol. 29, no. 2, pp. 943–957, 2014.
- [97] Z. Shuai, W. Huang, C. Shen, J. Ge, and Z. J. Shen, “Characteristics and restraining method of fast transient inrush fault currents in synchronverters,” *IEEE Transactions on Industrial Electronics*, vol. 64, no. 9, pp. 7487–7497, 2017.

- [98] R. Prez, A. R. Cabero, and M. Prodanovic, "Parallel current-controlled synchronverters for voltage and frequency regulation in weak grids," *The Journal of Engineering*, vol. 2019, no. 17, pp. 3516–3520, 2019.
- [99] V. Natarajan and G. Weiss, "Synchronverters with better stability due to virtual inductors, virtual capacitors, and anti-windup," *IEEE Transactions on Industrial Electronics*, vol. 64, no. 7, pp. 5994–6004, 2017.
- [100] G. C. Kryonidis, K.-N. D. Malamaki, J. M. Mauricio, and C. S. Demoulias, "A new perspective on the synchronverter model," *International Journal of Electrical Power & Energy Systems*, vol. 140, pp. 1–12, 2022.
- [101] R. Prez, A. R. Cabero, and M. Prodanovic, "Harmonic virtual impedance design for parallel-controlled grid-tied synchronverters," *IEEE Journal of Emerging and Selected Topics in Power Electronics*, vol. 7, no. 1, pp. 493–503, 2019.
- [102] T. Shao, T. Q. Zheng, H. Li, and X. Zhang, "Parameter design and hot seamless transfer of single-phase synchronverter," *Electric Power Systems Research*, vol. 160, pp. 63–70, 2018.
- [103] S. Dong and Y. C. Chen, "Adjusting synchronverter dynamic response speed via damping correction loop," *IEEE Transactions on Energy Conversion*, vol. 32, no. 2, pp. 608–619, 2017.
- [104] K. Y. Yap, C. M. Beh, and C. R. Sarimuthu, "Fuzzy logic controller-based synchronverter in grid-connected solar power system with adaptive damping factor," *Chinese Journal of Electrical Engineering*, vol. 7, no. 2, pp. 37–49, 2021.
- [105] S. Dong and Y. C. Chen, "A method to directly compute synchronverter parameters for desired dynamic response," *IEEE Transactions on Energy Conversion*, vol. 33, no. 2, pp. 814–825, 2018.

-
- [106] S. M. Ashabani and Y. A. R. I. Mohamed, "A flexible control strategy for grid-connected and islanded microgrids with enhanced stability using nonlinear microgrid stabilizer," *IEEE Transactions on Smart Grid*, vol. 3, no. 3, pp. 1291–1301, 2012.
- [107] Q. C. Zhong and D. Boroyevich, "Structural resemblance between droop controllers and phase-locked loops," *IEEE Access*, vol. 4, no. 99, pp. 5733–5741, 2016.
- [108] M. K. Ghartemani and M. Iravani, "A nonlinear adaptive filter for online signal analysis in power systems: Applications," *IEEE Transactions on Power Delivery*, vol. 17, no. 2, pp. 617–622, 2002.
- [109] X. Wang, L. Chen, D. Sun, L. Zhang, and H. Nian, "A modified self-synchronized synchronverter in unbalanced power grids with balanced currents and restrained power ripples," *Energies*, vol. 12, pp. 1–18, 2019.
- [110] L. Huang, H. Xin, Z. Wang, K. Wu, H. Wang, J. Hu, and C. Lu, "A virtual synchronous control for voltage source converters utilizing dynamics of DC-link capacitor to realize self-synchronization," *IEEE Transactions on emerging and selected topics in power electronics*, vol. 5, no. 4, pp. 1565–1577, 2017.
- [111] D. Dong, B. Wen, D. Boroyevich, P. Mattavelli, and Y. Xue, "Analysis of phase locked loop low frequency stability in three phase grid connected power converters considering impedance interactions," *IEEE Transactions on Industrial Electronics*, vol. 62, no. 1, pp. 310–321, 2015.
- [112] M. R. Amin and S. A. Zulkifli, "A framework for selection of grid-inverter synchronisation unit: Harmonics, phase-angle and frequency," *Renewable and Sustainable Energy Reviews*, vol. 78, pp. 210–219, 2017.
- [113] M. Amin, A. Rygg, and M. Molinas, "Self-synchronization of wind farm in MMC-based HVDC system: A stability investigation," *IEEE Transactions on Energy Conversion*, vol. 32, no. 2, pp. 458–470, 2017.

- [114] T. Younis, M. Ismeil, E. K. Hussain, and M. Orabi, "An improved single-phase self-synchronized synchronverter with enhanced dynamics and current limitation capability," *IET Power Electronics*, vol. 12, no. 2, pp. 337–344, 2019.
- [115] Q. C. Zhong, W.-L. Ming, and Y. Zeng, "Self-synchronized universal droop controller," *IEEE Access*, vol. 4, pp. 7145–7153, 2016.
- [116] S. Dong, J. Jiang, and Y. C. Chen, "Analysis of synchronverter self-synchronization dynamics to facilitate parameter tuning," *IEEE Transactions on Energy Conversion*, vol. 35, no. 1, pp. 11–23, 2020.
- [117] S. Dong and Y. C. Chen, "A fast self-synchronizing synchronverter design with easily tuneable parameters," in *IEEE Power and Energy Society General Meeting (PESGM)*, Portland, August 2018, pp. 1–5.
- [118] W. Gil-Gonzalez, O. D. Montoya, A. Escobar-Mejia, and J. C. Hernandez, "LQR-based adaptive virtual inertia for grid integration of wind energy conversion system based on synchronverter model," *Electronics*, vol. 10, no. 9, pp. 1–16, 2021.
- [119] R. Aouini, B. Marinescu, K. B. Kilani, and M. Elleuch, "Synchronverter-based emulation and control of HVDC transmission," *IEEE Transactions on Power Systems*, vol. 31, no. 1, pp. 278–286, 2016.
- [120] S. Peyghami, P. Davari, H. Mokhtari, P. C. Loh, and F. Blaabjerg, "Synchronverter-enabled DC power sharing approach for LVDC microgrids," *IEEE Transactions on Power Electronics*, vol. 32, no. 10, pp. 8089–8099, 2017.
- [121] M. Onate, J. Rosada, J. Lopez, J. Quintero, and M. Aredes, "Control of a back-to-back converter as a power transfer system using synchronverter approach," *IET Generation, Transmission and Distribution*, vol. 12, no. 9, pp. 1998–2005, 2018.

- [122] R. Wu, L. Ran, G. Weiss, and J. Yu, "Control of a synchronverter-based soft open point in a distribution network," *The Journal of Engineering*, vol. 2019, no. 16, pp. 720–727, 2019.
- [123] M. Blau and G. Weiss, "Synchronverters used for damping inter-area oscillations in two-area power systems," *Renewable Energy and Power Quality Journal*, vol. 1, no. 16, pp. 45–50, 2018.
- [124] B. W. Franca, M. Aredes, L. F. d. Silva, G. F. Gontijo, T. C. Tricarico, and J. Posada, "An enhanced shunt active filter based on synchronverter concept," *IEEE Journal of Emerging and Selected Topics in Power Electronics*, vol. 10, no. 1, pp. 494–505, 2022.
- [125] L. d. N. Gomes, A. J. G. Abrantes-Ferreira, R. F. d. S. Dias, and L. G. B. Rolim, "Synchronverter-based STATCOM with voltage imbalance compensation functionality," *IEEE Transactions on Industrial Electronics*, vol. 69, no. 5, pp. 4836–4844, 2022.
- [126] X. Li, Y. Tan, X. Liu, Q. Liao, B. Sun, G. Cao, C. Li, X. Yang, and Z. Wang, "A cost-benefit analysis of V2G electric vehicles supporting peak shaving in Shanghai," *Electric Power Systems Research*, vol. 179, pp. 1–9, 2020.
- [127] M. Singh, P. Kumar, and I. Kar, "A multi charging station for electric vehicles and its utilization for load management and the grid support," *IEEE Transactions on Smart Grid*, vol. 4, no. 2, pp. 1026–1037, 2013.
- [128] M. A. Lopez, S. D. Torre, S. Martin, and J. A. Aguado, "Demand-side management in smart grid operation considering electric vehicles load shifting and vehicle-to-grid support," *International Journal of Electrical Power & Energy Systems*, vol. 64, pp. 689–698, 2015.
- [129] S. Li, S. Wu, S. Xiang, Y. Zhang, J. M. Guerrero, and J. C. Vasquez, "Research on synchronverter-based regenerative braking energy feedback system of urban rail transit," *Energies*, vol. 13, no. 17, pp. 1–23, 2020.

- [130] X. Huang, K. Wang, G. Li, and H. Zhang, "Virtual inertia-based control strategy of two-stage photovoltaic inverters for frequency support in islanded micro-grid," *Electronics*, vol. 7, pp. 1–20, 2018.
- [131] W. Yan, L. Cheng, S. Yan, W. Gao, and W. Gao, "Enabling and evaluation of inertial control for PMSG-WTG using synchronverter with multiple virtual rotating masses in microgrid," *IEEE Transactions on Sustainable Energy*, vol. 11, no. 2, pp. 1078–1088, 2020.
- [132] A. J. Sonawane and A. C. Umarikar, "Small-signal stability analysis of PV-based synchronverter including PV operating modes and DC-link voltage controller," *IEEE Transactions on Industrial Electronics*, vol. 69, no. 8, pp. 8028–8039, 2022.
- [133] J. Fang, H. Li, Y. Tang, and F. Blaabjerg, "Distributed power system virtual inertia implemented by grid-connected power converters," *IEEE Transactions on Power Electronics*, vol. 33, no. 10, pp. 8488–8499, 2018.
- [134] G. P. da Silva Junior, L. S. Barros, and C. M. V. Barros, "Synchronverter coupled to a lithium-ion bank for grid frequency and voltage supports and controlled charge-discharge," *Electric Power Systems Research*, vol. 197, pp. 1–8, 2021.
- [135] K. R. Vasudevan, V. K. Ramachandaramurthy, G. Venugopal, J. M. Guerrero, and G. D. A. Tinajero, "Synergizing pico hydel and battery energy storage with adaptive synchronverter control for frequency regulation of autonomous microgrids," *Applied Energy*, vol. 325, pp. 1–12, 2022.
- [136] Z. Kustanovich and G. Weiss, "Synchronverter based photovoltaic inverter," in *IEEE International Conference on the Science of Electrical Engineering in Israel (ICSEE)*, Eilat, December 2018, pp. 1–5.
- [137] R. V. Ferreira, S. M. Silva, D. I. Brandao, and H. M. A. Antunes, "Single-phase synchronverter for residential PV power systems," in *17th International Conference on Harmonics and Quality of Power (ICHQP)*, Belo Horizonte, October 2016, pp. 861–866.

-
- [138] P. Kundur, *Power System Stability and Control*, 1st ed. McGraw-Hill, 1994.
- [139] S. Chapman, *Electric Machinery Fundamentals*, 5th ed. McGraw-Hill, 2012.
- [140] N. Yu, J. Yang, S. Chen, and M. Ye, “Design of LCL filter based three level active power filters,” *Indonesian Journal of Electrical Engineering*, vol. 12, no. 1, pp. 48–56, 2014.
- [141] M. Ben, S. Romdhane, M. W. Naouar, I. S. Belkhodja, and E. Monmasson, “Simple and systematic LCL filter design for three-phase grid-connected power converters,” *Mathematics and Computers in Simulation*, vol. 130, pp. 181–193, 2016.
- [142] M. Dursun and M. K. Dosoglu, “LCL filter design for grid connected three-phase inverter,” in *2nd International Symposium on Multidisciplinary Studies and Innovative Technologies (ISMSIT)*, Ankara, October 2018, pp. 1–4.
- [143] J. Liu, L. Zhou, X. Yu, B. Li, and C. Zheng, “Design and analysis of an LCL circuit-based three-phase grid-connected inverter,” *IET Power Electronics*, vol. 10, no. 2, pp. 232–239, 2017.
- [144] M. Liserre, F. Blaabjerg, and S. Hansen, “Design and control of an LCL-filter based three-phase active rectifier,” *IEEE Transactions on Industrial Applications*, vol. 41, no. 5, pp. 1281–1291, 2005.
- [145] K. Y. Yap, C. R. Sarimuthu, and J. M. Y. Lim, “Grid integration of solar photovoltaic system using machine learning-based virtual inertia synthesis in synchronverter,” *IEEE Access*, vol. 8, pp. 49 961–49 976, 2020.
- [146] T. Gonen, *Electrical Power Transmission System Engineering*, 3rd ed. CRC Press, 2014.
- [147] B. T. Gwynn and R. D. Callafon, “Demodulation of three-phase ac power transients in the presence of harmonic distortion,” *Energies*, vol. 13, no. 2341, pp. 1–18, 2020.

-
- [148] N. V. Kuznetsov, M. V. Blagov, E. Kudryashova, J. Ladvanszky, M. Yuldashev, and R. Yuldashev, “Non-linear analysis of a modified QPSK costas loop,” *IFAC-PapersOnLine*, vol. 52, no. 16, pp. 31–35, 2019.
- [149] A. Loukriz, M. Haddadi, and S. Messalti, “Simulation and experimental design of a new advanced variable step size incremental conductance MPPT algorithm for PV systems,” *ISA Transactions*, vol. 62, pp. 30–38, 2016.
- [150] P. Sivakumar, A. Abdul Kader, Y. Kaliavaradhan, and M. Arutchelvi, “Analysis and enhancement of PV efficiency with incremental conductance MPPT technique under non-linear loading conditions,” *Renewable Energy*, vol. 81, pp. 543–550, 2015.
- [151] N. Mohan, T. M. Undeland, and W. P. Robbins, *Power Electronics; converters, applications and design*, 6th ed. Wiley, 1995.
- [152] W. Shepherd and L. Zhang, *Power Converter Circuits*, 1st ed. CRC Press, September 2019.